Summer 8-15-2019

Visual and Chemosensory Pathways Associated With Male Courtship Decisions in Drosophila melanogaster

Ross Mckinney
Washington University in St. Louis

WASHINGTON UNIVERSITY IN ST. LOUIS

Division of Biology and Biomedical Sciences
Neurosciences

Dissertation Examination Committee:
Yehuda Ben-Shahar, Chair
Bruce Carlson
Erik Herzog
Timothy Holy
Barani Raman

Visual and Chemosensory Pathways Associated With Male Courtship Decisions in *Drosophila melanogaster*

by
Ross McKinney

A dissertation presented to
The Graduate School
of Washington University in
partial fulfillment of the
requirements for the degree
of Doctor of Philosophy

August 2019
St. Louis, Missouri

Table of Contents

List of Figures

List of Tables

Acknowledgments

There are many people that I would like to thank who have helped me tremendously through my time at Washington University.

Firstly, I am extremely grateful for all of the help and support provided by my advisor, Yehuda Ben-Shahar. Yehuda has allowed me a significant amount of leeway to explore various areas of research that are of interest to me. Though not all of our experimental ideas worked out as we thought they might, I have learned much about what it takes to become an independent researcher and am grateful for all of the skills and knowledge I picked up through these experiences. Thank you for mentoring me these past several years.

I am also very appreciative of the thought-provoking conversations I've had with members of the Ben-Shahar lab, especially to Eirik Søvik, who was my office mate, coffee-drinking companion, and experimental brainstorming backboard. In addition, I'd like to thank Cassie Vernier for our great talks and keeping our lab members connected with each other during our time in graduate school; we would not have had such a great lab were it not for her. Finally, I'd like to acknowledge Alexis Hill, Zhen Peng, and many other members of the lab who have offered great advice, insight, and friendship over the years.

Many people have also helped me with experimental preparations and procedures. In particular, I am indebted to Dianne Duncan for her help with confocal microscopy, Paula Kiefel for her help with generating transgenic flies, and Doris Ling for helping with calcium imaging.

I am also indebted to the members of my thesis committee: Erik Herzog, Bruce Carlson, Barani Raman, and Timothy Holy. The feedback that you have provided me has been invaluable for my maturation as an scientist. I know that it is time consuming to be a

mentor, and I appreciate all of your efforts to help me succeed here.

Finally, I would like to thank my partner Stephanie Takamatsu, without whose support I would not be where I am today. You have truly been the best friend I could ask for and your encouragement and companionship have been the most important aspects of my life. Thank you for all you've done for me throughout this process.

Ross McKinney

Washington University in St. Louis

August 2019

ABSTRACT OF THE DISSERTATION

Visual and Chemosensory Pathways Associated With Male Courtship Decisions in *Drosophila melanogaster*

by

Ross McKinney

Doctor of Philosophy in Biology and Biomedical Sciences

Neurosciences

Washington University in St. Louis, 2019

Professor Yehuda Ben-Shahar, Chair

Successful mating in diverse animal species often depends on ritualistic sequences of spatially and temporally coordinated behavioral elements. Yet, the sensory cues and neural circuits that mediate optimal mating display patterns are largely unknown. The courtship ritual in *Drosophila melanogaster* consists of a well-studied sequence of behavioral elements including orienting, chasing, tapping, singing, and licking that are known to depend on several sensory modalities, including both vision and chemosensation. However, the specific sensory inputs utilized by males to direct the spatial and temporal transitions between different elements of the courtship ritual are not well understood. In this thesis, I therefore first develop a new computational tool to quantitatively characterize male courtship behaviors with a high spatial and temporal resolution. Subsequently, I use this tool, in conjunction with genetic and microscopy approaches to map the visual and chemosensory neural pathways that drive some of the patterned behavioral elements of the male courtship ritual. I demonstrate that whereas visual circuits are important for mediating both spatial and temporal components of male mating behaviors, chemosensory circuits are mostly required for enhancing the duration and intensity of courtship bouts. Further, I identify a male-specific axonal architecture present in subpopulations of foreleg chemosensory neurons which is important for helping to sustain mating

behaviors. This thesis examines the inputs, processing centers, and neural architectures required for the proper organization of innate mating behaviors and should provide insight into understanding how animals transform sensory stimuli into complex behavioral outputs, which is a major goal in modern neuroscience.

Chapter 1: Introduction

All organisms are constantly tasked with making decisions. Some of these are conceptually simple and innate, such as a bacterium avoiding a toxic chemical within the environment [Tso and Adler, 1974]; whereas others are more complex and require learned or stored information, such as an animal navigating a maze [Morris, 1981, Krumin et al., 2018]. Regardless of the complexity, most decisions require that sensory stimuli be transformed into some form of motor output (as a behavioral response) that benefits the organism. While studies of unicellular organisms have provided great insight into the molecular mechanisms of simple, reflexive decisions [Bi and Sourjik, 2018], the sensorimotor pathways and neural circuit-level mechanisms that give rise to more complex choices in animals are less well understood.

In animals, environmental information is detected by sensory receptors that are present as part of either the peripheral (PNS) or central nervous system (CNS) and is transmitted along nerve fibers to central processing centers. Once in the CNS, sensory signals are thought to be integrated to help form or alter an animal's internal model of its environment [Gold and Shadlen, 2007, Huda et al., 2018]. These signals, along with subsequent proprioceptive signals from motor movements, ultimately feed into this internal model to coordinate subsequent behavioral outputs [Huda et al., 2018]. Much work has gone into understanding neural correlates of decision making [Platt and Glimcher, 1999, Padoa-Schioppa and Assad, 2006], and while these experiments have been instrumental in developing models of action selection in animals, many previous studies were not designed to identify specific neural circuits that regulate sensorimotor decisions.

Here, I help to further develop *Drosophila melanogaster* as model for understanding sensorimotor decision making. I highlight mating behaviors, and the male courtship ritual in particular, as a valid system for parsing the sensory and circuit-level mechanisms that

mediate particular behavioral states. Finally, I describe the current state of knowledge about neural circuits in the fly that lead to the generation of specific behaviors, with an emphasis on visual and chemosensory circuits.

1.1 Mating Behaviors as a Model for Understanding Decision Making

Mating behaviors provide a unique lens through which to examine decision making. These behaviors have an extremely rich diversity and are found across the animal kingdom, from the birds of paradise [Irestedt et al., 2009] to simpler invertebrates such as the fruit fly [Greenspan and Ferveur, 2000]. An important aspect of most mating behaviors is their innateness; these behaviors are not learned, but they are rather ingrained into an animal's behavioral repertoire from birth. That mating behaviors are innate makes them ideal targets for understanding the neural circuits that direct them, as these circuits are hard-wired into the animal. Therefore, one should be able to systematically identify all of the neurons involved in the decision to engage in a mating behavior, from the sensory stimuli important for its initiation to central and motor neurons required for its execution. Indeed, recent studies have taken advantage of the relatively simple nervous system of the model organism *Caenorhabditis elegans* to map all of the individual neurons that coordinate innate behaviors such as egg laying [Schafer, 2006, Collins et al., 2016], and studies in *D. melanogaster* have started to dissect the neural circuits underlying specific aspects of some mating behaviors [Ruta et al., 2010]. Further, unlike many other behavioral outcomes that involve simply deciding between one alternative or another, mating behaviors are often temporally linked into distinct sequences, collectively referred to as courtship rituals, where animals must choose between multiple behavioral outputs over time. Both their innateness and temporal relatedness make mating behaviors an interest-

ing and useful system for studying how animals choose between alternative behaviors.

1.2 The Courtship Ritual in *Drosophila*

The courtship ritual in the fly has been used as a tool for investigations into the genetics underlying behavior since at least the middle of the 20th century [Ehrman, 1960, Crossley and Zuill, 1970], and its behavioral components have been well described [Spieth, 1974, Greenspan and Ferveur, 2000, Sokolowski, 2001]. While the behavioral aspects of the male courtship ritual have been extensively addressed, female-specific courtship behaviors have not been well-studied and are, in general, less complex and more difficult to observe. Therefore, in this dissertation, I only examine male-specific courtship behaviors.

The male courtship ritual is composed of a series of stereotyped behaviors, often beginning with the male orienting towards the female (Figure 1.1). During orienting, the male visually fixates on the female and positions his body such that his antero-posterior body axis is aimed towards the female. Subsequently, the male may chase and sing towards the female, both behaviors which rely on visual inputs [Agrawal et al., 2014, Coen et al., 2014, 2016, Clemens et al., 2018]. As the female stops moving, the male can approach and tap and lick her to sample the chemical environment on the cuticle of the female [Vosshall, 2008, McKinney et al., 2015]. Finally, the male may attempt to copulate with the female. If copulation occurs, the courtship ritual ends; if not, then the male may enter into any of the behavioral states previously described, and the ritual may continue.

An important aspect of the male courtship ritual, which has made it immensely useful as tool for behavioral genetics research, is the fact that it is innate. Indeed, a male that has been isolated since eclosion, will engage in all of the behaviors of the courtship ritual immediately after being exposed to a female conspecific, even though he has never engaged in or observed any of these behaviors previously [Greenspan and Ferveur, 2000].

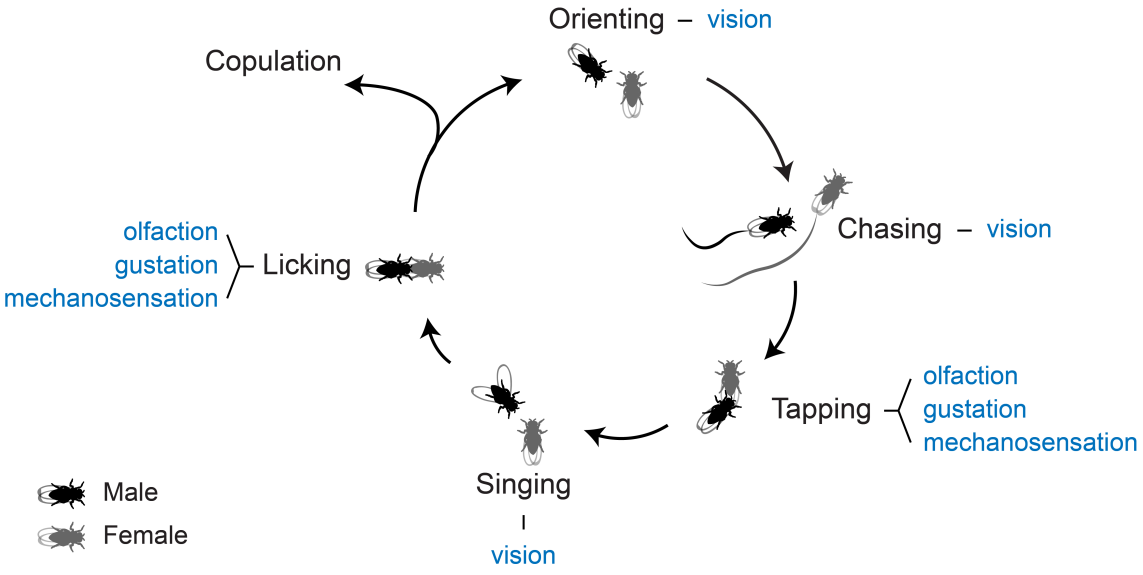

Figure 1.1: **Overview of the male courtship ritual.** The male courtship ritual in the fly consists of a male orienting towards, chasing, tapping, singing towards, licking, and attempting to copulate with a female courtship target. The sensory modalities utilized by the male to gain information about the female are colored in blue.

In addition to simply displaying these behaviors, the male courtship ritual also occurs with a specific temporal sequence [Markow and Hanson, 1981]. Even though these aspects of courtship suggest that there is a single, hardwired circuit which controls all aspects of male mating behaviors, loss of specific sensory stimuli can lead to alterations in the temporal sequencing of these behavioral displays [Markow, 1987]. Thus, the courtship ritual is plastic, and the interplay between various sensory circuits can direct alternative courtship decisions in the fly.

The courtship ritual in *Drosophila* relies on the proper acquisition of various sensory stimuli about the female, which the male can utilize to optimize his reproductive success. Indeed, the courtship ritual has long been used as a model for understanding the genetic and neural basis of chemosensation [Gailey et al., 1986, Ferveur et al., 1997, Lu et al., 2012, Thistle et al., 2012, Clowney et al., 2015], and has more-recently begun to be utilized to understand how visual signals and circuits coordinate behavioral responses [Pan

et al., 2012, Agrawal et al., 2014]. While other sensory modalities also mediate various courtship decisions in male flies [Tauber and Eberl, 2001, Ejima and Griffith, 2008], both vision and chemosensation have been shown to play dominant roles in these processes, and I therefore describe the function of each sensory modality in courtship in the following sections.

1.3 Visual Signals and Circuits Underlying Courtship Decisions in the Fly

Visual signals are utilized across the animal kingdom to regulate various mating behaviors [Gonzalez-Bellido et al., 2016, Darmaillacq et al., 2017, Ligon et al., 2018]. For instance, in many insects species, males often take advantage of motion-based cues to track, intercept, and mate with female conspecifics [Boeddeker et al., 2003]. And *Drosophila* males have also been shown to visually track the motion of a female to chase and court her [Kohatsu and Yamamoto, 2015, Ribeiro et al., 2018]. While motion-based cues have been presumed to be the predominant visual cue utilized by males during courtship [Greenspan and Ferveur, 2000], previous studies have also suggested the presence of other visual cues on the female that could direct courtship displays [Kimura et al., 2015], though none have been identified. Here, I describe the current state of knowledge about the various visual circuits that detect female-specific visual cues and direct male courtship decisions in the fly.

Recent advances in high-resolution mapping of neural circuits in the fly brain [Jenett et al., 2012, Zheng et al., 2018] have revealed distinct visual pathways that contribute to the regulation of various behaviors, including courtship. The fly visual system is composed of five layers of interconnected neurons that function together to collect light and process various visual stimuli. The first layer is the retina which contains photoreceptors, and the next four

layers include the lamina, medulla, lobula, and lobula plate and are contained within the optic lobes of the fly's brain [Borst and Helmstaedter, 2015]. While the photoreceptors and neurons present in more superficial layers of the visual system respond to more primitive forms of visual stimuli, such as changes in luminance, more selective responses to specific visual stimuli, including motion direction selectivity, start to appear at the level of the lobula and lobula plate where visual projection neurons (VPNs) reside [Krapp et al., 1998, Joesch et al., 2008]. VPNs have been well described both anatomically and physiologically [Fischbach and Dittrich, 1989, Krapp and Hengstenberg, 1996, Haag et al., 1999] and link visual processing with other brain centers [Otsuna and Ito, 2006, Strausfeld and Okamura, 2007, Wu et al., 2016]. Due to their anatomic location, response properties, and connectivity, VPNs have therefore been thought to be positioned such that they could mediate behavioral responses to visual stimuli. Indeed, recent studies have demonstrated that specific populations of VPNs respond to looming stimuli and directly induce escape behaviors (Figure 1.2A) [Sen et al., 2017, von Reyn et al., 2017, Ache et al., 2019]. In particular, looming-responsive VPNs were shown to directly synapse onto the giant fiber in the fly, which when depolarized, initiates a jump and flight response important for predator avoidance [Allen et al., 2006]. Thus certain VPNs themselves seem to function as decision centers that initiate innate behavioral responses to specific visual stimuli. Similar to initiating escape responses, VPNs have started to be investigated for their roles in coordinating mating behaviors in the fly, as I discuss below [Ribeiro et al., 2018].

Female motion is one of the best studied visual cues that helps to direct male courtship behaviors. In particular, both female and female-like motion entice males into chase behaviors [Cook, 1979, 1980, Agrawal et al., 2014, Kohatsu and Yamamoto, 2015], which were recently shown to require a subclass of VPNs termed Lobula Columnar (LC) cells [Ribeiro et al., 2018]. LC cells themselves have been extensively characterized and consist of at least 22 distinct neuronal populations (LC1-22) that are classified by their morphologies [Wu et al., 2016]. While LC neurons were originally classified by morphology,

they also show distinct physiological responses to various visual stimuli; moreover, ectopic activation of specific classes of LC neurons results in unique innate behavioral responses, such as backwards walking, reaching, and jumping [Wu et al., 2016]. Within the context of mating behaviors, Ribeiro et al. [2018] recently demonstrated that LC10 neurons are physiologically responsive to female-like movements and are required for males to chase and court females appropriately (Figure 1.2B). It is not known whether any other LC cell populations mediate male courtship behaviors, though several respond to common visual stimuli, such as looming, which are likely to be encountered by males during courtship.

In addition to motion cues, the visual system in the fly is also responsive to other stimuli such as shape, color, and pattern [Borst et al., 2010]; whether any of these features mediate male courtship decisions has not been well studied. However, at least one group found that the size, number, and spread of abdominal bands on a moving, robotic 'female' fly did not have an effect on male chase behaviors, though the physical size of the robot did [Agrawal et al., 2014]. Along with abdominal bands present on the female, the eyes are a prominent visual feature that could be utilized by males to direct certain aspects of courtship, though no studies have specifically addressed this question. Further, the specific neural circuitry that might underlie the detection of these features are not known. In subsequent chapters, I address how static visual features present on a female mediate male courtship decisions.

1.4 Chemosensory Signals and Circuits Underlying Courtship Decisions in the Fly

The mating ritual in *Drosophila* is also regulated by diverse gustatory and olfactory cues, termed pheromones. These structurally-diverse chemical compounds are present on the cuticle of flies, many of which originally evolved to function as anti-desiccants, that were subsequently co-opted to function in insect social communication [Yew and Chung, 2015].

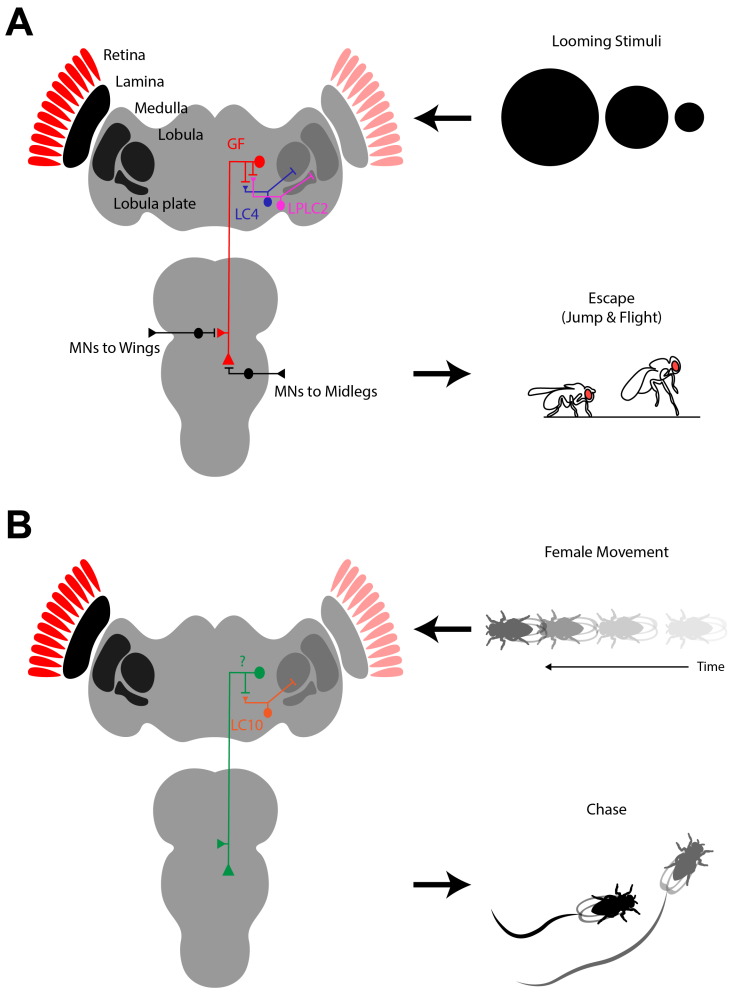

Figure 1.2: **VPNs help coordinate behavioral responses to visual stimuli. (A)** Lobula columnar (LC) and lobula plate/lobula columnar (LPLCs) cells detect looming stimuli and connect to the fly's escape circuitry by directly synapsing onto the giant fiber (GF) [von Reyn et al., 2017, Klapoetke et al., 2017, Ache et al., 2019]. Escape image modified from von Reyn et al. [2017]. **(B)** LC10 detects female-like movements and helps males engage in chase behaviors [Ribeiro et al., 2018]. The post-synaptic partners of LC10, which mediate behavioral responses, are not known.

Chemosensory receptor neurons are responsible for sensing different pheromones and translating their detection into neural impulses that can signal the saliency of a particular compound or potential mate. These neurons are distributed across the body of the fly and consist of gustatory receptor neurons (GRNs), which detect non-volatile compounds, and olfactory receptor neurons (ORNs), which detect volatile molecules. Both GRNs and ORNs participate in the detection of male- and female-specific pheromones and can either promote or inhibit various aspects of the male courtship ritual. The dual roles of chemosensory receptors, and their pheromonal agonists, in modulating courtship behaviors makes them prominent targets for interrogating the sensory mechanisms underlying decision making in the fly.

A major class of pheromones utilized by males during courtship are the cuticular hydrocarbons (CHCs), which are long-chain, non-volatile hydrocarbons covering the cuticles of flies. While there are approximately 30 distinct CHCs within various *Drosophila* species [Ferveur, 2005], the most abundant CHC present on females is 7,11-heptacosadiene (7,11-HD), which has been shown to promote courtship in males [Antony et al., 1985]. This pheromone is detected via a specific class of foreleg GRN that expresses the transcription factor *fruitless* (*fru*), which is a neuro-developmental gene that includes perhaps the entirety of the central and peripheral circuitry required for the initiation and maintenance of courtship along with other sex-specific behaviors such as aggression [Lee et al., 2000, Manoli et al., 2005, Vrontou et al., 2006]. While the specific identity of the chemoreceptor responsible for the detection of 7,11-HD in GRNs is not known, the expression of the degenerin/epithelial sodium channel *pickpocket23* (*ppk23*) has been shown to specifically overlap with *fru* in GRNs, and exogenous application of 7-11HD onto *ppk23*$^{+}$ gustatory sensilla leads to depolarization of these cells [Lu et al., 2012, Thistle et al., 2012, Toda et al., 2012]. Nevertheless, following activation of *fru/ppk23*$^{+}$ GRNs in the forelegs, pheromonal signals propagate along ascending interneurons in the ventral nerve cord (VNC) of the male until they reach P1 neurons, which also express *fru* and act as a

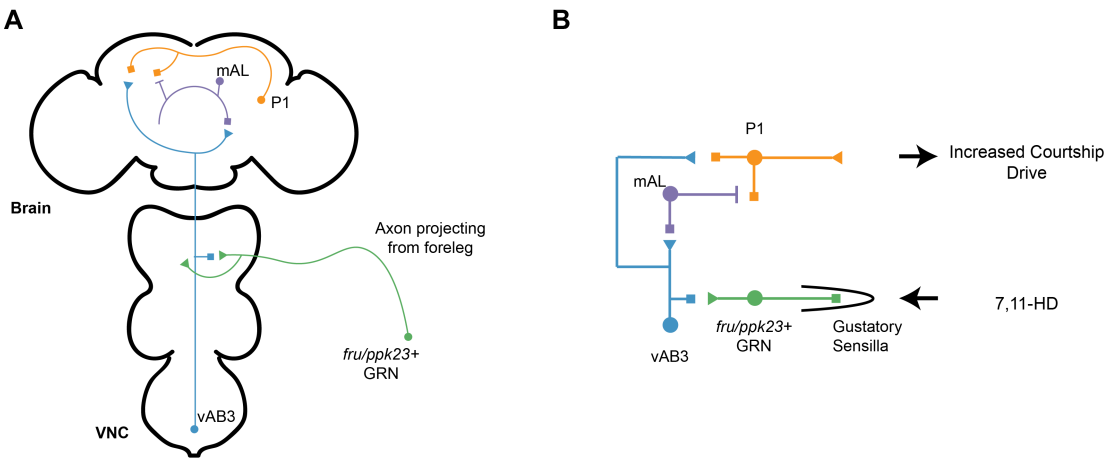

Figure 1.3: **Foreleg GRN circuitry regulating male courtship behavior. (A)** Schematic of neural circuitry, with approximate anatomic locations, that detects the female-specific pheromone 7,11-HD. *fru/ppk23*$^{+}$ GRNs initially detect 7,11-HD at the periphery, and the signal is subsequently sent through ventral abdominal 3 (vAB3) and medial antero-lateral (mAL) interneurons before arriving at P1 neurons in the brain. P1 neurons ultimately regulate male courtship drive. **(B)** Same as in (A), but shown as a simplified circuit diagram with chemosensory inputs and behavioral outputs.

central processing center to manage the sexual state of the male (Figure 1.3) [Kohatsu et al., 2011, Kallman et al., 2015]. Specifically, depending on the activity of P1 neurons, the male's sexual drive can change, such that lower activity within these neurons corresponds to lower levels of courtship and vice versa. Interestingly, the P1 neuronal cluster has been shown to not only respond to multiple chemosensory signals propagated by ORNs and GRNs [Clowney et al., 2015], but it has also been shown to respond to visual signals [Kohatsu and Yamamoto, 2015, Pan et al., 2012], suggesting that this cluster could act as a multisensory integration center in the fly brain. Exactly how chemosensory and visual signals interact within P1 — or other neural integration centers — is unclear.

While CHCs are an important component of the chemical environment to which males are exposed during the courtship ritual, other classes of volatile pheromones are also important for regulating courtship behaviors. For example, 11-cis-vaccenyl acetate (cVA) is a lipid produced in the male ejaculatory bulb that is transmitted from male to female

following copulation and functions as a volatile pheromone to inhibit courtship of the female by subsequent males [Butterworth, 1969, Guiraudie-Capraz et al., 2007, Kurtovic et al., 2007]. Whereas CHCs are largely detected by the contact-chemoreceptor GRNs, cVA is detected by ORNs in the antennae [Datta et al., 2008]. cVA signals also seem to converge on P1 neurons in the brain of the male to suppress neural activity and subsequent courtship behaviors [Clowney et al., 2015], suggesting that P1 neurons play an important role in regulating courtship drive in males. Though it is clear that both GRNs and ORNs play important roles in directing male courtship behavior, for the remainder of this dissertation, I will focus on the role of gustatory pheromones and GRN circuitry in male courtship decisions.

Pheromonal signals must propagate from the periphery into the CNS following a specific neural code that allows males to decide between engaging in alternative mating behaviors. Importantly, neurons must be wired in configurations that allow for the maintenance of sensory signals along circuits that involve potentially hundreds-to-thousands of synaptic connections [Zheng et al., 2018] and which ultimately encode valuable information about a particular stimulus. Sensory circuits, which often arise from bilaterally-paired sensory organs, in particular often contain neural circuit architectures which participate in this process. For example, sensory signals in the avian — and to a lesser extent, mammalian — auditory system travel along unique axonal delay lines, which allows for the parsing of interaural timing differences and determination of the azimuthal direction of a sound [Carr and Konishi, 1988, McAlpine and Grothe, 2003, Grothe et al., 2010]. Similarly, flies utilize asymmetric synapses in their olfactory circuitry to determine the location of volatile odorants [Gaudry et al., 2013]. Whether or not the fly pheromonal system contains specific neural circuit architectures which aid in the transmission of social stimuli remains unknown.

Interestingly, there are aspects of some pheromone-detecting circuits that suggest spe-

cific circuit configurations could function in the regulation of male courtship behaviors. For instance, morphological analyses of *fru/ppk23*$^{+}$ neurons initially revealed that the axonal projections of foreleg-specific GRNs are sexually-dimorphic [Possidente and Murphey, 1989, Mellert et al., 2010]. Whereas, GRN axons project contralaterally into and cross the midline of the VNC in males, these same neurons only project ipsilaterally in females. As the presence of sexually-dimorphic circuitry usually indicates its utility in sex-specific behaviors, the role of *fru/ppk23*$^{+}$ neurons in the regulation of male courtship behavior was quickly tested, and these neurons were confirmed to convey mostly excitatory signals to sustain courtship drive in male flies [Lu et al., 2012, Toda et al., 2012, Thistle et al., 2012]. While these neurons seem to intensify male courtship — likely by detecting CHCs, including 7,11-HD [Thistle et al., 2012, Kallman et al., 2015] — the specific role of midline crossing axons, and their function in directing courtship behaviors, has never been directly tested. The fact that these foreleg GRNs are present bilaterally, utilized for collecting chemosensory stimuli, and mediate elevated levels of courtship suggest that midline crossing axons could be functioning in an important, yet unrecognized, aspect of neural processing during male mating behaviors.

1.5 Summary and Overview

Understanding how animals make complex decisions is difficult task, however the male courtship ritual in *Drosophila melanogaster* provides a rich framework for understanding the mechanisms of action selection in animals. The courtship ritual consists of several independent, easily identifiable, and well-characterized behaviors that depend on several sensory modalities including vision and chemosensation. In this dissertation, I focus on delineating the specific sensory cues and circuits — with an emphasis on vision and chemosensation — that allow for male flies to choose between alternative behaviors during courtship.

In Chapter 2, I first take advantage of recent technological advancements in computer vision and machine learning to classify fly behaviors from video data. I describe the development of software that is capable of tracking the position and body postures of pairs of courting flies and provide a programmatic interface which allows users to use this data to classify video frames containing males engaged in specific behaviors. Ultimately, knowing when and where males participate in behavioral elements of the courtship ritual should allow for the determination of a rich and high-resolution description of male courtship in the fly. In subsequent chapters, I show that these data are useful for understanding how sensory cues and neural circuits affect behavioral decisions during social interactions.

In Chapter 3, I utilize the above software to develop a spatiotemporal description of the courtship ritual and examine the visual cues and neural circuits that regulate male courtship behaviors. I find that specific visual cues, unrelated to female motion, are important for the proper spatial positioning of the male with respect to the female and also affect the choice to engage in particular behaviors during courtship. I further show that specific classes of VPNs in the optic lobes of the fly participate in the recognition of female visual features that coordinate male behavioral displays. These data highlight previously unknown visual cues and circuits that regulate male courtship and provide new methodologies for characterizing the courtship ritual, which should be useful for future studies on the mechanisms underlying action selection during mating behaviors.

In Chapter 4, I examine how chemosensory cues regulate the male courtship ritual and show that specific aspects of foreleg GRN circuitry are necessary for regulating male courtship drive. In particular, I show that manipulations of female pheromones leads to overall decreases in courtship, but does not effect the spatial positioning or overall temporal structure of male courtship behaviors. Further, I highlight axonal midline crossing by foreleg GRNs as a necessary component of the male sex circuit which is required for sustained courtship. Consequently, my findings suggest that excitatory pheromones and

their sensation by GRNs largely regulate the decision of a male to court a female but do not impact the choice of which behaviors to engage in following entry into the courtship ritual.

Together, the findings presented in this dissertation develop the courtship ritual as an important tool for understanding complex behavioral decisions, as I discuss in Chapter 5. They suggest that distinct sensory systems can play alternative roles in directing behavioral displays and identify various circuits which mediate these effects. Whereas vision coordinates both spatial and temporal decisions within the courtship ritual, chemosensation seems to mostly regulate the decision to enter into and remain in a behavioral state that enhances courtship. These experiments, along with previous studies examining chemosensory and visual inputs which regulate courtship behavior, provide the foundation for examining exactly how brain circuits combine information across sensory systems to regulate complex behaviors.

Chapter 2: A Computational Method to Quantitatively Characterize Male Courtship Behaviors in *Drosophila*

Courtship in *Drosophila melanogaster* has traditionally been hand-scored in a binary manner, whereby a male fly is either courting or not courting a target female. The vast majority of studies which use courtship as a behavioral output utilize these simple binary data to calculate two main parameters: the fraction of time a male spends courting a female and the time taken for a male to initiate courtship, termed the courtship index (CI) and courtship latency (CL), respectively. While these parameters have been instrumental in advancing diverse areas of research, they are not capable of capturing the full complexity of the courtship ritual, especially in the context of understanding the spatiotemporal relationships between individual behavioral elements of male courtship.

Therefore, in this chapter, I develop computational tools and software designed to help analyze both individual courtship behaviors and the relationships between them. In particular, I utilize computer vision techniques to track and analyze videos of courting flies and subsequently use machine learning algorithms to classify video frames containing males engaged in specific behavioral elements of the courtship ritual. I am able to identify video frames containing specific behaviors with high accuracies and can subsequently use these classifications to examine both durations of time males spend in specific behavioral states and frequencies of transitions from one behavioral state to another. Further, by mapping frames containing males engaging in a particular behavior back onto the spatial position of the male in that frame, my software enables the examination of the precise locations of specific courtship behaviors. These tools, in conjunction with the genetic tools currently available in *Drosophila*, should enable the courtship ritual to be used as a model system for understanding the genetics and neural circuits that coordinate complex

behavioral decisions.

2.1 Introduction

In trying to understand the extremely difficult problem of relating brain function to behavior, scientists have often sought to reduce the complexity of both neurophysiological preparations and behavioral assays [Gomez-Marin et al., 2014, Krakauer et al., 2017]. For instance, the courtship ritual exhibited by *Drosophila melanogaster* males has been used for decades as a means to understand the sensory and genetic determinants of behaviors [Spieth, 1974]. While the courtship ritual is comprised of a rich sequence of spatiotemporally linked behaviors, it is very often described in the literature by only a few quantitative parameters, such as the courtship index (CI) and courtship latency(CL) [Siegel and Hall, 1979, Eastwood and Burnet, 1977]. This has generally been due to the laborious efforts required to hand-score individual bouts of behavior, rather than a disinterest in fully exploring the varied behavioral routines observed during courtship. Yet, even hand-scoring the times and durations of behavioral epochs is insufficient to capture the relationships between courtship behaviors; for this, we would need to know both the position and behavioral state of each individual for every time point during courtship.

With the advent of new technologies, such as video analysis by computer vision algorithms, it has become possible to track an animal's position and postures throughout every frame of a video during a behavior of interest [Kain et al., 2013, Wang and Wang, 2013, Berman et al., 2014, Uhlmann et al., 2017]. Advances in the field of machine learning have further allowed for the use of position/posture data to be utilized to classify video frames that contain animals engaging in particular behaviors [Klibaite et al., 2017, Berman et al., 2014, Robie et al., 2017]. By inputting tracking data into classification algorithms, it has therefore become possible to determine both positional and behavioral information about an animal over the course of a video-recorded behavioral trial. While there are sev-

eral software suites designed to track the positions of *Drosophila* from videos [Branson et al., 2009, Dankert et al., 2009], most are not designed to incorporate tracking, behavioral classification, and analysis into a single package. Further, the packages that are available are often written in proprietary languages, such as MATLAB, that do not allow for use by researchers without a software license [Dankert et al., 2009, Kabra et al., 2013, Swierczek et al., 2011].

In this chapter, I describe the development of a software package, written in the open-source Python programming language, that allows for a user to (1) track pairs of courting flies, (2) classify behaviors, and (3) analyze spatiotemporal behavioral sequences. This package not only enables use in a pure Python environment, but provides a graphical user interface (GUI) that enables tracking and analysis in a more user-friendly manner. In this and subsequent chapters, I use this package to quantitatively describe the spatial and temporal characteristics of individual male courtship behaviors and their relationships to one another.

2.2 Methods

The software described in this chapter has a particular use case: to track a male fly that is courting a stationary female target. Therefore, pairs of flies must be setup as follows.

2.2.1 Video Recording Chamber

In order to ensure a high quality video recording that was usable for tracking, we built a custom video-recording chamber (Figure 2.1). We first built a light box containing an array of white light emitting diodes (LEDs) and mounted a light diffuser on top of the box. We then adhered a single female fly to a transparent piece of plastic using UV-hardening glue (RapidFix) and placed the female onto the center of the light box. We built

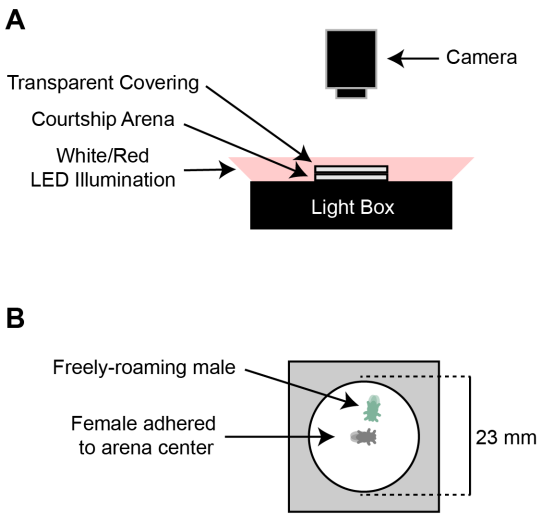

Figure 2.1: **Video recording chamber used for tracking. (A)** Side view of the recording chamber. It consists of a light box with white LEDs, a courtship arena, and an overhead camera. **(B)** Top-down view of the recording chamber showing the position of male and female during recording.

custom courtship arenas which were made from 38mm x 38mm x 6.5mm thick pieces of transparent plexiglass and contained a circular hole in the middle which was 23mm in diameter. We placed this arena on top of the female and covered the chamber with a piece of transparent plastic. Finally, we mounted a camera (Raspberry Pi NoIR) above the arena and surrounded the entire apparatus with a cloth box to eliminate shadows from overhead lights.

2.2.2 Videos

Videos were recorded for 10 minutes at 24 frames per second using a Raspberry Pi NoIR camera, though any camera can be used for this task. We recorded videos at a resolution of 640 pixels x 480 pixels and tried to assure that each fly occupied $\sim$1500 pixels in each frame. We initially recorded videos in .h264 format, and subsequently converted videos to .fmf format using custom scripts before tracking [Straw and Dickinson, 2009]. For tracking with the provided GUI, all videos must first be converted to .fmf format.

2.2.3 Tracking Algorithms

Videos were converted to a single color channel before tracking, and a single background image from the video was calculated by taking the mean pixel intensity across 200 randomly selected images.

Female Position. Since each female was immobilized and fixed to the center of the courtship arena, their detection was accomplished by allowing users to specify an elliptical region that fully enclosed the female through use of the GUI (see Section 2.2.4). Since there could be variation in the user-defined ellipse surrounding the female from trial to trial, the absolute position of the female within the ellipse was further refined by first thresholding and then binarizing the image based on a user-defined value. The largest area of connected pixels within the user-defined ellipse was defined as the 'female' (Figure 2.2). An ellipse was then fit to this region of connected pixels and its centroid, major axis length, minor axis length, and orientation were calculated using Scikit-image [van der Walt et al., 2014]. The female's head and rear positions were also calculated as the extremities of the fitted ellipse's major axis length, and directionality was determined via user input.

Male position. To calculate the position of the male, the ellipse fitted to the female was first excluded from the frame. A user-defined threshold was applied to the image and all pixels were converted to binary values. The largest region of connected pixels within the courtship arena — and outside of the ellipse fit to the female — was taken as the 'male'. An ellipse was fit to this region and the centroid, major axis length, minor axis length, and orientation were recorded.

The wing positions on the male were then calculated by (1) subtracting the current frame from the background image, (2) subtracting off the pixels occupied by the male's body position (which was calculated above), and (3) binarizing the resulting image based on

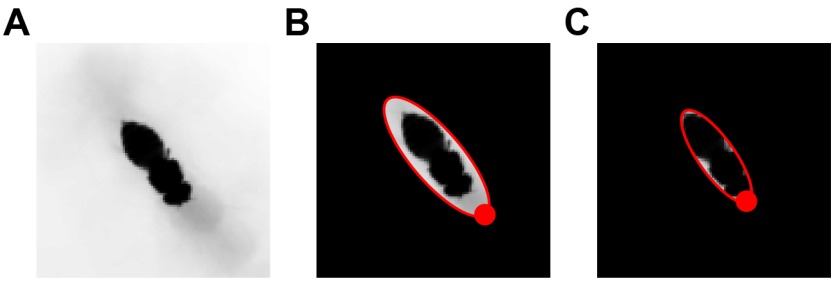

Figure 2.2: **Determining female position during tracking. (A)** Background-subtracted image of female. **(B)** User-defined ellipse; the filled red circle highlights the head of the female. This ellipse is slightly larger than the actual size of the female, which could affect male tracking and subsequent classification. **(C)** Refined ellipse. The ellipse has been tightened to the female based on the user-defined ellipse. Refining the ellipse in this manner ensures consistent tracking results from video to video.

a second user-defined threshold (see Figure 2.3). A small (100 pixel x 100 pixel) region containing the male was then cropped and the male was rotated such that his major axis aligned with the image's horizontal axis. The image was summed along the horizontal axis, and the appropriate orientation of the male was determined based on the half of the body containing more non-zero pixels: the head was defined as the half containing less pixels and the rear was defined as the half containing more pixels (Figure 2.3A-3). The image was then oriented such that the male's posterior-anterior axis was facing from left to right along the horizontal axis (Figure 2.3A-4), the image was split into quarters (Figure 2.3A-5), the two right-most quarters were discarded (Figure 2.3A-6), and an ellipse was fit to the areas with the greatest number of connected pixels in the top left and bottom left quarters (Figure 2.3A-7). These two regions represent the left and right wings, respectively.

Finally, head and rear positions of the male were assigned according to the distal most points along the major axis of the ellipse fitted to the male. Head and rear were distinguished from one another based on wing position (calculated above), where the head

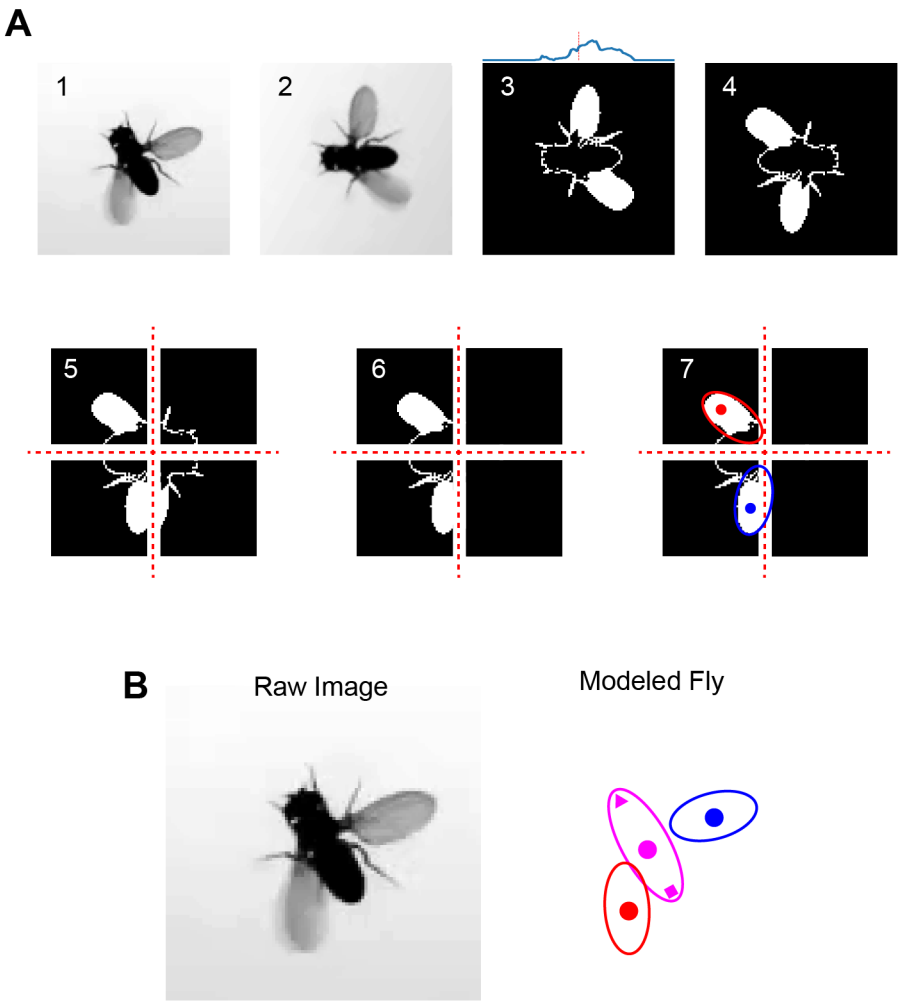

Figure 2.3: **Determining male position during tracking. (A)** Overview of algorithm used to determine male position. (1) Background-subtracted image of male. (2) Image of male rotated such that the male's major axis is aligned with the image's horizontal axis. (3) Binarized image of male with body pixels subtracted. The plot along the top of the image shows the summed pixels along the horizontal axis. Since more pixels were present in the right half of the image, the male is facing towards the left. (4) Same as in (3), except rotated so that the male is facing towards the right. (5) Same as in (4), split into quarters. (6) The right two quarters are excluded from further consideration. (7) Ellipses are fit to the regions containing the greatest number of connected pixels in the top left and bottom left quarters. These are the left (red) and right (blue) wings. **(B)** Raw image and tracked and modeled fly. Ellipse and points shown in pink represent the male's body (triangle: head, circle: centroid, square: rear). Ellipses and points shown in red and blue represent the male's left and right wings, respectively.

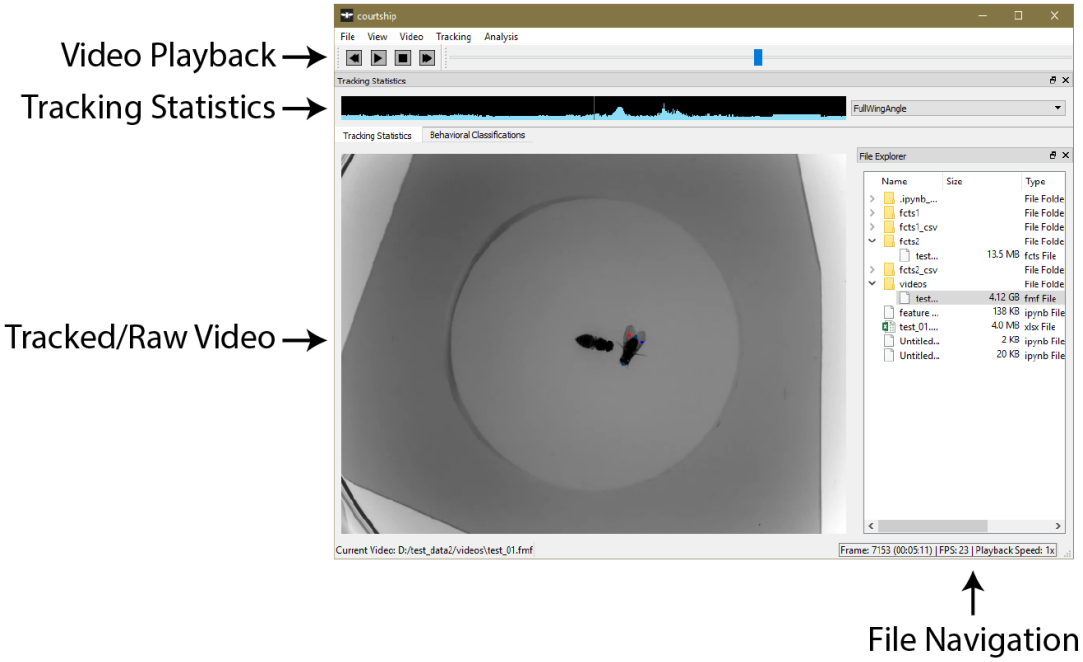

Figure 2.4: **Main graphical user interface (GUI) window.** The main window within the GUI allows a user to load and play through a single tracked or untracked video.

position was the point furthest from the wings. All points that were tracked and modeled on the male fly are shown in Figure 2.3B.

2.2.4 Graphical User Interface

In order to facilitate ease of tracking by users, we designed a custom GUI (Figure 2.4). Within the GUI, a user can load and track either a single or multiple video files. Following tracking, the GUI can be used to visualize the tracked position of the male overlaid on each frame of the video as well as per-frame tracking statistics (see Section 2.2.6) and behavioral classifications for the male fly.

The ability to track multiple videos simultaneously is an important consideration when designing software for experimental biologists. Since user input is required for the appropriate tracking of pairs of courting flies, we designed a “Batch Processing” dialog window,

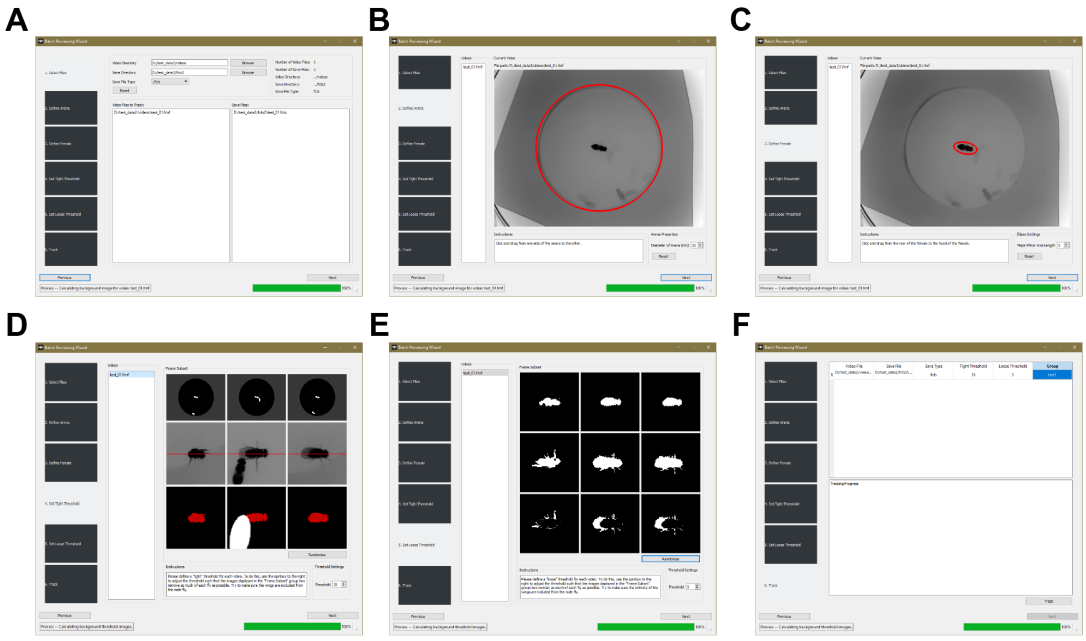

Figure 2.5: **Batch processing dialog windows.** **(A)** The user is prompted to load a batch of video files for tracking and specify their output format and save location. **(B)** The user designates the perimeter of the courtship arena for each video. **(C)** The user designates the ellipse which defines the stationary female for each video. **(D)** The user defines a pixel threshold used to identify the body of the male fly. **(E)** The user defines a pixel threshold used to identify the wings of the male fly. **(F)** The user can assign a group label to each video and then begin tracking. Tracking logs are outputted to the text box on this window.

where the user is able to load and setup tracking parameters for multiple video files (Figure 2.5). For each video, the user is allowed to specify: the save format, the perimeter of the courtship arena, the ellipse which defines the stationary female, a threshold for determining the pixels which represent the male's body, a threshold for determining the pixels which represent the male's wings, and an experimental group label (ie. 'control' or 'experimental') for the courting pair. When all parameters have been set, the user can begin tracking, and tracking will continue until all videos have been processed. The duration of time required to track a single video is approximately equal to the duration of the video.

2.2.5 Tracking Output

Tracked files may be saved as either Microsoft Excel spreadsheets (.xlsx) or as serialized Python objects (.fcts, for Fixed Courtship Tracking Summary). For further analysis in Python, it is recommended to save files in .fcts format; this substantially decreases the load times for importing these files into a Python environment. Nevertheless, both files contain the fields listed in Tables A.1-A.2, and can be loaded and accessed in Python as object attributes.

2.2.6 Python Package and Behavioral Classification

Having access to fly positions over the course of a courtship trial not only allows for the user to calculate simple statistics about spatial locations and movements, but these data can also be used to predict when and where a fly is located when it is engaged in particular behaviors by using classification algorithms. In particular, recent studies have shown that boosted decision trees are especially useful at making accurate predictions from animal tracking data [Branson et al., 2009, Kabra et al., 2013]. Therefore, within the software presented here, we implement boosted decision trees using Scikit-learn [Freund and Schapire, 1997, Pedregosa et al., 2012]. In particular, we built a Python package using Python 2.7 that enables users to input tracking data into this classification algorithm and train and predict the occurrence of specific behaviors within video data. From this classification data, our package also enables users to map flies spatial locations during behavioral occurrences, calculate the relative proportions of time spent within specified behavioral states, and calculate the rates of transitioning between multiple behaviors. A list of the tracking features used to generate specific behavioral classifiers is shown in Table A.3, and the package is freely available, along with documentation and examples at: http://github.com/regginold/drosophila-courtship.

2.3 Results

2.3.1 Male and Female Positions Are Accurately Tracked During Courtship Trials

To ensure that our tracking algorithms were reliable, we video recorded pairs of courting flies and compared tracking results to hand-annotated positions (Figure 2.6). Specifically, we calculated the tracking error as the total distance, in pixels, between the tracked and hand-annotated positions. For males, our tracking software was capable of tracking the body, head, rear, left wing, and right wing positions with mean tracking errors of less than 6 pixels (n=10 randomly selected frames per video, N=5 videos; Figure 2.6A,C), a distance approximately equal to $1/5$ of the body length of the male fly. Similarly, the mean tracking error in determining the body, head, and rear positions of the female was less than 3 pixels (N=5; Figure 2.6B,D). These results suggest that our tracking algorithms work reliably in our experimental setup. Example output from the full courtship trial, along with various statistics calculated from these tracking data, are further shown in Figure 2.7.

2.3.2 Behavioral Classifiers Can Be Used to Accurately Predict Different Courtship Behaviors

We next used our tracking software to track courting flies and classify video frames containing several common non-courtship-specific and courtship-specific behaviors (Figure 2.8). We first built a classifier to detect video frames containing males engaging in any form of body centroid movement, including forwards, backwards, or sideways walking. The mean accuracy of this classifier, validated across 5 videos and 1,742 frames, was 100% (Figure 2.8A), suggesting that non-courtship-specific behaviors could be reliably classified. Next, we generated a classifier to detect video frames containing male flies engaging in any courtship behavior. Surprisingly, this classifier also achieved a very high

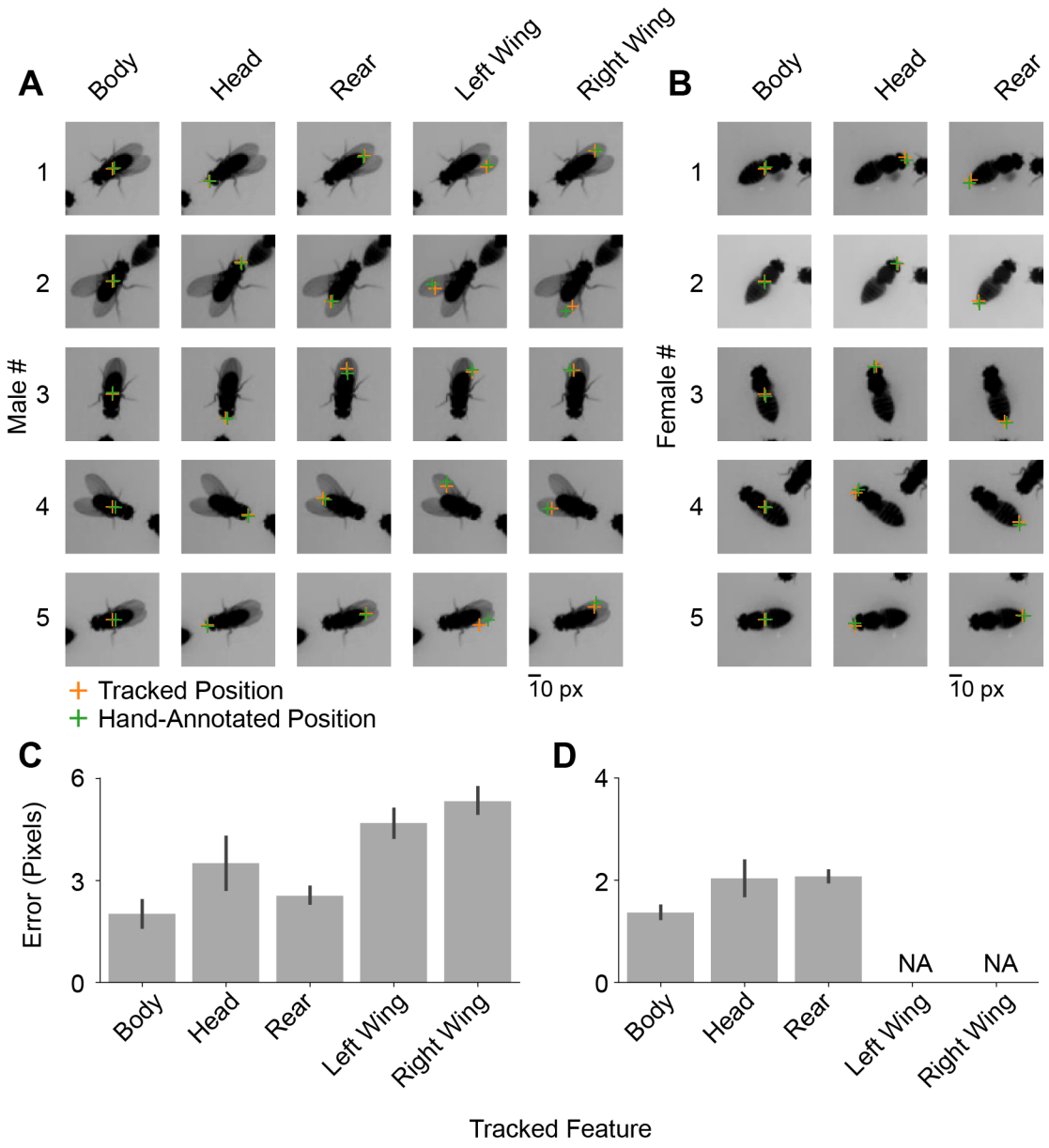

Figure 2.6: **Tracking male and female body position is reliable. (A-B)** Tracked positions of male (A) and female (B) flies are shown along with hand-annotated positions for a single randomly-selected video frame from 5 different videos. **(C)** The mean tracking error for the body, head, rear, left wing, and right wing of male flies was less than 6 pixels (n=10 frames/video, N=5 videos). **(D)** The mean tracking error for the body, head, and rear of female flies was less than 3 pixels (n=1 frame/video, N=5 videos). Error bars represent the standard error around the mean.

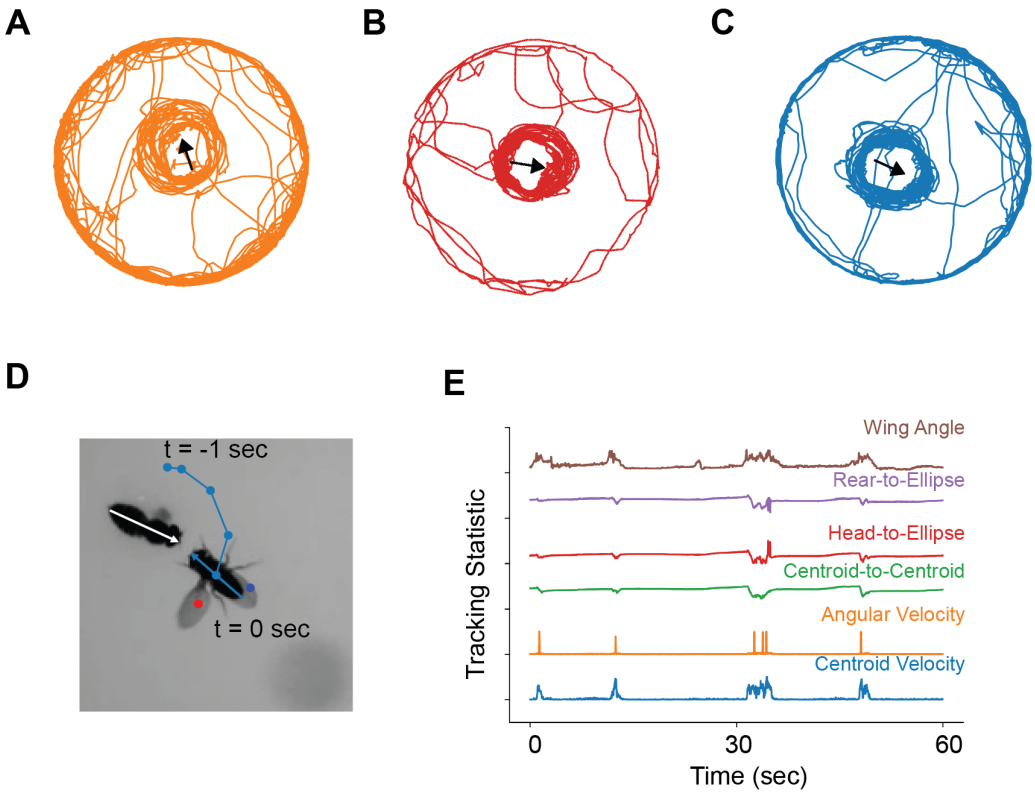

Figure 2.7: **Examples of tracking output.** **(A-C)** Tracked body centroid positions of different males are shown over the course of a 10-minute courtship trial. The position and orientation of each female is shown by an arrow. **(D)** Example of a video frame showing the tracked body centroid position of the male over a 1-second period of the courtship trial (same male as in C). **(E)** Various statistics calculated from tracking data are shown over a 60-second period (same male as in C).

accuracy (mean accuracy validated across 5 videos and 4,238 frames: 99.3% Figure 2.8A), suggesting that classifiers could be generated which detected not only single behaviors, but groups of behaviors. Finally, we generated two classifiers to detect individual courtship behaviors, including touching and singing. We defined touching to include any frame where the male was close enough to reach out and physically contact the female with any part of his body, including his forelegs or proboscis. This classifier was capable of correctly classifying video frames with a mean accuracy of 95.4%, a false negative rate (FNR) of 1.1%, and a false positive rate of 3.5% (cross validated against 5 videos including 2,596 frames, Figure 2.8A,B,D). We next defined singing as any behavior where the male was extending and vibrating either wing and made a behavioral classifier to identify video frames containing singing males. This singing classifier was again capable of classifying video frames with high accuracies (accuracy: 91.2%, FNR: 3.5%, FPR: 5.9%; Figure 2.8A,C,E). These results suggest that our software can be used to generate accurate and predictive classifiers to identify video frames containing many different behaviors of interest.

To ensure that our classifiers were utilizing appropriate tracked features to classify behaviors, and were not fixed on features that were predictive but irrelevant to the behavior, we examined the feature importance of touching and singing classifiers. Feature importance is proportional to the weight that each classifier attributes to a specific feature when making a prediction [van der Walt et al., 2014]. Whereas the touching classifier was heavily reliant on tracked features that included some transformation of the distance between the male and female (Figure 2.8B), the singing classifier was more reliant on features that monitored the intra-wing distances or minor axis length of the male fly (Figure 2.8C). These data suggest that our software generates behavioral classifiers that are both highly accurate and which predict behaviors based on relevant tracking statistics.

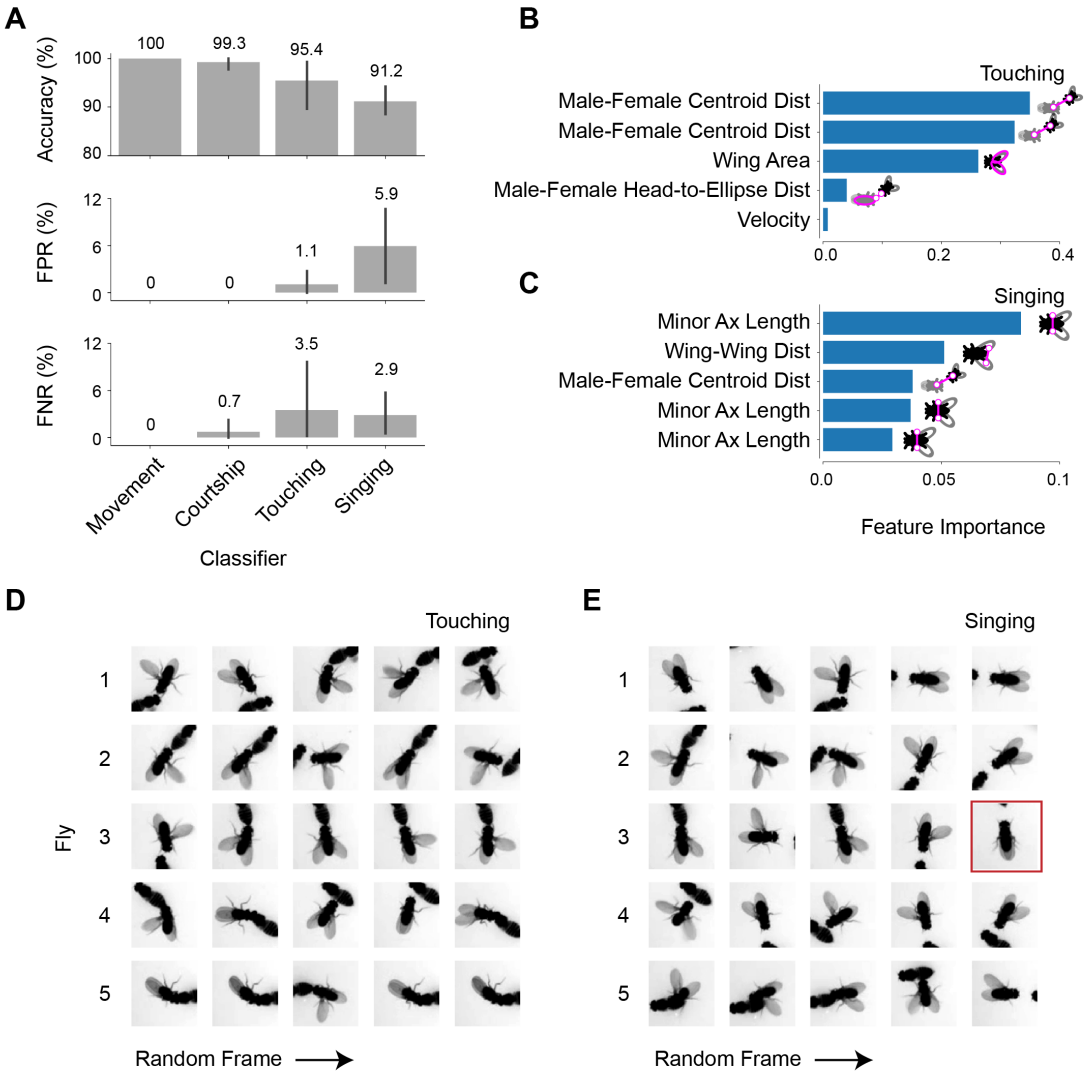

Figure 2.8: **Behavioral classifiers can be used to predict different courtship behaviors. (A)** Classifier accuracy (top), false positive rates (FPR, middle), and false negative rates (FNR, bottom) are shown for movement, courtship, touching, and singing classifiers. Bar heights represent the mean classifier accuracy across 5 different videos; error bars represent standard error around the mean (SEM). **(B-C)** Feature importance for the touching (B) and singing (C) classifiers. Features listed to the left of each plot indicate that some transformation of the specified feature was important for classifier prediction. Note that the x-axis is an arbitrary scale showing the relative importance of each feature, and all feature importance sum to 1. **(D)** Random video frames from 5 flies showing positively classified video frames containing touching. **(E)** Random video frames from 5 flies showing positively classified video frames containing singing. The image bordered in red was mis-classified.

2.4 Discussion

Previous studies that have utilized courtship as an assay for investigations into the genetics or neural circuits involved in regulating social behaviors have often examined simple temporal characteristics of the courtship ritual, such as the CI and CL. Here, we have developed quantitative tools necessary for describing the courtship ritual in a much more rich and detailed manner, which allows for the mapping of both the spatial distributions and temporal inter-relationships between courtship behaviors. Along with developing a graphical user interface to allow users to easily track many videos of pairs of courting flies, we have also built a Python package to allow for users to easily classify behaviors and analyze their tracking results. Together, these tools should enable researchers to investigate the mechanisms underlying more complex forms of social interaction.

Chapter 3: Visual Cues Regulate Spatiotemporal Courtship Decisions in *Drosophila*

Like many other mating behaviors, the courtship ritual exhibited by male *Drosophila* in response to the presence of a virgin female is comprised of temporal and spatial sequences of stereotypic innate behavioral elements. Yet, the specific signals and neural circuits that determine when and where behavioral elements are released by males during courtship are not well understood. Consequently, we investigated the role of visual object recognition in the selection of specific mating behaviors by males during bouts of courtship. By using novel computer vision and machine learning based approaches for high resolution analyses of the male courtship ritual, we show that the release of distinct elements of the male courtship ritual occurs at stereotyped locations around the female and depends on the ability of males to recognize visual landmarks present on the female. Specifically, we show that independent of target motion, males utilize several populations of visual projection neurons to recognize the location of females' eyes, which is essential for the release of courtship behaviors at appropriate spatial locations. Together, these results provide a mechanistic explanation for how relatively simple visual cues could play a role in driving both spatially- and temporally-complex social interactions.

3.1 Introduction

Courtship and other social interactions between conspecifics often depend on ritualistic spatio-temporal transitions between distinct innate behavioral elements [Markow and Hanson, 1981, Krstic et al., 2009]. Yet, the specific sensory stimuli and neuronal circuits that drive the spatial and temporal aspects of social behaviors remain unknown for most species. During courtship behaviors, many animals rely on the visual system to identify salient patterns, colors, or motion cues that promote (or inhibit) copulation [Elias et al.,

2012, Irestedt et al., 2009]. In insects, motion cues have been shown to be particularly important for male chase behaviors during courtship [Boeddeker et al., 2003, Cook, 1979, 1980, Agrawal et al., 2014, Kohatsu and Yamamoto, 2015]. These motion cues are detected and processed by visual projection neurons in the brain, which connect to downstream motor centers to generate relevant behavioral outputs [Wu et al., 2016, Sen et al., 2017, Ribeiro et al., 2018]. While motion cues are important for keeping a male close to a moving female during courtship, how specific visual cues and neural pathways might regulate the proper spatio-temporal coordination of other mating displays remains largely unknown.

In the fruit fly *Drosophila* melanogaster, the copulation success of males depends on a pre-mating courtship ritual that consists of a sequence of stereotyped behavioral elements including chasing, orienting, singing, scissoring, tapping, licking, and attempted copulation [Greenspan and Ferveur, 2000, Sokolowski, 2001, 2010]. Although different courtship elements are somewhat independent of one another, there is a strong temporal inter-relationship between each of these behaviors, where the probability of transitioning from one behavior to another is relatively fixed [Markow and Hanson, 1981]. However, sensory deficits can lead to alterations in these transitions and can also have an effect on both courtship latency and intensity [Markow, 1987, Wilhelm and Doschek, 1979, Krstic et al., 2009]. Similarly, male mating behaviors include important spatial components which support successful copulation, including extension of the wing nearest the female's body to allow auditory cues to be heard more clearly [Markow, 1987, Kohatsu and Yamamoto, 2015, Pan et al., 2012]. However, the specific sensory cues that drive the appropriate spatial and temporal transitions between individual elements of the male courtship ritual are not well understood.

Previous work has suggested that visual recognition of female motion is sufficient to trigger male courtship and that males use motion cues to orient towards and chase their

target females [Kohatsu and Yamamoto, 2015, Ribeiro et al., 2018, Cook, 1979, 1980, Agrawal et al., 2014]. Recently, a subset of visual projection neurons in the Lobula Column (LC) of the male brain was shown to be tuned to female-like movements and specifically required for the proper orientation of a male towards a female during courtship [Ribeiro et al., 2018]. However, which and how other motion-independent visual cues contribute to male courtship remains mostly unknown.

Here we investigate the visual features and neural circuits that regulate both spatial and temporal components of the courtship ritual in *Drosophila* males. By using computer vision- and machine learning-based analyses of male courtship behaviors towards motion-less female targets, we demonstrate that the timing and positioning of males during specific courtship elements depends on visual signal processing. Specifically, we show that males use the eyes of their courtship targets as a visual guide to release bouts of tapping, scissoring, and orienting at appropriate times and spatial locations surrounding the female. Further, we find that the spatial positioning of the male depends on the activity of several classes of LC neurons in the visual system. Together, these data suggest that *Drosophila* males use specific visual features present on the female's body to regulate appropriate spatio-temporal distributions of courtship behavioral elements.

3.2 Methods

3.2.1 Flies

Animals were housed at 25 ^{o}C and 70% humidity under a 12h:12h light:dark cycle, and reared on a corn-meal based food (Archon Scientific). All flies used in this study are available from Bloomington *Drosophila* Stock Center (BDSC) (see Table 3.1).

Canton-S male and female flies were used for courtship experiments under white and red

BDSC #	Description	Reference	Figure(s)
NA	Canton-S (CS)	NA	3.1-3.12
NA	CS; w^{1118} (wCS)	NA	3.5, 3.8
68259	LC4	Wu et al. [2016]	3.10-3.12
68342	LC9	Wu et al. [2016]	3.10-3.12
68337	LC10-1	Wu et al. [2016]	3.10-3.12
68331	LC16	Wu et al. [2016]	3.10-3.12
68356	LC17	Wu et al. [2016]	3.10-3.12
28996	UAS-TNT^{-}	Sweeney et al. [1995]	3.10-3.12
28841	UAS-TNT^{+}	Sweeney et al. [1995]	3.10-3.12

Table 3.1: **Fly lines used in chapter 3.**

light (Figures 3.1-3.4) and for decapitation and head-transplantation experiments (Figure 3.5A-J). White-eyed females were derived from w^{1118} flies that had been back-crossed into Canton-S for at least 6 generations, and these flies, along with their red-eyed Canton-S counterparts, were used as courtship targets in the red- versus white-eyed experiments (Figure 3.5K-O). Canton-S females were used as courtship targets in the LC-inactivation experiments (Figures 3.10-3.12), and males were derived from crosses between each LC-GAL4 line (LC4, BL68259; LC9, BL68342; LC10-1, BL68337; LC16, BL68331; LC17, BL68356) and flies containing either the active (UAS-TNT^{+}, BL28996) or inactive (UAS-TNT^{-}, BL28841) version of the Tetanus Toxin gene [Wu et al., 2016, Sweeney et al., 1995].

3.2.2 Courtship Assay

All courtship trials were conducted at Zeitgeber Time (ZT) 1–5, using 4–6 day old virgin male and female flies. Both males and females were collected immediately following eclosion and moved into 25 mL plastic vials containing corn-meal-based food. Both males and females were kept in single-sex groups of 10–12 for two days, at which time individual males were moved into 5 mL glass vials containing a small amount of fly food and isolated for at least two additional days before testing. On test day, legs and wings were surgically removed from each female target, which was subsequently adhered to a rectangular piece

of plastic weigh-boat (approx. 30mm x 30mm) using UV-hardening glue (RapidFix). A circular courtship arena (approx. 23mm diameter x 6mm height) was placed over the fixed female, and males were aspirated into the chamber and allowed to freely court the female for 10 minutes. The orientation of the antero-posterior body axis of each target female was random across trials.

3.2.3 Video Recordings

Videos were recorded on a Raspberry Pi NoIR camera with a Navitar 8–48 mm lens for 10 minutes at 24 frames per second and were backlit using LEDs. To record under red-light conditions, LEDs were covered with long-pass, red filters (Neewer).

3.2.4 Tracking and Behavioral Classification

All videos were analyzed on a per-frame basis using custom software that tracks body and wing positions of courting flies and subsequently classifies whether or not a male was engaging in a particular behavior (see Chapter 2). Three classifiers were created for identifying frames that contained males engaging in bouts of (1) tapping or touching, (2) stationary orienting, and (3) stationary scissoring/wing extensions. For each frame, several features were calculated from tracking data for use in an AdaBoost decision tree classifier (see Table 3.2). These features were selected based on both previous studies and empirical classifier cross-validation which yielded greater accuracies [Freund and Schapire, 1997, Branson et al., 2009, Kabra et al., 2013].

Classifiers were created for each experiment by hand-scoring a subset of frames from at least 4 videos containing control males and 4 videos containing experimental males. All classifiers had accuracies $>$95% (see Table 3.3-3.4). To further improve classification accuracies, all videos were hand-scored for bouts of courtship, and any positive behavioral

Tap	Ori	Sci	Feature	Description	units
		✓	θ_{wings}	Angle between $C_{LW} > C_{body} > C_{RW}$	rad
		✓	θ_{LW}	Angle between $C_{LW} > C_{body} >$ x-axis	rad
		✓	θ_{RW}	Angle between $C_{RW} > C_{body} >$ x-axis	rad
		✓	A_{LW}	Area of left wing	mm^2
		✓	A_{RW}	Area of right wing	mm^2
		✓	D_{wing}	Total distance between C_{LW}, C_{body}, C_{RW}	mm
✓	✓	✓	D_{CC}	Male-to-female distance (centroid)	mm
✓	✓	✓	D_{HE}	Male-head to female-ellipse distance	mm
✓	✓	✓	D_{RE}	Male-rear to female-ellipse distance	mm
✓	✓	✓	ΔD	$D_{RE} - D_{HE}$	mm
✓	✓	✓	Θ_{Rel}	Relative heading of male w.r.t female	rad
✓	✓	✓	$\lvert\Theta_{Rel}\rvert$	Absolute value of Θ_{Rel}	rad
✓	✓	✓	v_Θ	Angular velocity of male	rad/sec
✓	✓	✓	$\lvert v_\Theta\rvert$	Absolute value of v_Θ	rad/sec
✓	✓	✓	$\lvert v_C\rvert$	Velocity of male centroid	mm/sec
✓	✓	✓	L_{maj}	Maj. axis length of male ellipse	mm
✓	✓	✓	L_{min}	Min. axis length of male ellipse	mm
✓	✓	✓	A	Area of male ellipse	mm^2
✓	✓	✓	Θ	Angle of male ellipse w.r.t. x-axis	rad
✓	✓	✓	D_{CE}	Male-centroid to arena edge distance	mm

Table 3.2: **Features used to generate behavioral classifiers.** First and second derivatives, as well as windowed statistics, were calculated for all features. Abbreviations are as follows: C_{LW}, centroid of male fly's left wing; C_{RW}, centroid of male fly's right wing; C_{body}, centroid of male fly's body. Windowed statistics, are shown in Table A.4 and were also calculated for all features listed in this table.

Classifier	N_{videos} Scored	N_{frames} Scored		Cross Validation		
		+	-	Acc (%)	FPR (%)	FNR (%)
Tap	8	1137	1431	95.92 ± 1.14	2.21 ± 0.74	1.86 ± 0.74
Ori	8	4243	4412	97.59 ± 1.57	0.62 ± 0.58	1.79 ± 1.55
Sci	8	4277	5248	98.18 ± 1.03	1.37 ± 0.95	0.46 ± 0.18

Table 3.3: **Behavioral classifier cross-validations.** Leave-one-out cross validation was used to determine classifier accuracies, false positive rates (FPRs), and false negative rates (FNRs), as well as standard errors around the mean ($\pm$ SEM) for each of the behavioral classifiers.

Classifier	Acc (%)	FPR (%)	FNR (%)
Tap	99	0.763	0.211
Ori	99.4	0.128	0.507
Sci	98.9	0.696	0.434

Table 3.4: **Behavioral classifier testing.** Each classifier was tested on 17,000 hand-scored frames from a single video which was not included in each classifier's training data set.

classifications falling outside of courtship were discarded.

Each of the individual courtship behaviors we classified were defined to be mutually exclusive of one another. We specified a behavioral hierarchy whereby tapping/touching took the highest precedence, followed by scissoring/wing extensions, and then orienting. If a video frame contained multiple behavioral classifications, we used the behavioral hierarchy to determine which behavior to retain and eliminated all other classifications from that frame. This was done to eliminate the strong overlap between bouts of scissoring and orienting and allowed for us to more easily determine when a fly transitioned from one behavior to another. Further, this let us calculate pertinent spatial correlations between behaviors (see Figure 3.2).

3.2.5 Data Analysis

Prior to each analysis, the orientation of the female in the courtship arena (along with all tracking data) was rotated such that the females antero-posterior body axis was aligned

along the x-axis, with the head centered at 0 radians and facing to the right (as shown in Figure 3.1A-B).

Courtship Path. The courtship path of each male was calculated by dividing the angular space surrounding the female into 50 bins and taking the mean centroid-to-centroid distance between the male and female during bouts of courtship. For some experiments, both control and experimental males attempted to copulate with the female for extended periods of time. While these males were not physically able to copulate since the female was fixed in place, these long durations of minimal movement had a significant effect on the courtship path, and for our purposes, represented bouts of copulation; they were therefore removed from all analyses.

Anterior-Posterior Distance Ratio (D_A/D_P). The D_A/D_P ratio was calculated as the ratio of the maximum courtship path when the male was on the front half of the female ($-\pi/2 < \theta_{male} < \pi/2$) to when the male was on the rear half of the female ($\theta_{male} < -\pi/2$ or $\theta_{male} > \pi/2$).

Angular Locations of Courtship Elements. The mean angular position of the male with respect to the female was calculated across all frames containing positive classifications for each behavior of interest. Rayleigh values (represented as arrow length in circular plots) were calculated for populations of males.

Bimodal Rayleigh Test. Raw angular distributions were first compared to uniformity using the Rayleigh test. If no significant difference was found, we then tested for bimodality as follows. Angular distributions were transformed using the following equation, as in [Landler et al., 2018]: $\theta = 2t \mod 2\pi$, where t are the original angles and θ are the transformed angles. This distribution was subsequently compared to the uniform distribution using a Rayleigh Test.

Courtship Latency and Index. The courtship index was calculated as the total fraction of time a male spent courting a female from the first occurrence of any courtship element until the end of the 10-minute trial ($t_{courting}/(t_{end-trial} - t_{start-courtship})$). The courtship latency was calculated as the time taken until the first occurrence of courtship during the trial.

Behavioral Indexes. Behavioral indexes were calculated for each of the classified behavioral states. These indexes represent the fraction of time a male spent in a particular behavioral state with respect to the duration of time the male spent courting ($t_{in-state}/t_{courting}$).

Behavioral Transitions. The frequency of transitioning from one behavior to another was calculated by taking the number of transitions between each behavior over the total number of behavioral transitions ($n_{b1\to b2}/n_{total}$, $n_{b2\to b3}/n_{total}$, etc.).

All software and scripts used for tracking, classification, and data analysis were written in Python and are freely available at www.github.com/regginold/drosophila-courtship.

3.3 Results

3.3.1 Male Courtship Behaviors Occur at Stereotyped Locations Around the Female

Female motion is an important visual cue which male flies use to initiate and direct chase behaviors during bouts of courtship [Agrawal et al., 2014, Cook, 1979]. However, whether other visual cues also play a role in regulating spatial or temporal aspects of courtship elements is mostly unknown. Therefore, here we hypothesized that in addition to responding to female motion, males also use visual features present on the female's body to direct courtship elements at distinct spatial locations. To separate the effects of female body

morphology from motion on the spatial positioning of the male during courtship, we developed a simplified courtship paradigm which eliminates female motion-related visual cues and used custom tracking and behavioral classification software to determine the spatial localization of males during specific elements of the courtship ritual (see Section 3.2.4; Figure 3.1A).

Using this assay, we first characterized the spatial aspects of male courtship behaviors in wild-type Canton-S males. We found that males take an asymmetric and stereotyped path around the female during courtship whereby they position themselves $\sim$1.5 times further away from the female's head than her abdomen ($p < 0.001$, 1-Sample T-Test; Figures 3.1B-C). We further trained and used classifiers to identify video frames containing males engaging in three easily-recognizable courtship behaviors: (1) tapping or touching, (2) orienting, and (3) scissoring or wing extension (Figure 3.2A-E). In our paradigm, these behaviors accounted for $\sim$95% of the time that males were actively courting (Figure 3.2F). Spatial analyses of these three courtship elements indicated that bouts of tapping largely occurred when the male was on the posterior half of the female, whereas bouts of orienting and scissoring occurred when the male was on the anterior half of the female (Figure 3.1D). Accordingly, tapping positions were largely anti-correlated with scissoring and orienting positions, whereas orienting and scissoring positions were highly correlated with one another (Figure 3.2H-I). This was likely the result of a high frequency of transitions between orienting and scissoring bouts (Figure 3.2G), often with little to no male movement occurring during transitions between these two courtship elements.

3.3.2 Visual Inputs Are Required for Stereotyped Behavioral Positioning During Courtship

We next sought to determine whether vision was driving the differential spatial positioning of males during specific courtship elements by comparing males courting females under

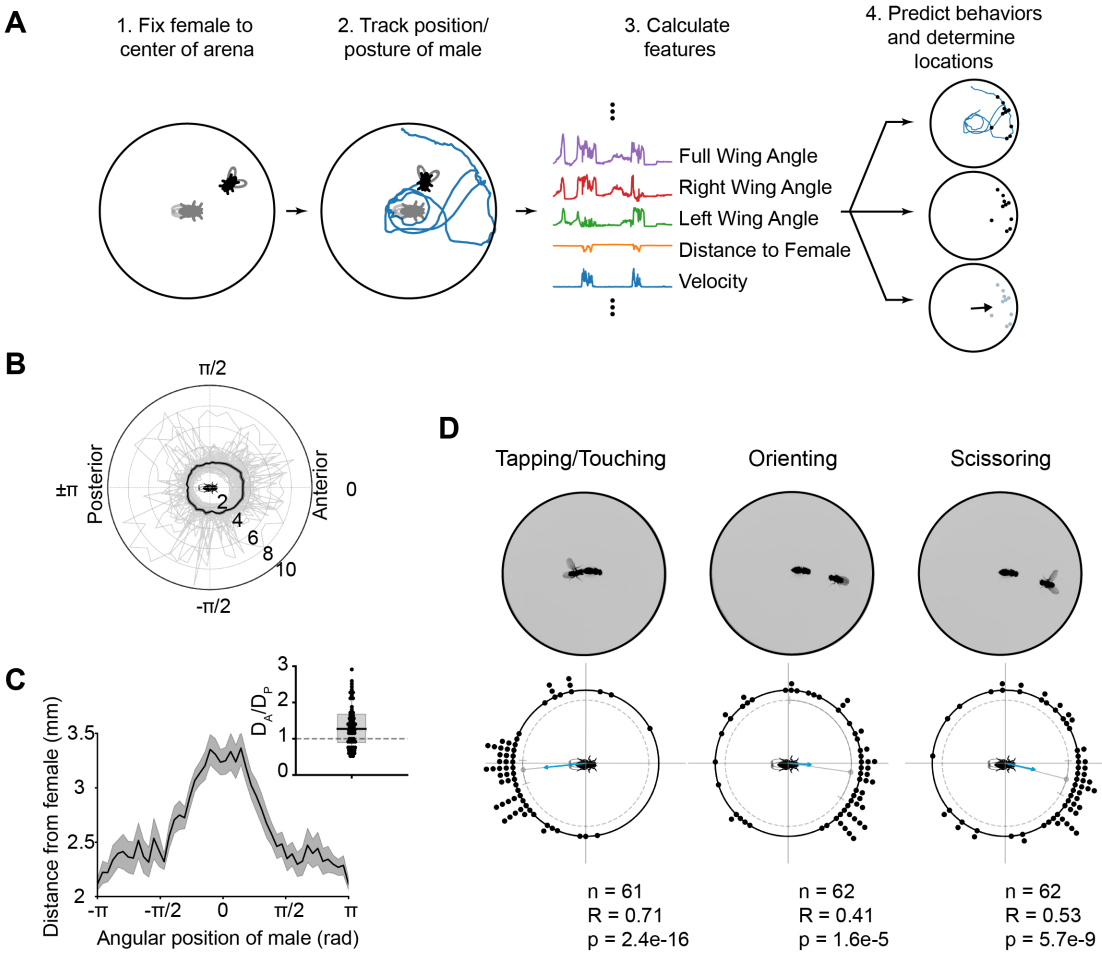

Figure 3.1: **Male courtship behaviors occur at stereotyped locations around the female. (A)** Overview of algorithm used to determine locations of male mating behaviors during courtship: (1) a female is first fixed to the center of a courtship arena, and then a male is introduced and allowed to court the female for 10 minutes; (2) the male is tracked; (3) tracked features are used in a boosted decision tree classifier to predict frames containing a behavior of interest; (4) the position of the male in positively-classified frames is determined, and the mean behavioral position over the trial is recorded. **(B)** The average courtship path of Canton-S males (n=62) over the course of a courtship trial. Each thin gray line represents the average path of an individual male. The thick black line represents the mean of all males. Note that for each behavioral trial, all male tracks have been rotated with respect to the female such that the females anterior-posterior axis is aligned along the horizontal with the anterior end near 0 and the posterior end near $\pm\theta$ rad. **(C)** The mean courtship path (same as in B) of Canton-S males, shown in Cartesian coordinates. (Inset) The ratio of the maximum male-female distance when the male is on the anterior half of the female (D_A) to when the male is on the posterior half of the female (D_P). Note that this is significantly greater than 1 ($p < 0.001$, 1-Sample T-Test). Caption continued on next page.

Figure 3.1: **(D)** Examples of individual frames containing positively-classified behaviors are shown above mean angular locations, across flies, for each behavior. Each black point represents the mean behavioral location of an individual fly, and the direction of the arrow represents the mean behavioral location of all flies. The length of the arrow is proportional to the Rayleigh R-value for the total population of flies. The median and 95% confidence intervals surrounding the median are shown as a gray point and lines just beneath the points representing the individual flies.

either red light (limited vision) or white light (intact vision; Figures 3.3-3.4). We found that in contrast to white light conditions, males courting under red light positioned themselves more distant from the posterior end of females ($p < 0.001$, 1-Sample T-Test; Figure 3.3A-C), tapped females on both the posterior and anterior ends ($p < 0.001$, Bimodal Rayleigh Test; Figure 3.3D), and oriented towards the posterior end of females ($p < 0.05$, Rayleigh Test; Figure 3.3D). Similar to tapping, males courting under red light also showed a bimodal distribution in their scissoring locations ($p < 0.05$ Bimodal Rayleigh Test; Figure 3.3D). Further, we found that although red light conditions reduced the overall courtship index of males (Figure 3.4D), the relative time spent tapping was increased, scissoring was decreased, and orienting remained constant (Figure 3.4E). Consistent with these results, under red light conditions, the frequency of transitioning from orienting to tapping increased whereas orienting to scissoring decreased (Figure 3.4F-H). These data suggest that although vision is not required for courtship in general, nor for the release of any of its individual behavioral elements, visual cues provide important sensory input for directing spatiotemporal courtship displays. Furthermore, males seem to have the remarkable ability to compensate for the loss of visual sensory information by increasing chemo- and/or tactile sensory inputs via increased physical contact through tapping.

3.3.3 The Eyes of the Female Are Used as a Visual Marker for Directing Male Courtship Behaviors

Having established that vision plays an important role in regulating the spatiotemporal patterns of male courtship, we next asked which specific morphological features of the

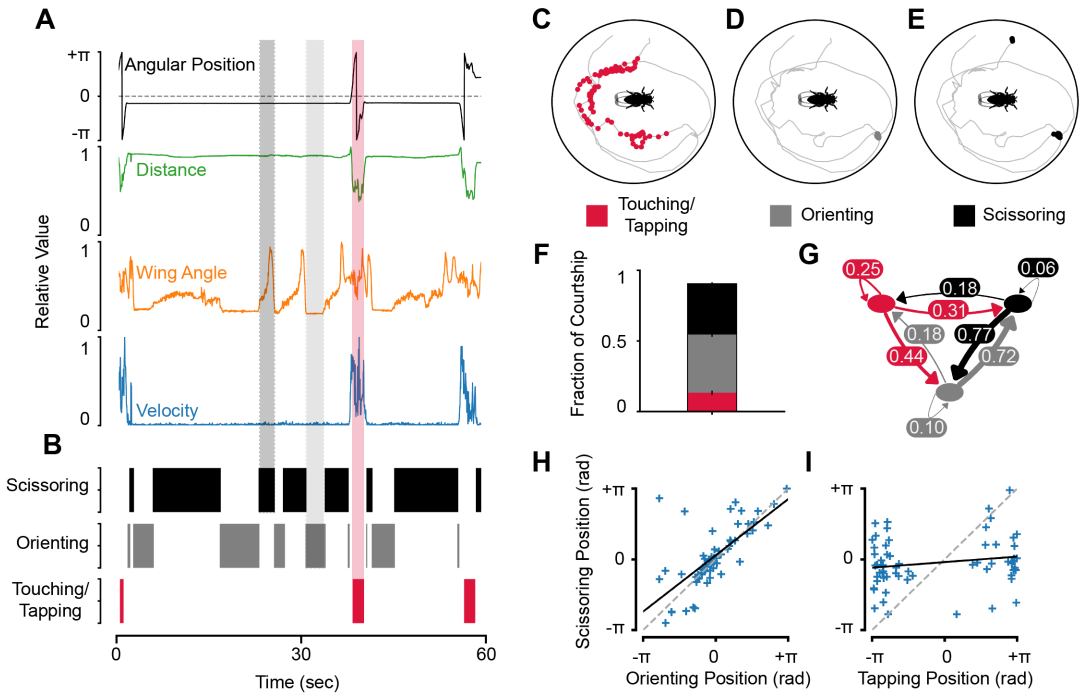

Figure 3.2: **Relationships between individual courtship elements.** **(A)** Examples of some of the important features extracted from tracking data. **(B)** Frames classified as Scissoring, Orienting, or Touching/Tapping are shown for an individual male over the course of 1 minute. Behavioral epochs classified as Scissoring are associated with large increases in the angle defined by the males left wing, right wing, and body centroid as well as low velocities. Those classified as Orienting are associated with no changes in the wing angle and low velocities. And those classified as Tapping/Touching are associated with decreased distances between the male and female. **(C-E)** Locations of the male during each of the behavioral epochs from (A-B) are shown along with the track (gray line) produced by the male during the 1 minute segment of courtship. **(F)** Each of the three classified behaviors account for 95% of the behaviors occurring during the courtship ritual. The remaining time is largely spent transitioning between behaviors. **(G)** Transitions between each of the three classified behaviors. **(H)** Mean Scissoring and Orienting positions are highly correlated with one another. **(I)** Mean Scissoring and Tapping positions are highly anti-correlated with one another.

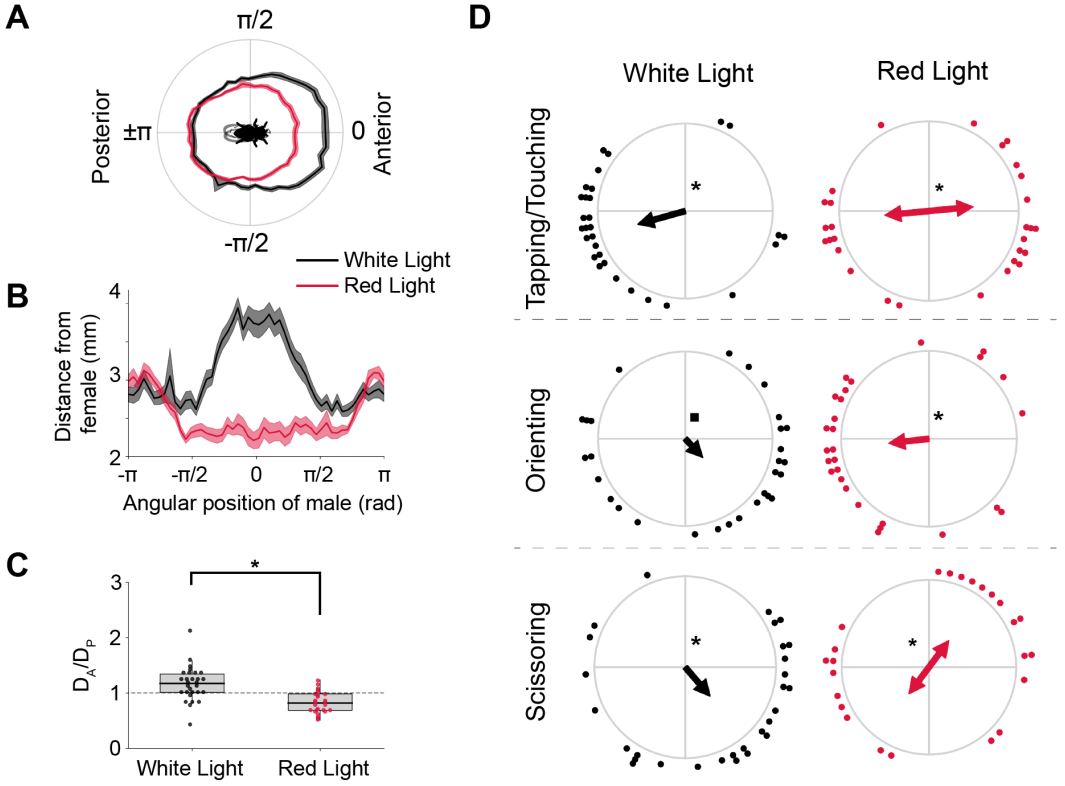

Figure 3.3: **Spatially-stereotyped courtship elements depend on vision. (A)** Average courtship path for Canton-S males that were allowed to court under either white- (black line) or red-light (red line) (n=32/group). **(B)** Same as (A), shown in Cartesian coordinates. **(C)** Maximum distance ratio of male on anterior versus posterior end of female. Males allowed to court under white light had a $D_A/D_P > 1$ ($p < 0.001$, 1-Sample T-Test), whereas males courting under red light had a $D_A/D_P < 1$ ($p < 0.001$, 1-Sample T-Test). **(D)** Average angular positions of males during individual courtship behaviors under either white- or red-light. Under white-light, males positioned themselves to the posterior side of the female during bouts of Tapping/Touching ($p < 10^{-5}$, Rayleigh Test), whereas they positioned themselves to the anterior side of the female during bouts of either Orienting or Scissoring (Orienting: $p = 0.08$; Scissoring: $p < 0.01$; Rayleigh Test). Males courting under red light displayed Tapping and Scissoring behaviors which were bimodally distributed along the anterior-posterior axis of the female ($p < 0.001$ for Tapping/Touching and $p < 0.05$ for Scissoring; Bimodal Rayleigh Test). Additionally, these males oriented towards the female while on her posterior half ($p < 0.01$; Rayleigh Test). Note that the female is oriented as in (A).

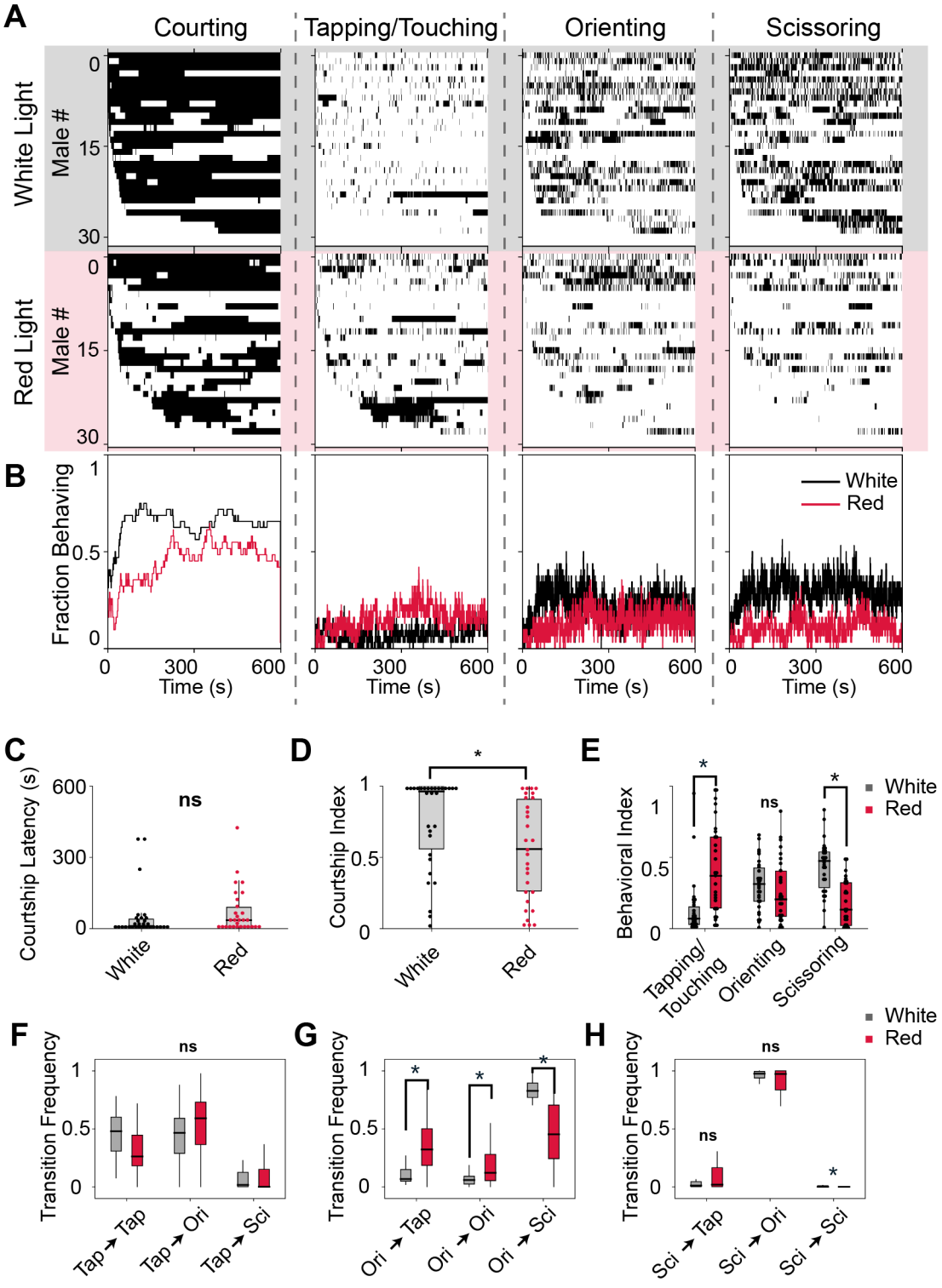

Figure 3.4: **Overall courtship drive and the relative frequencies of individual courtship elements depend on visual inputs.** Caption on next page.

Figure 3.4: **(A)** Behavioral ethograms are shown for Courtship, Tapping/Touching, Orienting, and Scissoring. Each row represents a courtship trial for one male; areas of black represent frames where the male was engaging in the specified behavior. **(B)** Total fractions of males engaging in each behavior over time. **(C-D)** Males courting in red light take longer to start courting females (C, $p < 0.05$, Kruskal Test) and court for shorter periods of time (D, $p < 0.01$, Kruskal Test). **(E)** Behavioral indices are shown for each of the classified behaviors as a fraction of total courtship. Males courting in red light had greater levels of tapping ($p < 0.001$, Kruskal Test) and lower levels of Scissoring ($p < 0.001$, Kruskal Test) than males courting in white light. **(F-H)** Transitions between individual courtship behaviors. Behavioral transitions from Orienting to all other behavioral states are significantly different between males courting in either white or red light ($p < 0.001$, Kruskal Test).

female body might serve to visually guide males during courtship. We hypothesized that anatomical features with high visual contrast could serve as salient spatial landmarks to delineate the body axis and orientation of courted females. Specifically, because the red-pigmented eyes of flies are highly contrasted with the lighter-colored cuticle, we hypothesized that they could serve as a robust visual marker for the antero-posterior body axis of courted females.

To test this hypothesis, we first asked whether the head of females is necessary for regulating any spatial aspects of the male courtship ritual (Figure 3.5A-E and Figure 3.6). We found that when courting headless females, male courtship paths were symmetric and equidistant from either end of the antero-posterior body axis of females (Figure 3.5A-D), and the mean angular positions of tapping, orienting, and scissoring behaviors were either bimodally or uniformly distributed around the female ($p < 0.05$ for tapping, Bimodal Rayleigh Test; $p > 0.05$ for orienting and scissoring, Rayleigh Test; Figure 3.5E). While the overall courtship latencies and indices were unaffected for males courting headless females (Figure 3.6A-D), these males exhibited a decreased scissoring frequency, suggesting that the female head is particularly important for visually triggering for the release of this specific courtship element ($p < 0.05$, Kruskal Test; Figure 3.6E-H).

Next, to determine whether visual cues associated with the female head are sufficient for

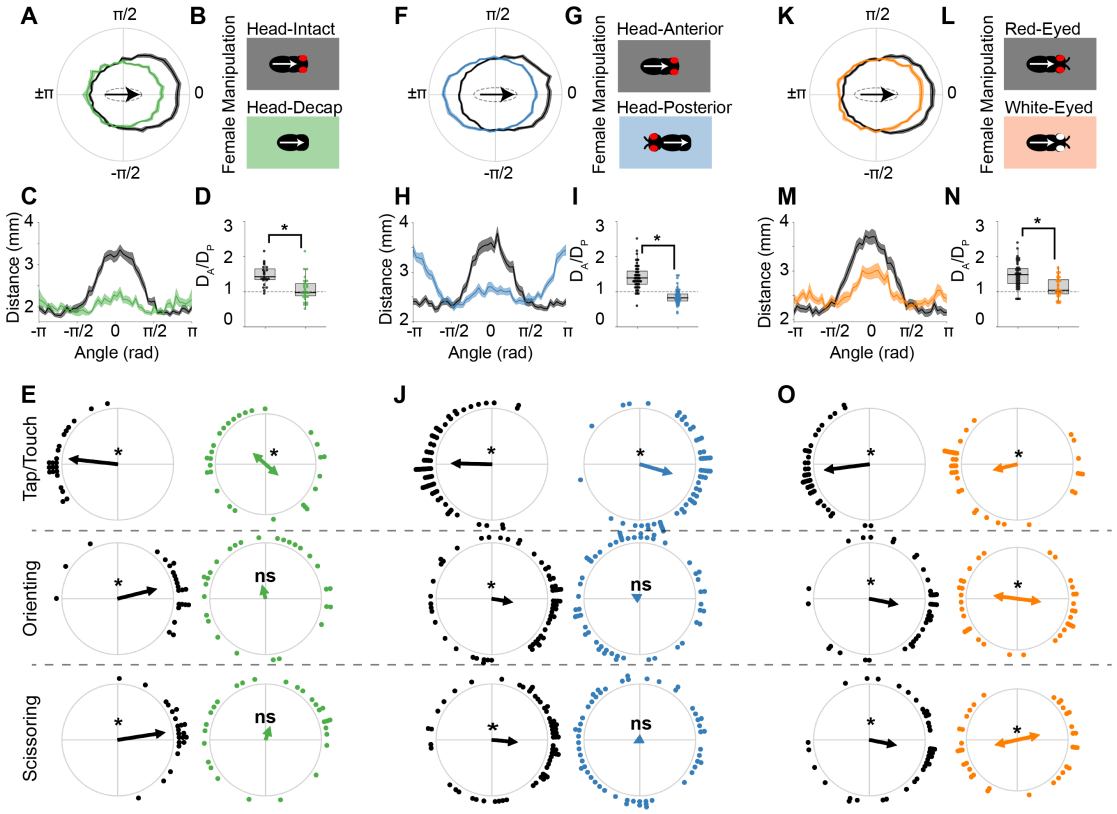

Figure 3.5: **The female's head and eye coloration are important visual features for proper male positioning during courtship. (A)** Average courtship paths of males courting either intact females ("Head-Intact", n=32, black line), or females that had been decapitated ("Head-Decap", n=32, green line). **(B)** Manipulations for intact and decapitated females. Arrows show the anterior-posterior axis of the female as it has been plotted in (A). **(C)** Average courtship paths of males courting either intact or decapitated females (same as in A), shown in Cartesian coordinates. **(D)** Maximum distance ratio of male on the anterior (D_A) versus posterior (D_P) end of the female. Males courting intact females positioned themselves significantly further from the females anterior end versus their posterior end ($p < 10^{-5}$, 1-Sample T-Test). However, males courting decapitated females did not position themselves significantly further when on either side of the female ($p > 0.1$, 1-Sample T-Test). Thus, males courting intact females had a significantly greater D_A/D_P ratio than males courting decapitated females ($p < 10^{-4}$, One-way ANOVA). **(E)** Behavioral locations of males courting either intact or decapitated females (asterisks denote significance at $p < 0.05$, Rayleigh Test or Bimodal Rayleigh Test). Note that females are oriented as in (A). **(F)** Average courtship paths of males courting either intact females ("Anterior", n=64, black line), or females that had their heads transplanted to their posterior end ("Posterior", n=63, blue line). **(G)** Female manipulations of either the "Anterior" or "Posterior" group. Note that arrows are the same as in B. Caption continued on next page.

Figure 3.5: **(H)** Average courtship path of males courting either "Anterior" or "Posterior" females (same as in F), shown in Cartesian coordinates. **(I)** D_A/D_P ratio for males courting either Head-Anterior ("Anterior") or Head-Posterior ("Posterior") females. "Anterior" males positioned themselves significantly further from the females anterior rather than posterior end ($p < 10^{-5}$, 1-Sample T-Test), whereas "Posterior" males positioned themselves significantly more distant from the females posterior rather than anterior end ($p < 0.01$, 1-Sample T-Test). **(J)** Behavioral locations of males courting either "Anterior" or "Posterior" females (asterisks same as in E). Note that females are oriented as in (F). **(K)** Average courtship path of males courting either females with red eyes ("Red-Eyed", n=47, black line) or white eyes ("White-Eyed", n=48, orange line). **(L)** Female manipulations of Red-Eyed and White-Eyed groups. Arrows same as in B. **(M)** Same as in K, shown in Cartesian coordinates. **(N)** D_A/D_P ratio for males courting either Red-Eyed or White-Eyed females. Both groups have ratios significantly different from 1 (Red-Eyed, $p < 10^{-5}$; White-Eyed, $p = 0.03$; 1-Sample T-Test); however, males in the Red-Eyed group have significantly greater ratios than males in the White-Eyed group ($p < 10^{-5}$, One-way ANOVA). **(O)** Behavioral locations of males courting either Red-Eyed or White-Eyed females (asterisks same as in E). Note that females are oriented as in (K).

regulating the spatiotemporal patterns of individual courtship elements, we examined the behavior of males courting females whose head had been transplanted from the anterior to posterior end. We found that although head position had no effect on the overall levels of courtship or on the frequencies of expressing individual courtship elements (Figure 3.7), males that courted females with a posterior head position ("Head-Posterior") exhibited an asymmetric courtship path that was biased towards greater distances from the posterior, rather than the anterior, end of her body axis (Figure 3.5F-I). Thus, males utilize the head as a visual marker to delineate the antero-posterior body axis of the female during courtship. Further, we found that when courting "Head-Posterior" females, males switched their tapping location to the anterior end of the female body axis. In contrast, the spatial distributions of orienting or scissoring behaviors towards "Head-Posterior" females were randomly distributed (tapping: $p < 0.05$, Rayleigh Test; orienting and scissoring: $p > 0.05$, Rayleigh Test; Figure 3.5J). These results indicate that the location of the female head is required and sufficient to drive the spatial release of tapping behaviors during courtship. However, female head location is required, but not sufficient, to drive

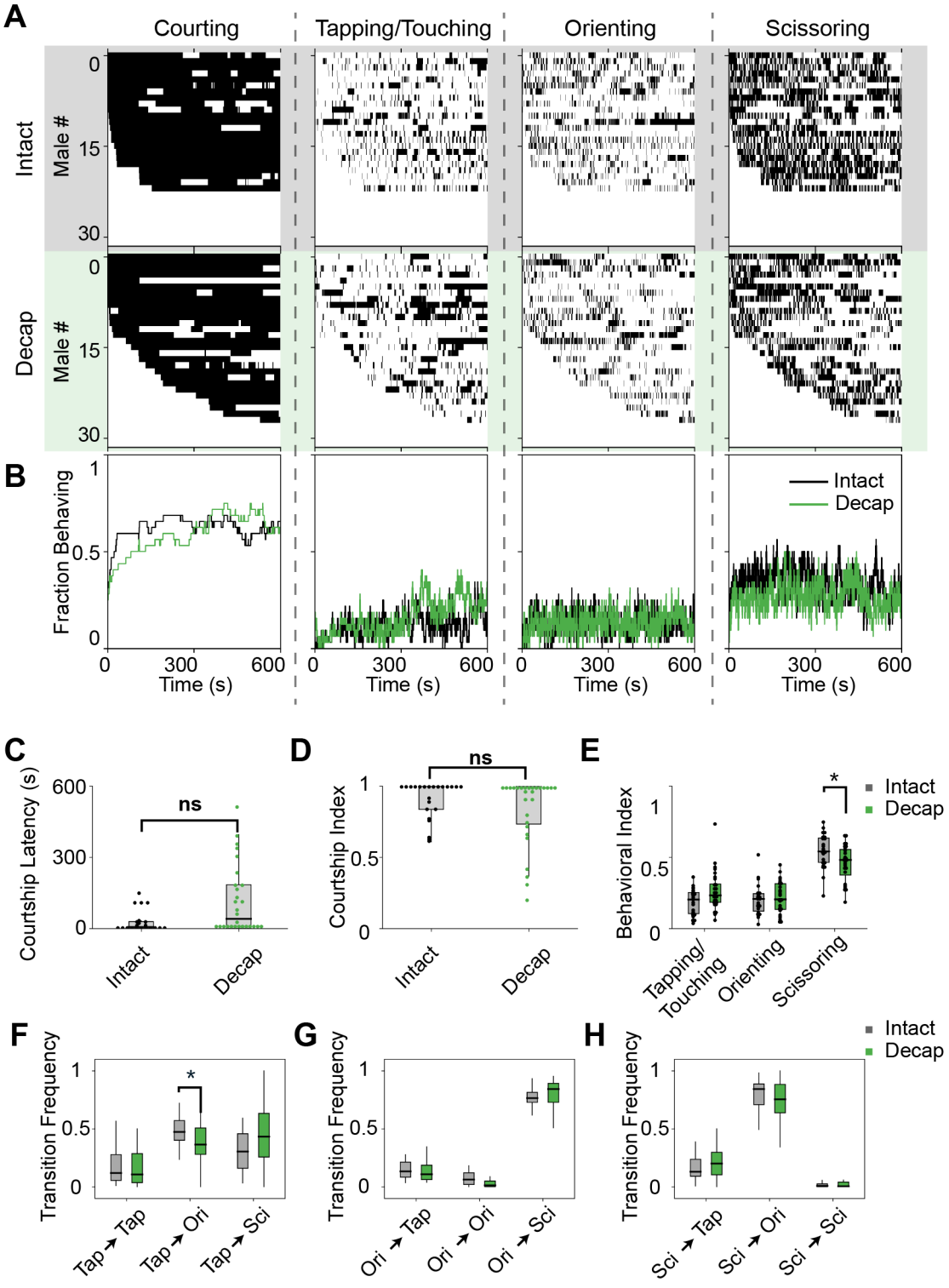

Figure 3.6: **The female's head is important for mediating temporal aspects of courtship.** Caption on next page.

Figure 3.6: **(A)** Behavioral ethograms for males courting either Intact or Decap females (n=32/group). Each row represents an individual fly and each column represents a video frame that has been classified as containing (black) or not-containing (white) a specified behavioral state. **(B)** Fractions of flies engaging in each behavioral state shown in (A) over time. **(C-D)** Courtship latency (C) and courtship index (D) are not significantly different between groups ($p > 0.05$, Kruskal Test). **(E)** Behavioral indices for touching/tapping and orienting are not significantly different between groups, but males courting decapitated females have lower levels of scissoring ($p < 0.05$, Kruskal Test). **(F-H)** Transitions between individual states of courtship. Males courting decapitated females transition from tapping to orienting less frequently than controls ($p < 0.05$, Kruskal Test), but are otherwise normal.

the appropriate spatial release of orienting or scissoring behaviors.

Because one of the most striking visual features of the fly head is the contrast between the red-pigmented eyes and the surrounding cuticle, we next hypothesized that males specifically use the eyes of females as a visual landmark to determine the antero-posterior body axis of their courtship targets. To test this hypothesis, we generated two congenic lines of wild-type flies that differed in a single mutation in the *white* gene, resulting in red- and white-eyed females with inverted visual contrasts made between the eyes and surrounding cuticle (Figure 3.9). We found that although both female genotypes elicited asymmetric courtship paths, the distances of males from the anterior end of white-eyed females were significantly reduced when compared to males courting red-eyed females ($p < 0.05$, Student's T-Test; Figure 3.5K-N). Further, we observed that while males courting white-eyed females tapped mostly at the posterior end, the mean angular locations of both orienting and scissoring bouts were bimodally distributed around the antero-posterior axis of the female ($p < 0.001$ for tapping, Rayleigh Test; $p < 0.001$ for orienting and scissoring, Bimodal Rayleigh Test; Figure 3.5O). In addition, while the relative durations of tapping and orienting were not affected by female eye color, we found that males courting white-eyed females spent significantly less time scissoring ($p < 0.01$, Kruskal Test; Figure 3.8). These data are similar to, though less pronounced than, those observed when males courted headless females, which suggests that males use the eyes of the female

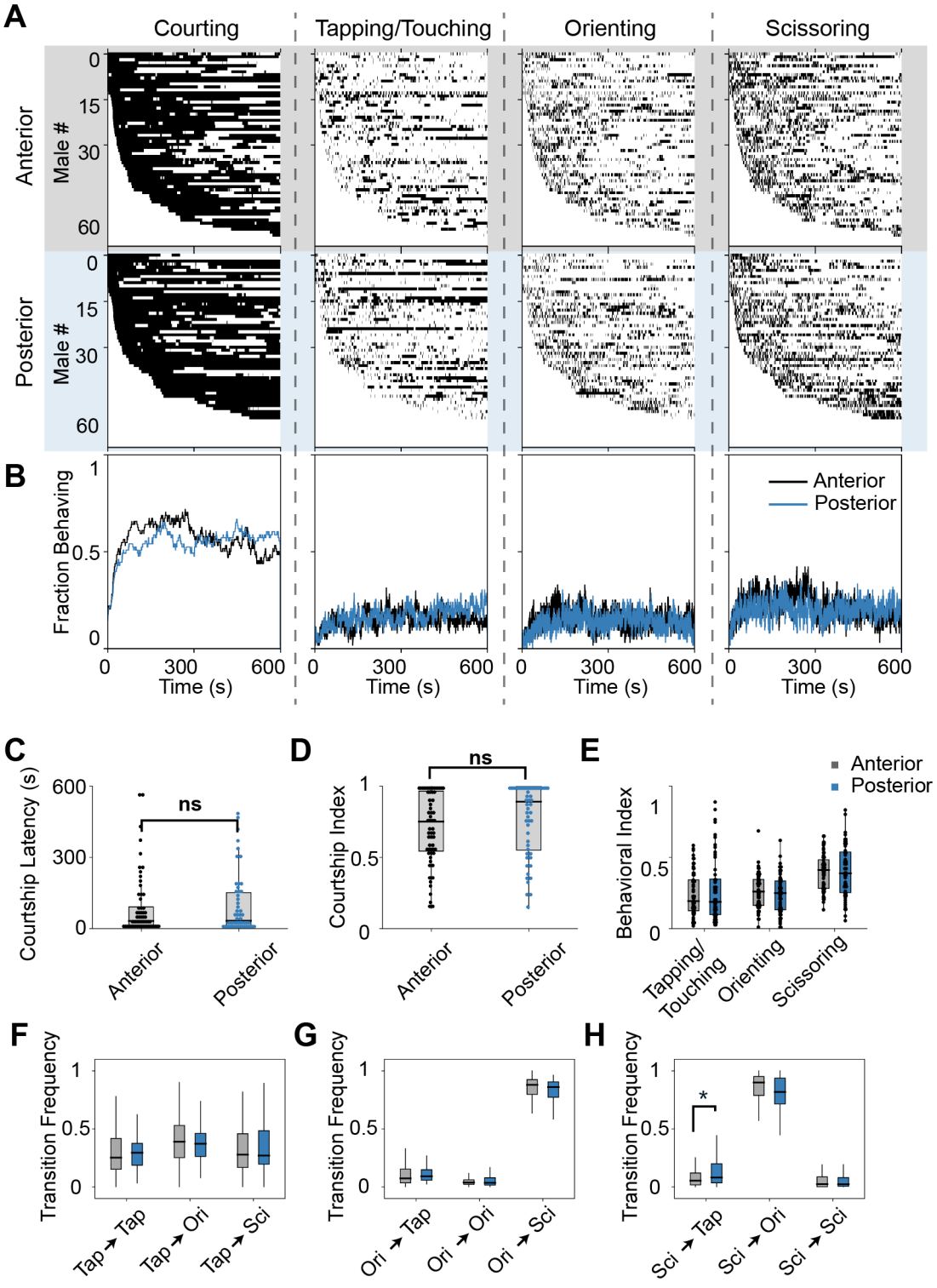

Figure 3.7: **The position of the female's head is not required for temporal elements of the courtship ritual.** Caption on next page.

Figure 3.7: **(A)** Behavioral ethograms for males courting either Head-Anterior ("Anterior", n=64) or Head-Posterior ("Posterior", n=63) females. Each row represents an individual fly and each column represents a video frame that has been classified as containing (black) or not-containing (white) a specified behavioral state. **(B)** Fractions of flies engaging in each behavioral state shown in (A) over time. **(C-D)** The courtship latency (C) and courtship index (D) are not significantly different between groups ($p > 0.05$, Kruskal Test). **(E)** Behavioral indices for tapping/touching, orienting, and scissoring are not significantly different between groups ($p > 0.05$, Kruskal Test). **(F-H)** Behavioral transition frequencies are shown for each group. Males courting "Posterior" females show a small but significant increase in transitioning from scissoring to tapping when compared to males courting "Anterior" females ($p = 0.047$, Kruskal Test).

as an important visual landmark for coordinating both spatial and temporal aspects of the courtship ritual.

3.3.4 LC Neurons Are Necessary for Spatiotemporal Aspects of Courtship

Our behavioral data suggest that males use a simple visual landmark, the red pigmented eyes of females, to define the antero-posterior body axis of courted females. Several recent studies have indicated that ectopic activation of specific classes of Lobula Columnar (LC) visual projection neurons can trigger various behaviors [Wu et al., 2016, Sen et al., 2017], including mediating responses to motion during courtship [Ribeiro et al., 2018]. Therefore, we next hypothesized that the spatiotemporal regulation of individual male courtship elements depends of the activity of a specific visual neuronal pathway for body axis recognition.

Based on previously published data, we chose to focus our investigation on four classes of LC neurons that could be involved in regulating various courtship behaviors, including: leg reaching (LC10), forward walking (LC17), backward walking (LC9, LC10, LC16, LC17), turning (LC16, LC17) [Wu et al., 2016]. We additionally chose to examine LC4 neurons because they have been shown to function in detecting looming stimuli [Wu et al., 2016, von Reyn et al., 2017], which is a visual feature that is likely to be encountered by males as they approach female courtship targets.

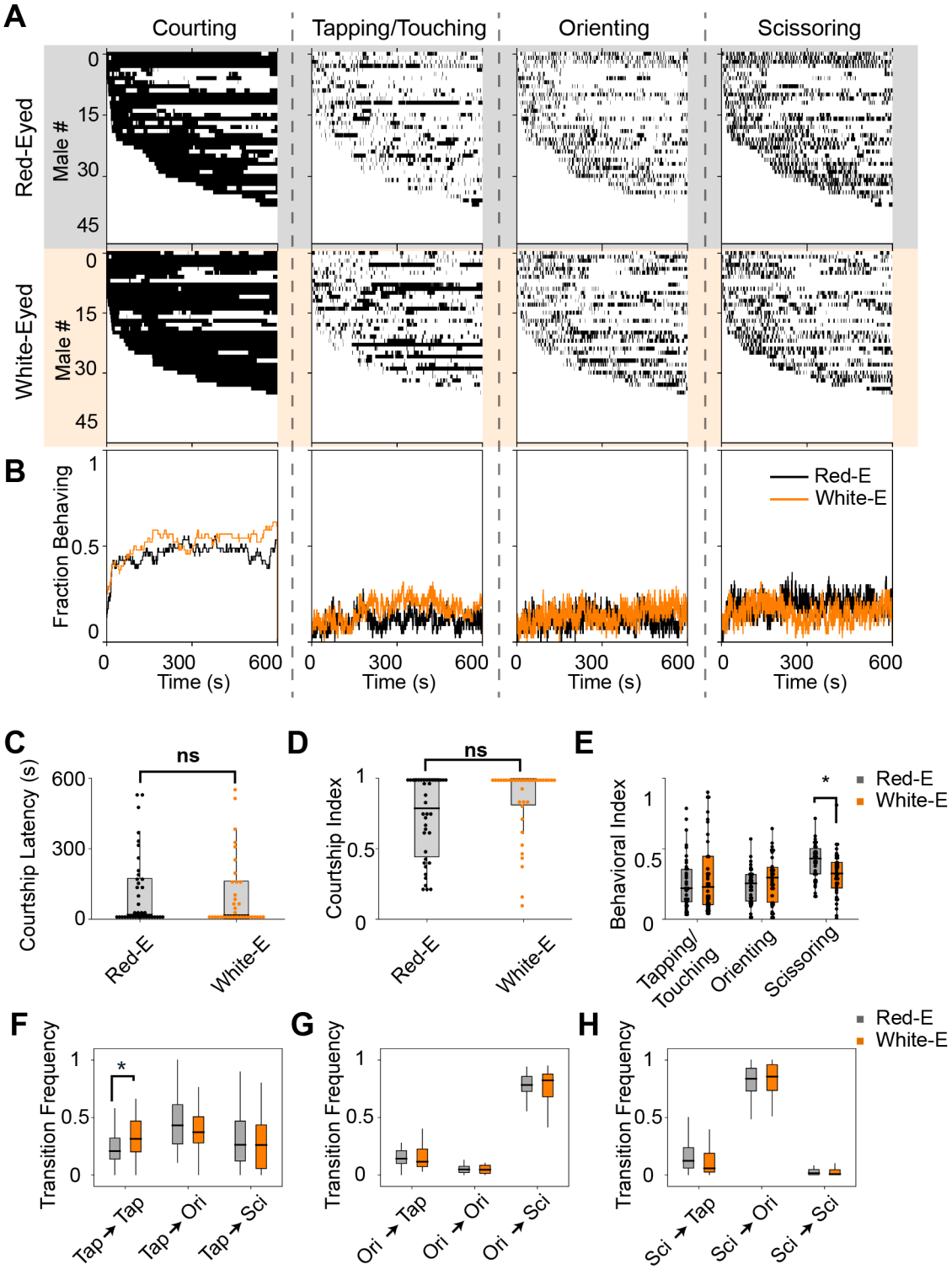

Figure 3.8: **Female eye color is important for mediating temporal aspects of male courtship behavior.** Caption on next page.

Figure 3.8: **(A)** Behavioral ethograms for males courting either Red-Eyed (n=47) or White-Eyed (n=48) females. Each row represents an individual fly and each column represents a video frame that has been classified as containing (black) or not-containing (white) a specified behavioral state. **(B)** Fractions of flies engaging in each behavioral state shown in (A) over time. **(C-D)** The courtship latency (C) and courtship index (D) are not significantly different between groups ($p < 0.05$, Kruskal Test). **(E)** Males courting White-Eyed females spend less time scissoring compared to controls ($p < 0.01$, Kruskal Test). **(F-H)** Behavioral transition frequencies are shown for each group. Males courting White-Eyed females tend to make more tapping→tapping transitions than males courting Red-Eyed females (shown in F; $p < 0.05$, Kruskal Test).

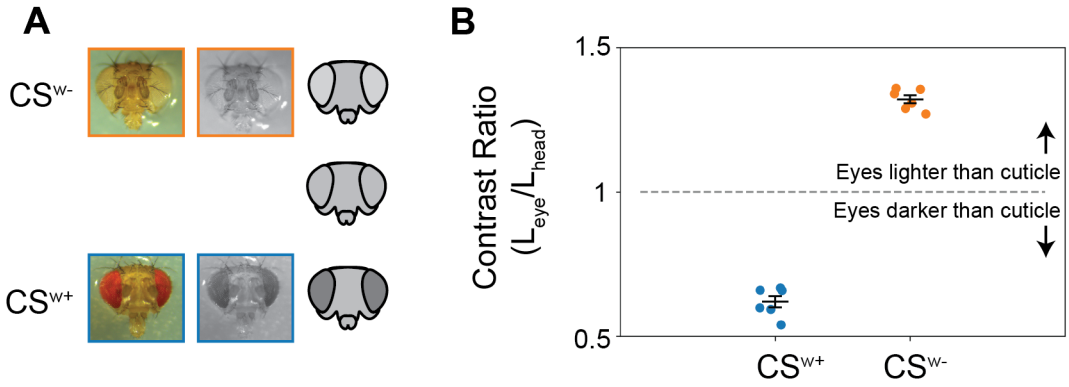

Figure 3.9: **Red-eyed and white-eyed females have inverted eye color contrasts. (A)** Images of the heads of Canton-S (CS^{w^+}) and congenic females with a single mutation in the *white* gene (CS^{w^-}) are shown next to a schematic of flies with varying eye contrasts. **(B)** Contrast ratios for CS^{w^+} and CS^{w^-} flies (n=6/group). Ratios were calculated by converting images to luminances and comparing pixels comprising the eyes (L_{eye}) to pixels comprising the cuticle surrounding the eyes ($L_{cuticle}$).

We found that synaptic silencing of populations of LC neurons by using targeted transgenic expression of Tetanus Toxin (TNT) led to distinct courtship deficits across all lines we examined. Specifically, we found that different LC neuron subtypes play various roles in mediating both spatial and temporal aspects of the courtship ritual, including regulating the latency to court, fractions of time spent exhibiting each courtship element, and the transition frequencies between each behavioral state (Figure 3.10 and Figure 3.11). Importantly, the behavioral deficits we observed were different from line to line, suggesting that each subpopulation of visual descending neurons is involved in coordinating distinct behaviors based on the unique visual features they detect.

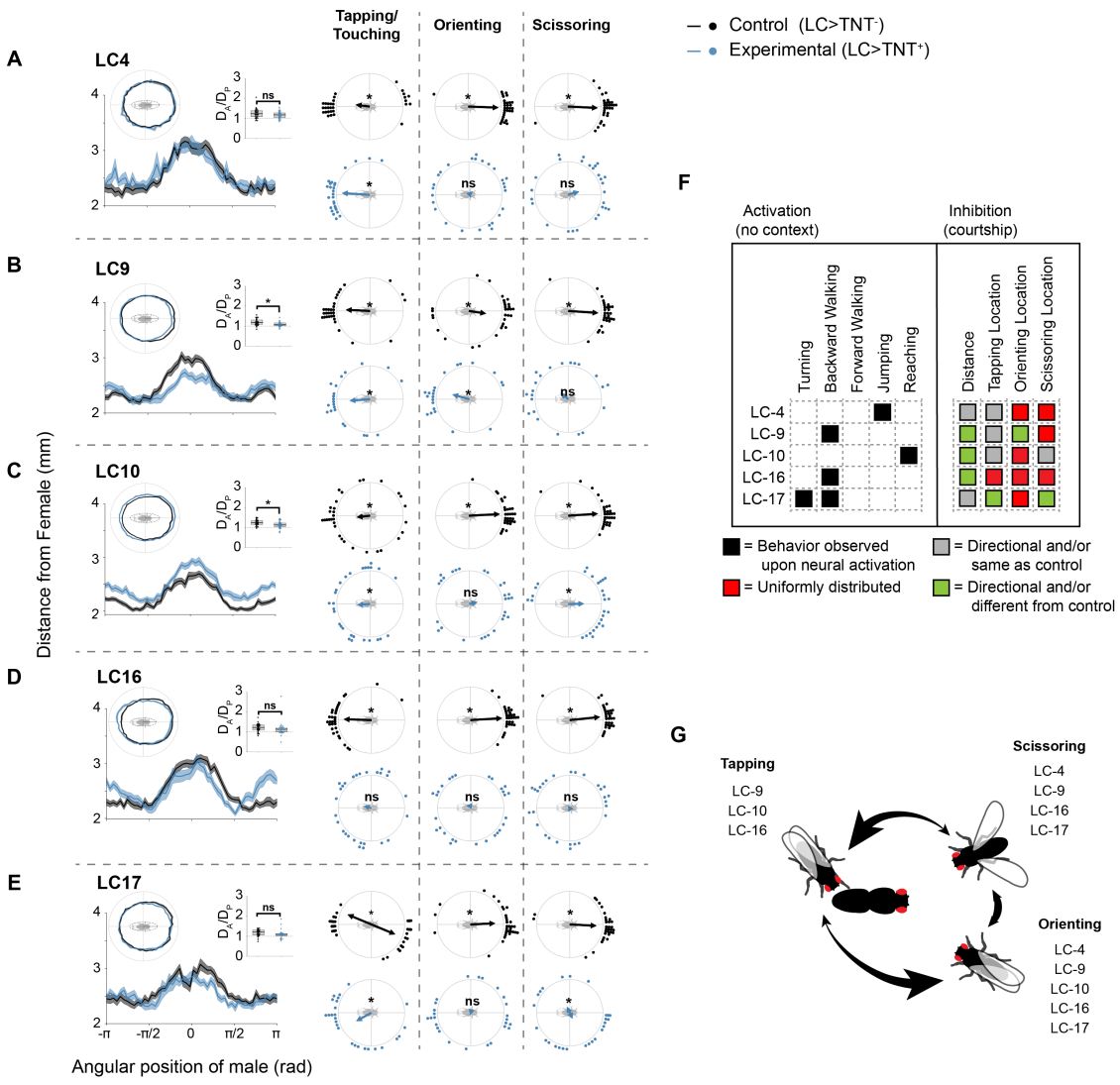

Figure 3.10: **Visual projection neurons are important for directing the spatial localization of male courtship behaviors. (A-E)** Average courtship paths, ratios of the maximum male-to-female distance when a male is on either the anterior or posterior end of the female (D_A/D_P), and average angular positions of the male during Tapping/Touching, Orienting, and Scissoring are shown for each LC line expressing either an inactive (Control, n=32 per line) or active (Experimental, n=32 per line) version of the Tetanus toxin gene (TNT). Asterisks on D_A/D_P plots represent significant differences between Control and Experimental groups ($p < 0.05$, One-way ANOVA). Asterisks on circular plots highlight distributions that were significantly different from uniformity ($p < 0.05$, Rayleigh Test or Bimodal Rayleigh Test). **(F)** (Left) Solid black squares denote LC lines that engaged in the specified behavior upon neural activation in the absence of a specific behavioral context (data from [Wu et al., 2016]). (Right) Gray and colored squares denote whether an LC line differed from controls in their spatial positioning during courtship following neural inactivation (data from this paper). **(G)** Summary plot showing which LC lines were important for the proper spatial positioning of males during Tapping, Orienting, and Scissoring.

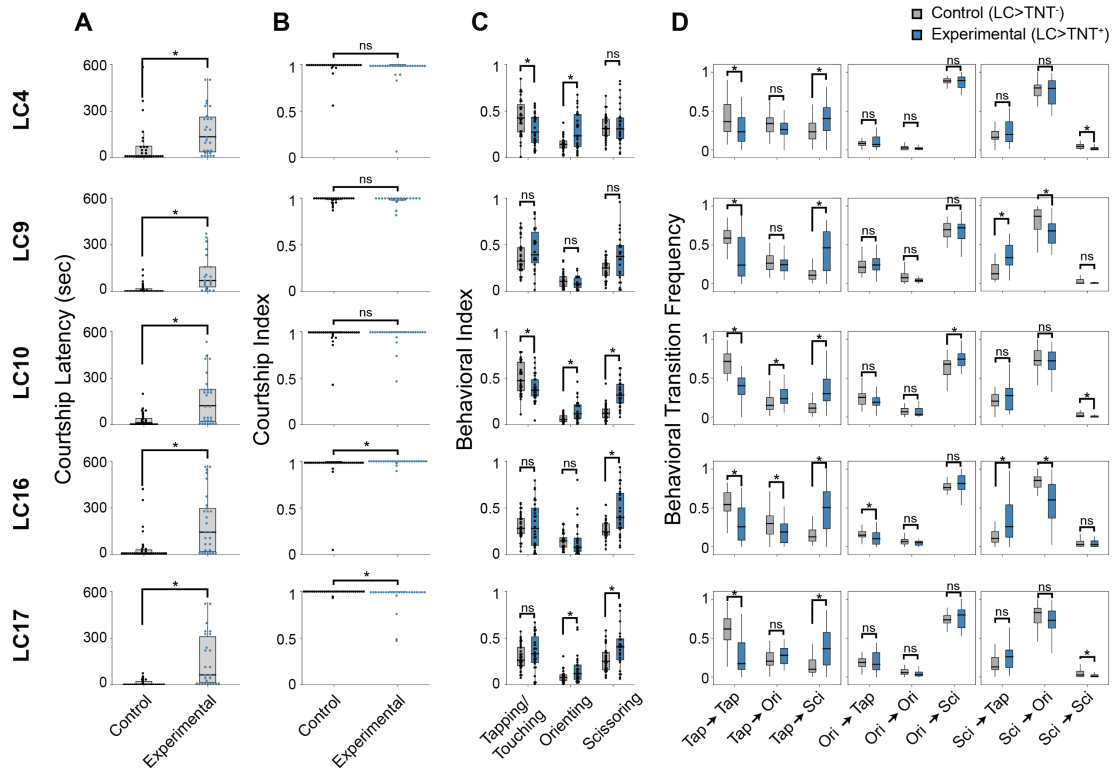

Figure 3.11: **LC neurons are required for temporal aspects of the courtship ritual.** **(A)** Inactivation of all LC lines led to significant increases in courtship latencies when compared to controls ($p < 0.05$, Kruskal Test). **(B)** Courtship indexes were mostly unaffected by LC inactivation (there were significant differences following inactivation of LC16 ($p = 0.049$) and LC17 ($p < 0.001$); however removal of outliers before statistical testing eliminated this effect). **(C)** Behavioral indexes for Tapping/Touching, Orienting, and Scissoring are shown for each LC inactivation. Asterisks represent significant differences between groups ($p < 0.05$, Kruskal Test). **(D)** Frequencies at which flies transitioned between each of the behavioral states during courtship are shown for each LC inactivation.

LC4 neurons have been previously shown to respond to looming stimuli and elicit jumping behaviors [Wu et al., 2016, von Reyn et al., 2017]. We reasoned that as a male approaches a female, she may appear as a looming object and thus require specific looming detection neurons to mediate appropriate behavioral responses during courtship. We found that while inactivation of LC4 neurons did not lead to any deficits in the distances that males placed themselves around the female, it did lead to deficits in their angular positioning during bouts of orienting and scissoring, but not tapping ($p > 0.05$ for Orienting and Scissoring, $p < 0.05$ for Tapping, Rayleigh Test; Figure 3.10A). These results suggest that males utilize LC4 neurons for the identification of visual features, possibly including looming stimuli, that are required for proper spatial positioning during bouts of specific courtship elements. Further, we found that inactivation of LC4 neurons leads to increased courtship latencies, decreased times spent tapping, and increased times spent orienting toward females (Figure 3.11). Together, these results suggest that LC4 visual projection neurons are an important feature detector for the spatial and temporal organization of courtship behaviors.

An important component of male behaviors during the courtship ritual includes sideways and backward movements that help males push themselves away from the female to release courtship elements at their appropriate spatial positions. Activation of several classes of LC neurons, including LC9, LC10, LC16, and LC17, was recently shown to elicit backwards walking behaviors in males [Wu et al., 2016, Sen et al., 2017]. We found that inactivation of each of these subpopulations of neurons in males led to both spatial and temporal courtship deficits, as follows.

LC9 inactivation led to decreased distances between males and their courtship targets when the male was on the anterior half of the female (D_A/D_P, $p < 0.05$, One-Way ANOVA; Figure 3.10B). Further, males positioned themselves on the posterior, rather than anterior, half of the female during bouts of orienting ($p < 0.05$, Watson-Williams Test) and showed

randomly distributed angular positions during bouts of scissoring ($p > 0.05$ for Scissoring, Rayleigh Test; Figure 3.10B). Finally, males displayed longer latencies to court but did not differ in their fractions of time spent engaging in any of tapping, orienting, or scissoring behaviors, following LC9 inactivation (Figure 3.11).

LC10 inactivation led to overall increased distances between males and females during courtship, while maintaining an asymmetric courtship path ($D_A/D_P > 1$, $p < 0.05$, 1-Sample T-Test; Figure 3.10C), and resulted in normal angular positioning during tapping and scissoring, but not during orienting bouts ($p < 0.05$ for Tapping and Scissoring, $p > 0.05$ for Orienting, Rayleigh Test; Figure 3.10C). Further, inactivation of LC10 resulted in longer latencies to court and decreased fractions of time males engaged in tapping, while increasing the time males engaged in both orienting and scissoring behaviors (Figure 3.11). In addition, the altered times spent in each behavioral state were likely the result of different transition frequencies from tapping to each other state (Figure 3.11D). Along with evoking backwards walking upon activation, LC10 neurons have been implicated in generating leg reach behaviors [Wu et al., 2016]. That both the male-to-female distance increased and overall levels of tapping decreased during courtship and following LC10 inactivation, suggest that LC10 could be important for bringing the male within reach of the female and initiating tapping behaviors.

We found that LC16 neurons were important for all spatial aspects of courtship we examined, as inactivation of LC16 altered the courtship path and eliminated stereotypy in tapping, orienting, and scissoring locations (Figure 3.10D). Specifically, while males were able to maintain asymmetry in their courtship paths and distance themselves further from the females anterior end, the effect was much smaller than controls ($p < 0.05$, One-Way ANOVA; Figure 3.10D). Additionally, the mean angular position of males during bouts of tapping, orienting, and scissoring were randomly distributed in males that had LC16 cells inactivated ($p > 0.05$, Rayleigh Test; Figure 3.10D). Finally, LC16-inactive males had in-

creased latencies to court, increased levels of scissoring, and significantly different levels of transitions between each of the courtship elements (Figure 3.11). These results suggest that LC16 is a critical visual cell type that is responsible for both spatial and temporal courtship decisions in male flies, which functions in eliciting backwards and/or sideways motor movements necessary for the coordination of courtship displays.

Finally, LC17 was also shown to generate sideways and backwards walking following neural activation [Wu et al., 2016], and we identified several spatio-temporal courtship deficits in males with synaptically-inactive LC17 neurons. Specifically, we found that LC17-inactive males positioned themselves at appropriate distances around the female, but did not display orienting or scissoring bouts along specific angular locations ($p > 0.05$ for Orienting and Scissoring, Rayleigh Test; Figure 3.10E). Temporally, LC17-inactive males tended to initiate courtship at later times and engage in higher levels of orienting and scissoring than controls ($p < 0.05$ for Orienting and Scissoring, One-Way ANOVA; Figure 3.11). Taken in whole, these results suggest that LC17, as well as other visual LC-subpopulations whose activation drives sideways and backwards movements, are critical for the appropriate spatial and temporal coordination of male courtship elements.

3.3.5 LC Neurons Mediate Stereotyped Courtship Movements

To begin to determine which visual features these LC neurons might be responding to in the spatiotemporal regulation of male courtship, we examined average movement speeds of males at different angular positions around female courtship targets. We found that control males had very stereotypical movement patterns around the female, where they accelerated and achieved high velocities while on either side of the females medial-lateral axis (V_{ML}, areas shown in green in Figure 3.12B); an effect which was mostly mediated via sideways movement (Figure 3.12A-C). These males then slowed down to much lower velocities when on either the female's anterior (V_A) or posterior (V_P) sides. In contrast,

males with inactive populations of LC neurons moved slower than controls overall, and while they were capable of speeding up when alongside the female's medial-lateral axis (with the exception of LC16), they failed to slow down to the same extent as controls when near the female's head (as shown by decreased V_{ML}/V_A ratios; Figure 3.12D). Interestingly, males courting decapitated females showed similar movement phenotypes (Figure 3.12E-G). These results again suggest that the female's head is an important visual signal — in part detected by LC cells — which males use to coordinate their movements during bouts of courtship.

3.4 Discussion

Innate behaviors, such as the courtship ritual in *Drosophila melanogaster*, provide unique opportunities to study the sensory cues and circuits that direct sophisticated behavioral motifs. In this paper, we developed computational tools to quantitatively characterize both spatial and temporal components of the male courtship ritual in the fly and highlighted the significant role that visual signals play in directing spatiotemporal aspects of the courtship ritual. Further, we identified several classes of visual projection neurons that recognize cues present on female courtship targets that are important for coordinating behavioral positioning. This work demonstrates that even simple visual cues, such as eye color, are salient enough signals to direct multiple aspects of complex and innate behaviors.

Visual cues present on the female are important not only for directing males to specific locations around the female, but they are also direct a specific 'mode' of courtship with enhanced scissoring and diminished tapping displays. While these results are most strikingly observed between males courting under either white or red light (Figure 3.3 and Figure 3.4), males courting either decapitated females or females with white eyes were also seen to have lower levels of scissoring and increased (though not significantly) levels of tapping (Figure 3.5 and Figures 3.6 and 3.8). From the male's perspective, these re-

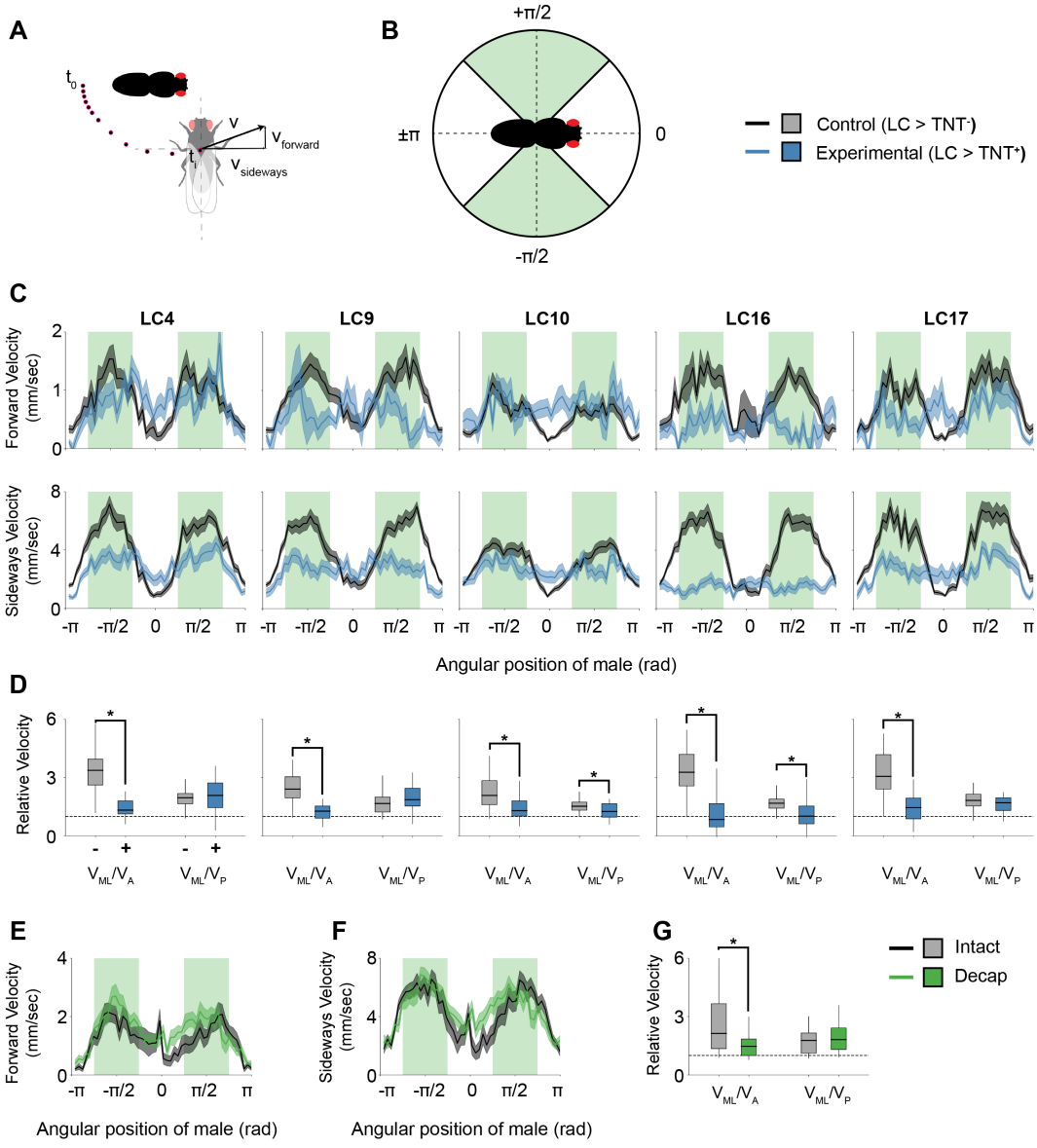

Figure 3.12: **Visual projection neurons mediate movements during courtship. (A)** Schematic showing the breakdown of the males velocity vector (v) at a specific time point (t_i) into forward ($v_{forward}$) and sideways ($v_{sideways}$) components. **(B)** Schematic highlighting the four spatial quadrants surrounding the female. **(C)** Line plots showing the average velocity ($\pm$SEM) of each population of males at each angular bin surrounding the female. Areas of green correspond to the spatial quadrants on either side of the female along the medial-lateral axis; areas of white correspond to spatial quadrants on either side of the anterior-posterior axis. Forward and sideways velocities are affected following the inactivation of most LC lines; however, the most severe deficits occur when males are along either side of the female along the medial-lateral axis. Caption continued on next page.

Figure 3.12: **(D)** Relative velocities showing both (1) the mean sideways velocity when the male is on either side of the females medial-lateral axis (V_{ML}) to the sideways mean velocity when the male is within the females anterior quadrant (V_A) and (2) the sideways mean velocity when the male is on either side of the females medial-lateral axis to the mean sideways velocity when the male is within the females posterior quadrant (V_P). Inactivation of all lines leads to decreased V_{ML}/V_A ratios when compared to controls ($p < 0.001$, One-way ANOVA). **(E-F)** Similar plots to those shown in (C) but for males courting females that were either intact or decapitated (see Figure 3.5). **(G)** Males courting decapitated females show a significantly smaller V_{ML}/V_A than controls ($p < 0.05$, One-way ANOVA).

sults could suggest that in the absence of vision, the male is trying to compensate for the loss of input through one sensory modality with increased input through others [Kupers and Ptito, 2014]. Therefore, males lacking visual inputs increase their levels of tapping to increase their tactile and/or chemosensory inputs. Alternatively, from the female's perspective, scissoring displays could be important for female acceptance and transitioning from courtship into copulation. In the absence of light, the female would not gain any information about the male's fitness via his displays of scissoring, which could be another reason for altered modes of courtship. Though not mutually exclusive, it would be interesting to try and parse the reasons for alternative modes of courtship in light and dark.

In this paper we focused on the role of the female's head in coordinating male spatial positioning during courtship, though there are other visual signals present. Three independent experiments showed that the females head is important for this positioning, and highlighted the female's eye color as a one salient feature which provides information about female orientation (Figure 3.5). However, transplantation of the female's head onto her abdomen did not lead to a full reversal of male spatial positioning (Figure 3.5F-J), and eliminating pigment from the female's eyes did not lead to full loss of the male's ability to localize the female (Figure 3.5K-O). These results suggest that while female head and eye color are important visual features that allow males to spatially orient themselves during courtship displays, they are not the only features. The only other area of the female's body that contains significant pigmentation is the banding pattern on the female's

abdomen. Though we did not directly test the significance of this banding pattern on male spatial positioning, the evolution of pigmentation patterns is under strong sexual selection [Protas and Patel, 2008, Wittkopp and Beldade, 2009], suggesting that it plays a role in courtship success. Nonetheless, our results suggest that there is likely an interplay between the pigmentation on both the abdomen and eyes that males utilize to direct their mating displays, though future experiments should more thoroughly address this issue.

LC neurons have previously been shown to be important for initiating behavioral responses to visual stimuli [Wu et al., 2016, Sen et al., 2017]. Here, we examined whether specific subsets of LC neurons were important for the detection of visual stimuli present on the female during courtship. Surprisingly, we found that synaptic inactivation of all LC lines we tested led to deficits in the spatial positioning of the male during courtship. Perhaps surprisingly, inactivation of LC4 — important for detecting looming stimuli and initiating an escape jump response [von Reyn et al., 2017] — also led to behavioral deficits. During approach behaviors, the female's image generated on the male's retina would appear to be looming, and thus neurons detecting looming might be expected to play a role in the behavioral coordination of courtship. LC4 neurons have been demonstrated to be directly wired to the giant fiber in Drosophila [von Reyn et al., 2017], which has been shown to be important for escape responses [Wyman et al., 1984, Card, 2012]. That inactivation of LC4 during courtship also leads to behavioral deficits suggest that parallel circuits, responding to similar visual stimuli, direct alternative behaviors in different contexts. Perhaps less surprising is the fact that manipulating visual circuits that help to direct reaching (LC10), backward walking (LC9, LC10, LC16, LC17), and turning (LC16, LC17) lead to behavioral defects in male positioning during courtship as these are all behaviors which occur during courtship. Further, though we attempted to limit the amount of visual stimuli present on or surrounding the female during courtship by studying males courting immobile females, there are still many visual signals both present on the female and generated by male-produced ego-motion that males need to account for during courtship. Each of

the LC neuron subtypes we examined likely responds to some of these features, which is why a wide array of LC neurons is required for the coordination of courtship behaviors. Studies have started to look at understanding exactly which features some of the neurons are responding to [Wu et al., 2016, Ribeiro et al., 2018], and future studies will likely tell the precise visual stimuli responsible for activation of the other cell types. Importantly, this study should place some ethological context onto the specific visual stimuli detected by LC neurons and their roles in directing behavioral outputs.

The courtship ritual entails one of the most well-understood behavioral sequences in the fly, and it has a long history of usefulness into investigations of the genes and circuits underlying the generation of specific behaviors [Sturtevant, 1915]. While the importance of vision in mediating courtship has also been known for some time [Spieth and Hsu, 1950, Connolly et al., 1969, Markow, 1975], the courtship ritual has been most often used in the study of other sensory modalities. With the advent of new methods for reliably tracking and classifying behavioral motifs in animal models [Dankert et al., 2009, Branson et al., 2009, Kabra et al., 2013], courtship has started to become a useful model for investigating the role of vision in *Drosophila* mating behaviors [Agrawal et al., 2014, Ribeiro et al., 2018]. We hope that the findings presented in this chapter will enable the courtship ritual to become a valuable system for exploring the role of visual processing in action selection.

Chapter 4: A Sex-Specific Neural Architecture in Foreleg Gustatory Neurons Regulates Courtship Drive in *Drosophila*

The detection and processing of pheromonal stimuli is crucial for appropriate behavioral decision-making in many insect species; yet, how specific neural circuit architectures function to relay chemosensory stimuli and convert these into specific behavioral outputs is largely unknown. Here, we highlight the necessity of an architectural feature of the sex circuit in *Drosophila melanogaster* — axonal midline crossing by foreleg gustatory receptor neurons (GRNs) in the ventral nerve cord — in mediating sustained bouts of courtship by male flies. Foreleg GRNs detect contact chemosensory stimuli on a female's cuticle during courtship and relay this information to central processing centers in the brain via ascending pathways that send sensory stimuli to both halves of the central nervous system. Our results show that the processing of contralateral chemosensory stimuli by foreleg GRNs is required for a male to fully engage in and maintain heightened levels of courtship, and without axonal midline crossing, courtship levels are severely impacted. The data presented in this chapter therefore identify a specific morphological feature of a neural circuit whose presence is required for the appropriate processing of social stimuli by enhancing levels of arousal in male flies.

4.1 Introduction

Pheromones are important for the regulation of social interactions in diverse insect species, including courtship behaviors in *Drosophila melanogaster* males. During courtship, males approach a female and use chemosensory cues, detected by in part by gustatory receptor neurons (GRNs) in the forelegs, to direct specific temporal aspects of the courtship ritual, such as the time taken to initiate and the total duration of courtship. Indeed, specific populations of foreleg GRNs have been shown to be important for detect-

ing multiple classes of pheromonal stimuli and regulating the excitatory state of central neurons which ultimately determine a male's level of arousal [Clowney et al., 2015, Lu et al., 2012, Thistle et al., 2012, Koh et al., 2014, Starostina et al., 2012, Toda et al., 2012]. Much research has gone into the genetic identification of foreleg GRNs that function to control male courtship levels, and the transcription factor *fruitless* (*fru*), along with several protein channels including *pickpocket23* (*ppk23*), has been shown to play a significant role in mediating arousal in males during courtship [Lee et al., 2000, Manoli et al., 2005, Demir and Dickson, 2005, Lu et al., 2012]. At the circuit level, these foreleg GRNs send axonal projections into the ventral nerve cord (VNC), where they make synaptic contacts with ascending interneurons that direct pheromonal stimuli to the brain which can ultimately place a male into an excitatory behavioral state [Clowney et al., 2015]. While the identification of specific genetic- and circuit-level elements has revealed much about how animals translate pheromonal stimuli into behavioral outputs, how specific morphological features of neural circuits play a role in these processes is still largely unknown.

One of the characteristic morphological features of foreleg GRNs that play a role in mediating male courtship behaviors is the presence of sexually-dimorphic axonal fibers that project into and cross the midline of the VNC within the prothoracic neuromere. The genetics underlying whether a GRN axonal fiber will cross the midline at this region has been at least partially worked out and depend on the transcriptional repression of the chemotrophic factor *roundabout1* (*robo1*) by *fru* [Orgogozo et al., 2004, Mellert et al., 2010, Neville et al., 2014, Ito et al., 2016]. While the mechanisms controlling the crossing status of a foreleg GRN's axonal projections have started to be determined, the behavioral and functional significance of these midline-crossing axons are not well understood.

Sensory systems often contain elements within their neural circuits that function to extract meaningful information from the environment. For instance, bilaterally-encoded auditory stimuli are sent along axonal 'delay lines' that parse interaural timing differences to local-

ize sounds in birds [Jeffress, 1948, Carr and Konishi, 1988, Stern et al., 1988]. Specific elements of olfactory circuits in flies have also been shown to extract location information about the source of odors [Louis et al., 2008, Duistermars et al., 2009, Gaudry et al., 2013]. Whether gustatory chemosensory cues traveling along GRNs are processed similarly to those of olfactory stimuli in *Drosophila* males to localize specific elements of the female during courtship are unknown, as are the specific circuit elements which might regulate GRN-mediated chemolocation. Alternative to the localization of sensory stimuli in the environment, bilateral chemosensory stimuli detected by GRNs could simply be a redundant mechanism to ensure that the entry into or maintenance of courtship remains intact following injury to one foreleg. Whether midline-crossing axons from foreleg GRNs function in either chemolocation or sensory redundancy is not known.

To determine whether midline-crossing axons play a role in either chemolocation or simply function as a redundant mechanism for eliciting courtship behaviors in males, we examined the spatiotemporal consequences of eliminating GRN foreleg axonal projections (GRN^{fap}) from the male's sex circuit. We initially show that pheromonal stimuli hold both spatial information about a female's position and promote the maintenance of courtship behavior by males, but demonstrate the GRN-detected pheromones do not play a role in the spatial localization of a female; rather, they function to sustain courtship bouts. Further, we highlight the separate roles of foreleg GRNs that contain axonal projections which cross the midline (GRN^{fap+}) from foreleg GRNs which do not contain crossing midline-crossing axonal projections (GRN^{fap-}), and show that GRN^{fap+} neurons, but not GRN^{fap-} neurons, are important for courtship maintenance. Finally, we specifically inhibit axonal crossing from GRN^{fap+} neurons and show inhibition of crossing axons also leads to a reduced ability of males to maintain courtship. Together, the experiments in this chapter demonstrate the importance of GRN^{fap+} neurons for maintaining male courtship behaviors in the fly.

4.2 Methods

4.2.1 Flies

All flies were housed at 25 ^{o}C and 70% humidity on a 12h:12h light:dark schedule, and reared on a standard corn-meal based food from Achron Scientific. All flies, except for the *ppk23*^{GAL4} line [Lu et al., 2012] and the *ppk23*^{GAL80} line described below, are available from Bloomington *Drosophila* Stock Center (BDSC) and are listed in Table 4.1.

The *ppk23*^{GAL80} line was generated by amplifying the 2.6 kb promoter sequence upstream of the *ppk23* genomic region from Canton-S flies and flanked by the following EcoRI-tagged primers: ACTCATCGCTCTGTAAGCTTCT (forward) and GTTCAGGGAGGTCAAAATCC (reverse). This PCR product was moved into the pENTR-1A vector (ThermoFisher) at EcoRI sites, and then the *ppk23* promoter was subsequently moved into the vector pBPGAL80Uw-6 [Pfeiffer et al., 2010] (Addgene #26236) via an LR Clonase (ThermoFisher) reaction. This construct was injected into BDSC line 24483 for integration onto the second chromosome at the attP cytological marker 51D9 and backcrossed into w^{1118} flies before use.

4.2.2 Courtship Assays

All spatial courtship assays were performed as described in Section 3.2.2. For experiments that only measured non-spatial parameters, courtship trials were run as follows. Males and females were collected upon eclosion and moved into same-sex grouped housing (10–12 individuals per 25 mL vial). When males were 2 days old, they were isolated and moved into individual, 5 mL glass vials. When flies were 4–6 days old, males and females were moved into circular arenas (13 mm in diameter) and were allowed to court for 10 minutes. Videos were recorded of courting flies using back-lighting from white LEDs,

BDSC #	Description	Reference	Figure(s)
NA	Canton-S (CS)	NA	4.1-4.9
65406	*desat*^{GAL4}; *tub*^{GAL80ts}	Billeter et al. [2009]	4.1-4.2
65403	*UAS-hid*	Billeter et al. [2009]	4.1-4.2
41263	*R44C09*	Jenett et al. [2012]	4.3
50210	*R44E04*	Jenett et al. [2012]	4.3
46607	*R69E01*	Jenett et al. [2012]	4.3
50051	*R39E06*	Jenett et al. [2012]	4.3, 4.5-4.6
48454	*R11D04*	Jenett et al. [2012]	4.3, 4.5-4.6
39323	*R64H04*	Jenett et al. [2012]	4.3, 4.5-4.6
NA	*R47D04*	Jenett et al. [2012]	4.3, 4.5-4.6
38824	*R52C06*	Jenett et al. [2012]	4.3, 4.5-4.6
48698	*R15F02*	Jenett et al. [2012]	4.3, 4.5-4.6, 4.7
49690	*R31H02*	Jenett et al. [2012]	4.3, 4.5-4.6
50150	*R42C06*	Jenett et al. [2012]	4.3, 4.5-4.6
39847	*R74C07*	Jenett et al. [2012]	4.3, 4.5-4.6
39078	*R54F03*	Jenett et al. [2012]	4.3
50199	*R44B02*	Jenett et al. [2012]	4.3
45796	*R13B12*	Jenett et al. [2012]	4.3
39201	*R58H10*	Jenett et al. [2012]	4.3
48673	*R15A08*	Jenett et al. [2012]	4.3
38829	*R52D09*	Jenett et al. [2012]	4.3
39465	*R68C02*	Jenett et al. [2012]	4.3
50014	*R38F11*	Jenett et al. [2012]	4.3
39078	*R54F03*	Jenett et al. [2012]	4.3
32185	*UAS-mCD8::GFP*	NA	4.4, 4.8-4.9
32198	*UAS-myr::GFP*	NA	4.4
NA	*ppk23*^{GAL4}	Lu et al. [2012]	4.3-4.4, 4.5-4.6, 4.7
NA	*poxn*^{GAL4} *(6-9)*	Boll and Noll [2002]	4.3, 4.8-4.9
NA	*UAS-kir*; *tub*^{GAL80ts}	Baines et al. [2001]	4.5-4.6, 4.7
NA	*UAS-Robo1*	Evans et al. [2015]	4.8-4.9

Table 4.1: **Fly lines used in chapter 4.**

and all bouts of courtship were hand-scored from these videos. Videos were recorded using either a Raspberry Pi NoIR camera or a Logitech C920 webcam.

For some experiments, a "Maintenance" index was calculated as the total number of males engaging in courtship at any particular time as a fraction of the cumulative number of males that had started to court. All other courtship parameters, including the courtship index and latency, were calculated as in Section 3.2.5.

4.2.3 Immunohistochemistry and Imaging

Ventral nerve cords were dissected and stained using 1:1000 rabbit anti-GFP primary antibody and 1:500 donkey anti-rabbit secondary antibody (ThermoFisher) as in [Wu and Luo, 2006]. VNCs were mounted ventral side up into slide wells (Electron Microscopy Sciences, EMS) containing either phosphate buffered saline (PBS) or hard-mounting medium (Vectashield), and imaged with a 20x oil-immersion objective using a Nikon A1 confocal microscope and a 1 mm step size in the Z-plane. All VNC images are shown as maximum-intensity projections along the Z-plane (Z-stacks). For some VNCs, a "Crossing Score" was calculated from this Z-stack as the pixel intensity (I) of GFP signal at the midline of the prothoracic neuromere relative to the pixel intensity of all neurites on either side of the prothoracic midline, as in [Mellert et al., 2010], and shown by Eq. 4.1:

$$\text{Crossing Score} = (I_{midline} - I_{background})/((I_{left} + I_{right} - 2I_{background})/2) \tag{4.1}$$

Note that $I_{background}$ was determined by taking the average GFP signal from four regions within the VNC that were surrounding, but which did not include, the axonal projections of interest.

Images of GRNs in the forelegs were collected by rearing flies expressing either *UAS-*

myr::GFP or *UAS-mCD8::GFP* for at least 2 days at 30 ^{o}C to increase expression in the extremities, then amputating foreleg tarsal segments and mounting and imaging raw GFP signal as above. All images of forelegs are shown as maximal intensity projections.

4.3 Results

4.3.1 Female Pheromones Direct Spatial and Temporal Aspects of Male Courtship

Pheromones are comprised of a diverse array of chemical compounds including hydrocarbon alkanes and alkenes. These chemicals are present on the cuticles of flies and are produced, in part, by fat-like cells called oenocytes, which contain desaturase enzymes that are involved in the production of pheromonal hydrocarbons [Ferveur, 2005, Marcillac et al., 2005, Krupp et al., 2008]. By over-expressing the pro-apoptoic gene *head involution defective* (*hid*) under the control of the *desaturase-1* (*desat1*) gene's regulatory elements, prior research has shown that oenocyte-specific ablation leads to a strong reduction in the overall levels of pheromones present on the cuticle of adult flies [Billeter et al., 2009]. We took advantage of this genetic manipulation to ask whether pheromones present on female flies were important for regulating either the ability of males to sustain bouts of courtship or coordinate spatial mating displays.

We found that ablation of female oenocytes led to both decreased levels of courtship in males and impaired their ability to engage in behavioral elements of the courtship ritual at appropriate locations (Figures 4.1 and 4.2). Specifically, while males courting oenocyte-less (oe-) females showed an asymmetric courtship path that resembled those of controls (Figure 4.1A-B), they were unable to release orienting and scissoring behaviors at specific angular locations around the female ($p > 0.05$, for Orienting and Scissoring, Rayleigh Test; Figure 4.1C). Further, males courting oe- females had a significantly decreased courtship index compared to controls ($p < 0.05$, Kruskal Test; Figure 4.1D), though their latency to

court was unaffected ($p > 0.05$, Kruskal Test; Figure 4.1E). Nonetheless, males courting oe- females did not show any differences in their levels of tapping, orienting, or scissoring as a fraction of overall levels of courtship ($p > 0.05$, Kruskal Test; Figure 4.1F), nor were transitions between individual courtship elements greatly affected (Figure 4.2). These results suggest that female pheromones regulate both spatial elements of the courtship ritual as well as overall levels of male courtship, by sustaining courtship bouts at elevated levels, but they do not bias the mode of courtship towards one that favors any individual courtship element.

4.3.2 There Are Two Major Morphological Classes of Foreleg Chemosensory Neurons

Pheromones are detected by several groups of chemosensory neurons which are distributed across the body of the fly, including GRNs located within the legs. We hypothesized that there are multiple classes of leg gustatory neurons that serve distinct functions in directing specific aspects of the male courtship ritual: whereas one class might regulate its temporal aspects, such as courtship intensity, another class might regulate its spatial aspects. To determine if multiple such classes of leg chemosensory neurons exist, we first screened populations of genetically distinct, GAL4 reporter lines [Jenett et al., 2012] for specific morphological features. Subsequently, we inactivated each of these lines by over-expressing an inwardly-rectifying potassium channel (*kir2.1*) in a temperature-dependent manner and searched for associations between morphology and behavior.

We initially screened 21 different GAL4 reporter lines that were driving the expression of a membrane-bound green fluorescent protein (GFP) and qualitatively scored each line for fluorescence expression in (1) foreleg tarsal neurons (Foreleg Tarsi), (2) axonal neurites which cross the midline of the VNC in the prothoracic neuromere (Midline Crossing), (3-5) axonal neurites that project into the prothoracic (Prothorax), midthoracic (Midthorax), or

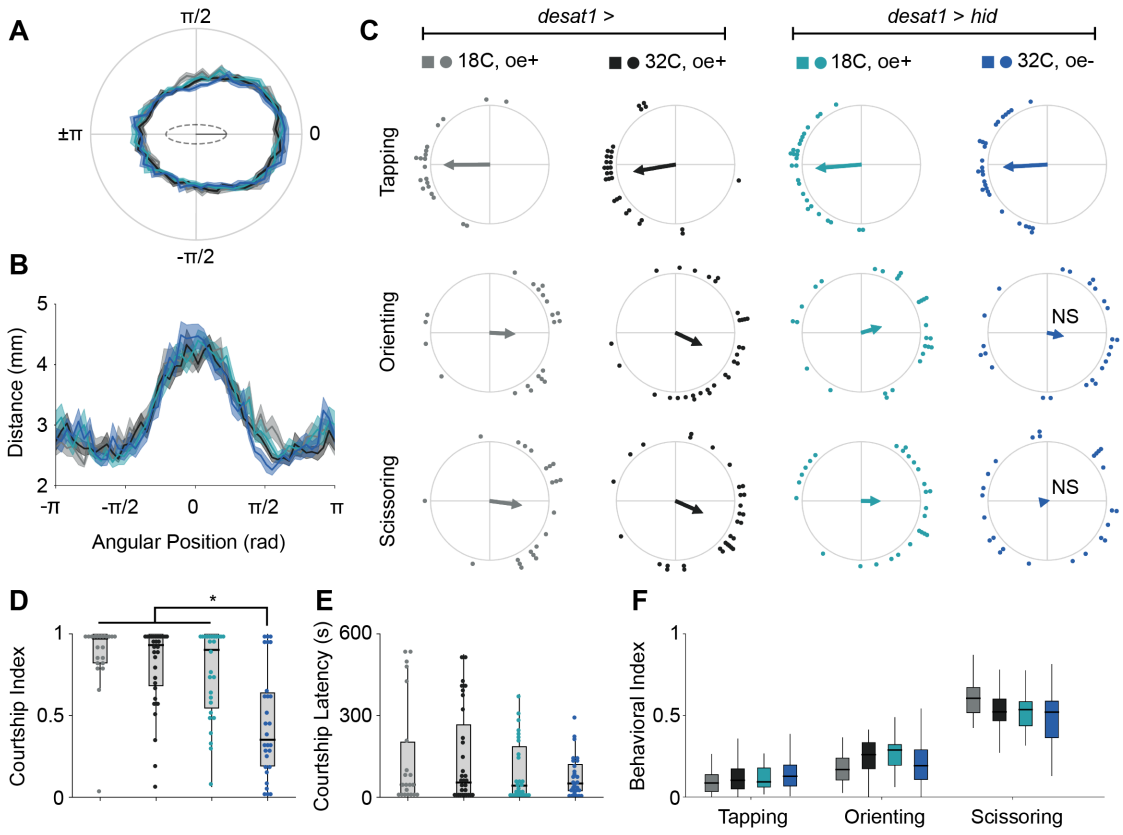

Figure 4.1: **Pheromones are important for spatial aspects of the courtship ritual and regulate courtship intensity. (A)** Average courtship paths of males courting pheromone-deficient females and their controls (color legend is shown in subplot C). **(B)** Same as (A), shown in Cartesian coordinates. **(C)** Average angular position of males during Tapping, Orienting, and Scissoring. Males courting oe- females did not display Orienting or Scissoring along locations significantly different from those of a uniform distribution ($p > 0.05$; Rayleigh Test). **(D)** The courtship index of males courting oe- females was significantly less than controls ($p < 0.05$; Kruskal Test with Bonferroni correction). **(E)** The courtship latency was not different between groups. **(F)** The fractions of time that each group spent in Tapping, Orienting, or Scissoring were not different between groups.

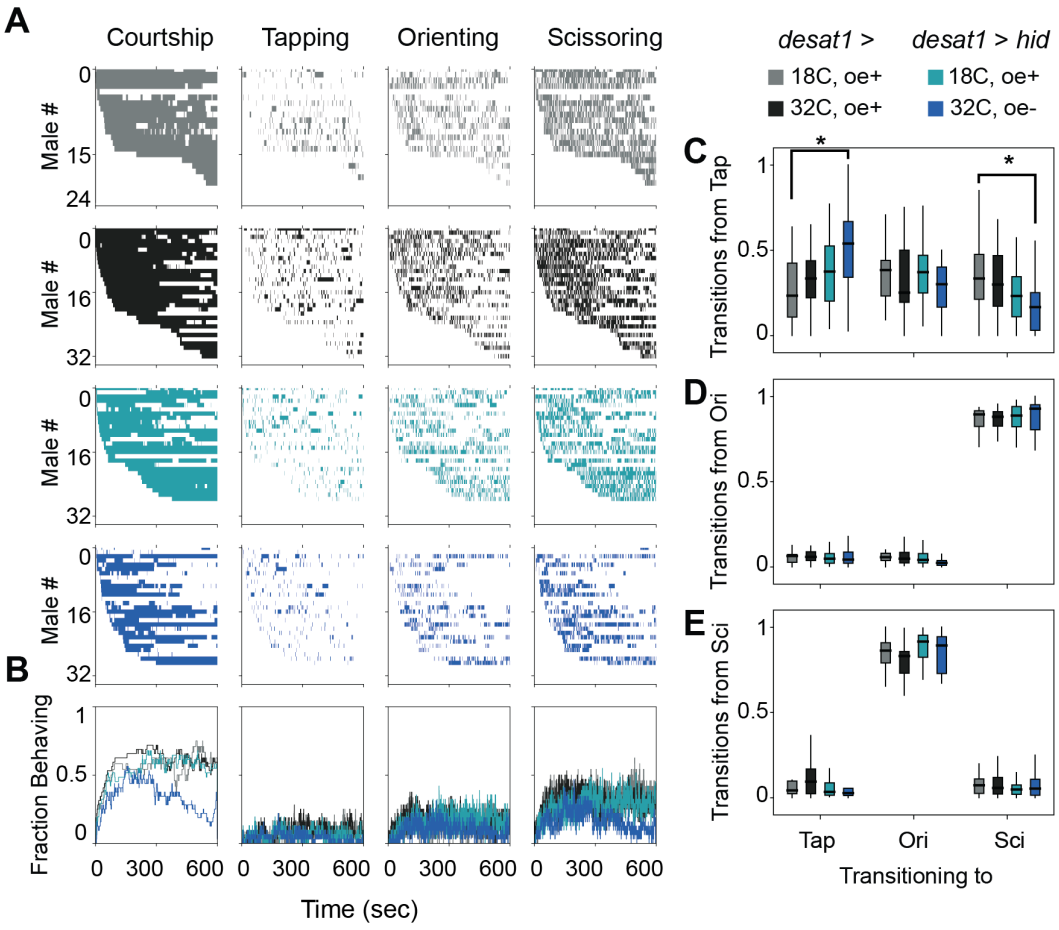

Figure 4.2: **Pheromones are important to sustain overall levels of courtship. (A)** Ethograms of bouts of Courtship, Tapping (Tap), Orienting (Ori), and Scissoring (Sci) (genotypes are shown in legend to the right). **(B)** Fractions of males engaging in Courtship, Tap, Ori, and Sci are shown over the entire duration of the courtship trial. **(C-E)** Behavioral transition frequency for flies transitioning from (C) Tap, (D) Ori, and (E) Sci to each of the behavioral states are shown for all groups. (C) Males courting oe- females transitioned from Tap to Tap more frequently than controls ($p < 0.05$; Krukal Test with Bonferroni correction) and transitioned from Tap to Sci less frequently than controls ($p < 0.05$; Krukal Test with Bonferroni correction).

hindthoracic (Hindthorax) neuromere in the VNC, and (6-7) axonal neurites that project into either the dorsal (Dorsal) or ventral (Ventral) portions of the VNC (Figure 4.3). Based on these various morphological characteristics, we were able to assign a hypothetical functional type to each cell population and identified 9 lines that marked neurons present in male legs with a likely sensory cell function (Figure 4.3A). The morphological feature that could best divide these sensory cells into the two biggest sub-groups was the presence (or absence) of 'Midline Crossing' neurites. We thus labeled these two groups as GRNs with foreleg axonal projections that cross the midline as GRN^{fap+} neurons and those that do not cross the midline as GRN^{fap-} neurons.

Previous studies have identified genetic markers that are expressed in leg neurons with GRN^{fap+} morphologies, including *pickpocket23* (*ppk23*), and have shown that *ppk23+* neurons are involved in mediating male courtship behaviors [Lu et al., 2012, Toda et al., 2012, Thistle et al., 2012, Lu et al., 2014]. However, whether *ppk23+* neurons encompass the entire population of GRN^{fap+} cells is not know. Therefore, we generated a transgenic line of flies that expresses that GAL4 inhibitor, GAL80, under the control of the *ppk23* promoter (*ppk23*^{GAL80}) to test the hypothesis that *ppk23+* cells include all GRN^{fap+} cells. We crossed this line to flies expressing GFP under the control of both GAL4 and the *pox neuro* (*poxn*^{GAL4}) promoter, which is a transcription factor expressed in every GRN, and found that no fluorescence was observable from midline-crossing neurites in offspring (Figure 4.3B). These results suggest that all GRN^{fap+} neurons are also *ppk23+* neurons, though we did not determine whether *ppk23+* cells are exclusively GRN^{fap+} cells. Nevertheless, *ppk23* can be used as a genetic marker for GRN^{fap+} cells (Figure 4.3).

We next sought to determine whether GRN^{fap+} cell bodies were enriched along any of the tarsal segments in male forelegs in an effort to better understand the organization of this group of neurons. To achieve this, we bilaterally amputated each of the foreleg tarsal segments in flies expressing GFP under the control of the *ppk23* promoter and then

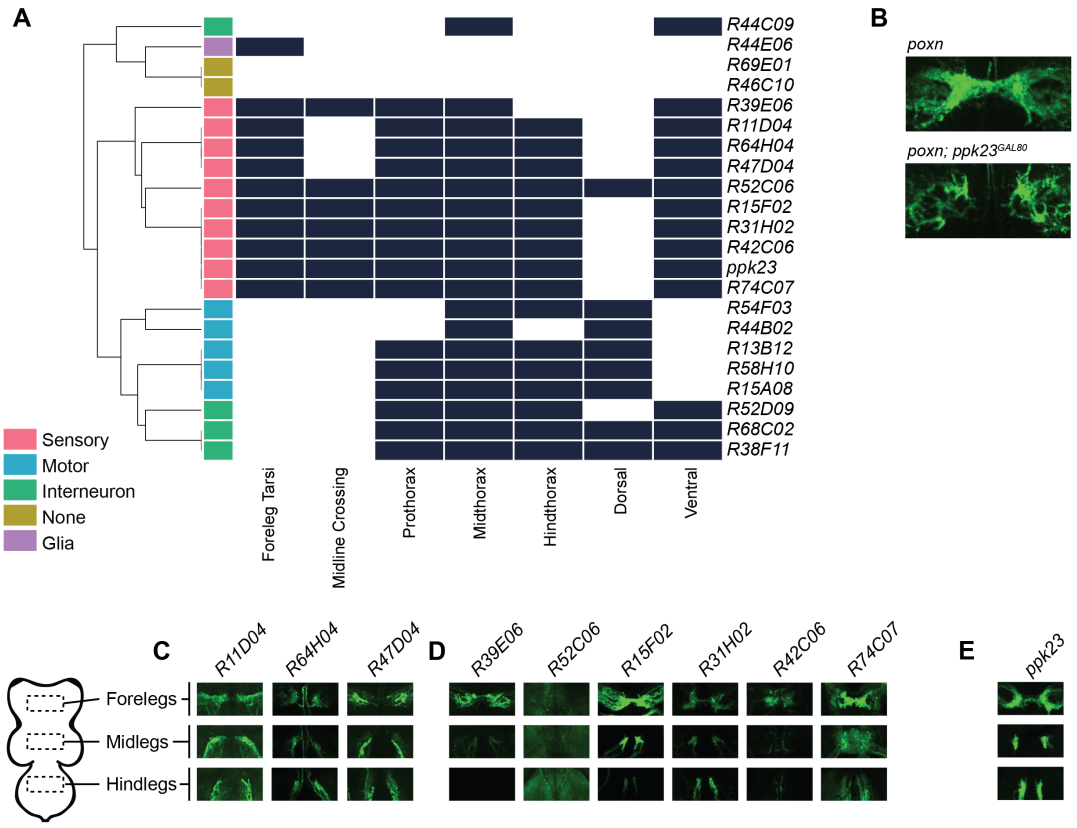

Figure 4.3: **There are two morphological classes of gustatory foreleg neurons. (A)** A morphological screen of 21 different Flylight lines revealed that foreleg sensory neurons come in two main classes: (1) those with axons that project across the midline of the VNC (GRN^{fap+}) and (2) those with axons that do not project across the midline (GRN^{fap-}). **(B)** All GRN^{fap+} neurons are encompassed by the *ppk23* promoter. Top image (*poxn>myr::GFP*) shows axonal projections in the VNC from foreleg GRNs. Bottom image (*poxn>myr::GFP; ppk23-GAL80*) shows axonal projections from foreleg GRNs, exclusive of *ppk23* neurites. **(C)** Confocal images (maximal intensity projection, Z-stacks) of axonal neurites projecting into the VNC from GRN^{fap-} neurons. Images are shown for neurons emanating from the forelegs (top), midlegs (middle), and hindlegs (bottom) for each line. **(D)** Same as in (C), shown for GRN^{fap+} neurons. **(E)** Confocal images of *ppk23+* axonal projections into the VNC.

quantified the amount of midline crossing (as GFP signal, termed the “Crossing Score”) present in the VNC (Figure 4.4). We found that as you sequentially amputate each of the tarsal segments (from T5 to T1), there is a near-linear decrease in the number of axonal fibers that cross the midline (Figure 4.4D). As *ppk23+* cell bodies are also distributed evenly across the tarsi (Figure 4.4B-C), these results suggest that GRN^{fap+} neurons are not enriched in any particular tarsal segment, but that they are distributed evenly across all tarsi.

4.3.3 GRN^{fap+} Neurons Regulate Courtship Maintenance

We next performed a neural inactivation screen on all of the sensory cell lines we identified in Section 2.3.2 and examined the effects of inactivation on courtship behavior. Specifically, we over-expressed the inwardly-rectifying potassium channel, *kir2.1*, in each of the GRN^{fap+} and GRN^{fap-} cell populations in a temperature-sensitive manner and recorded bouts of male courtship. We found large effects on the courtship index, but not on either the latency to court or the fraction of males engaging in courtship, following inactivation of GRN^{fap+} cells, but not GRN^{fap-} cells (Figure 4.5A). Further, the decrease in courtship index was a result of the inability of males to maintain bouts of courtship (Figure 4.6). Together, these results suggest that midline-crossing axons are an important feature of male foreleg GRNs that support sustained periods of courtship.

4.3.4 GRN^{fap+} Neurons Regulate Male-Female Distance, but Not Other Spatial or Temporal Aspects of Courtship

We then asked whether GRN^{fap+} neurons are important for regulating either the spatial positioning of males or the durations of time males spend within or transitioning between individual courtship elements. We therefore selected two GRN^{fap+} lines, *ppk23* and *R15F02*, along with a *UAS-kir2.1* control, and tracked and classified male bouts of

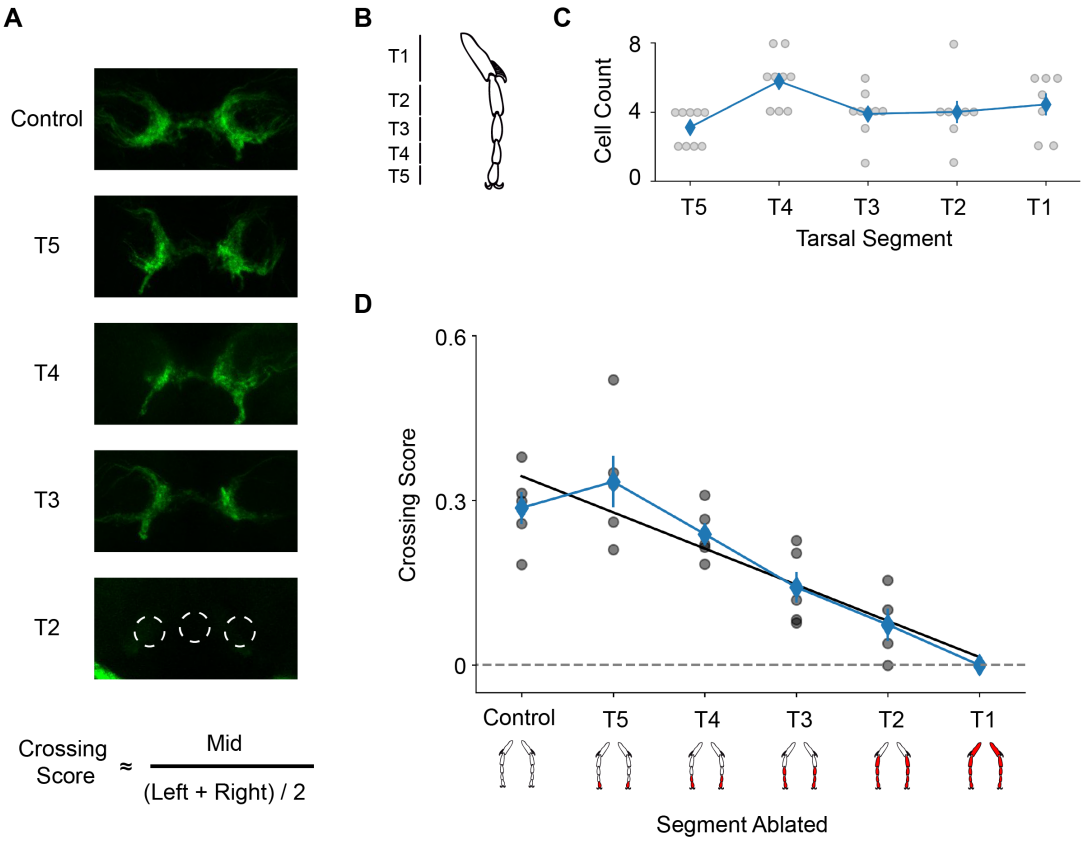

Figure 4.4: **GRN^{fap+} neurons are not enriched in any of the foreleg tarsi. (A)** Confocal images (maximal intensity projection, Z-stacks) of *ppk23+* axons projecting into the prothoracic neuromere of the VNC. Images are from flies that had not undergone tarsal amputation at the time of VNC dissection (Control), or from flies that had undergone bilateral amputation at their T5, T4, T3, T2, or T1 tarsi three days prior to VNC dissection. Crossing scores were calculated from these images and are approximately equal to the pixel intensity ratio of an area containing only GRN^{fap+} neurites to surrounding areas (see Eq. 4.1). **(B)** Schematic of the foreleg tarsal segments. **(C)** Total cell count of *ppk23+* neurons in each tarsal segment. **(D)** Crossing scores calculated following ablation of sequential tarsi. There is a mostly linear decrease in the crossing score, suggesting that GRN^{fap+} neurons are equally distributed across tarsi.

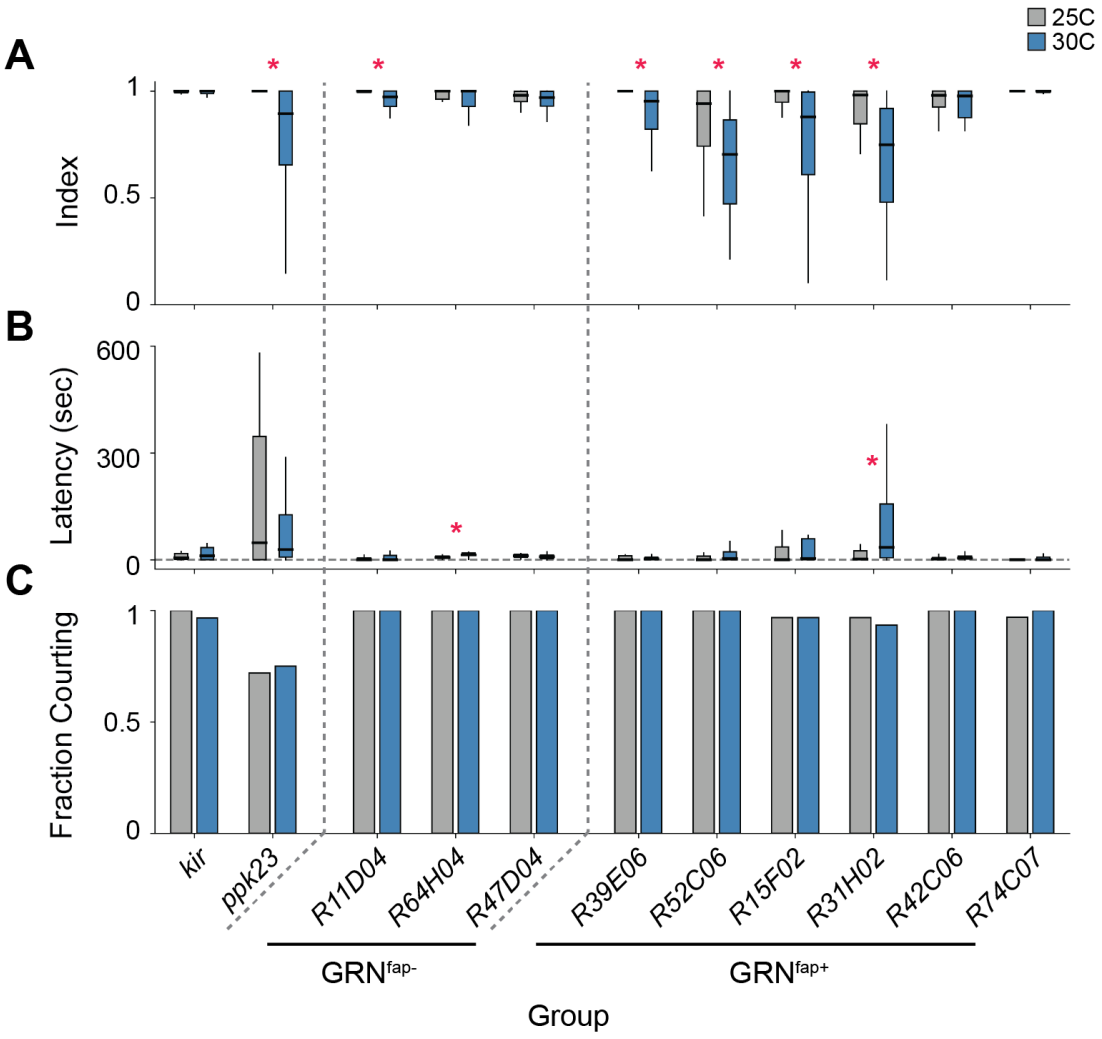

Figure 4.5: **GRN^{fap+} neurons regulate courtship intensity.** **(A)** Temperature-dependent inactivation of GRN^{fap+} neurons, but not GRN^{fap-} neurons, leads to large deficits in the courtship index. All flies in each comparison were the same genotype and included the inwardly-rectifying potassium channel, *kir2.1*, and the temperature-sensitive GAL80 (*GAL80ts*), which inhibits the expression of GAL4 at 25 ^{o}C, but not at 30 ^{o}C. Thus flies that were reared at 25 ^{o}C for the three days prior to the experiment do not express kir2.1, but those reared at 30 ^{o}C do express kir2.1. **(B-C)** Courtship latencies (B) and total fractions of flies engaging in courtship (C) were not associated with GRN$^{fap\pm}$ neurons.

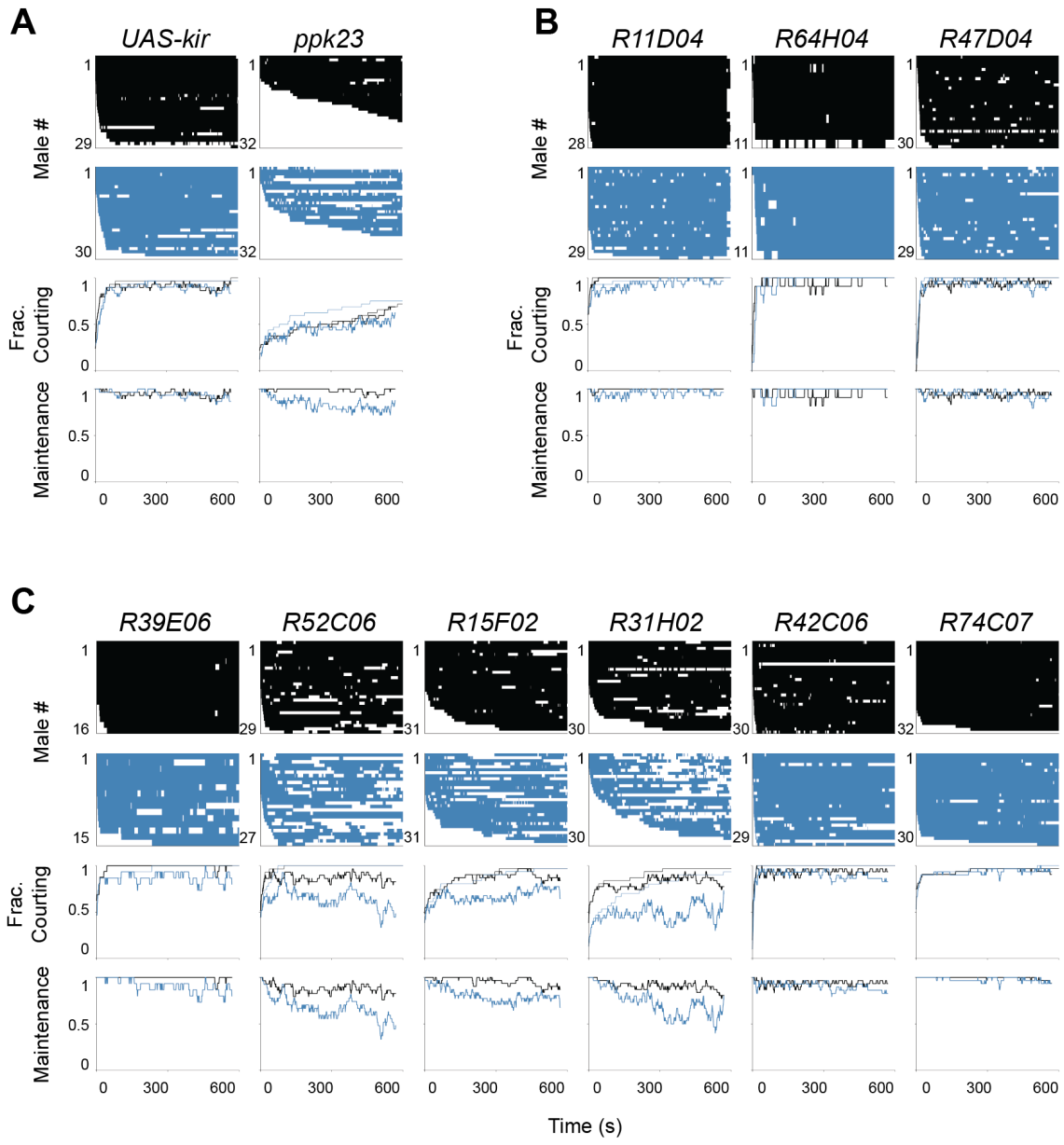

Figure 4.6: **GRN^{fap+} neurons are important for sustaining overall levels of courtship. (A)** Courtship ethograms for control (top, black) and experimental (top, blue) flies, along with total fractions of flies courting over time (middle) and maintenance indexes (bottom) are shown for the parental control, *UAS-kir*, and positive GRN^{fap+} control *ppk23*. **(B)** Same as in (A), shown for GRN^{fap-} lines. **(C)** Same as in (A), shown for GRN^{fap+} lines.

tapping, scissoring, and orienting during courtship trials following temperature-dependent inactivation of neurons by *kir2.1* (Figure 4.7). We found that there were deficits in the distances that males positioned themselves from females during courtship; more specifically, inactivation of both *ppk23*$^{+}$ and *R15F02*$^{+}$ neurons led to increases in male-female distance ($p < 0.05$ for mean distance across all angles, One-way ANOVA; Figure 4.7A). However, the mean angular locations of male tapping, orienting, and scissoring were unaffected following neural inactivation in all lines we examined ($p > 0.05$, Watson-Williams Tests comparing control to experimental groups for each genotype; Figure 4.7A). Oddly, the mean tapping locations for both temperatures in the control genotype (*UAS-kir*) were directed towards the anterior end of the female ($p < 0.05$, Rayleigh Test; Figure 4.7A, left panel). While we currently do not have an explanation for this, the background of the *UAS-kir* line appeared to have lighter-colored eyes than resultant offspring from crosses with *ppk23/R15F02* flies (data not shown); it is possible loss of visual acuity due to decreased eye pigmentation [Burnet et al., 1968] led to these deficits. Nevertheless, since both groups in the *UAS-kir* experiment were not different from one another, our findings that spatial courtship parameters are mostly unaffected following neural inactivation of GRN^{fap+} remains valid.

We further examined the fractions of time that males spent in each behavioral state during courtship and found no differences between control and experimental groups for all lines we examined (Figure 4.7B). Accordingly, the frequencies of transitioning from one behavioral state to another were similar between control and experimental groups for each line, though there were some minor differences (Figure 4.7C). These data, together with the data shown in Section 2.3.3, suggest that while GRN^{fap+} neurons regulate overall levels of courtship, they do not regulate most spatial aspects of courtship (with the exception of distance), nor do they regulate the time or frequency of transition between individual behavioral states. Rather, GRN^{fap+} neurons — and the pheromones they detect — are important for generating the drive to remain within a mating state that promotes courtship.

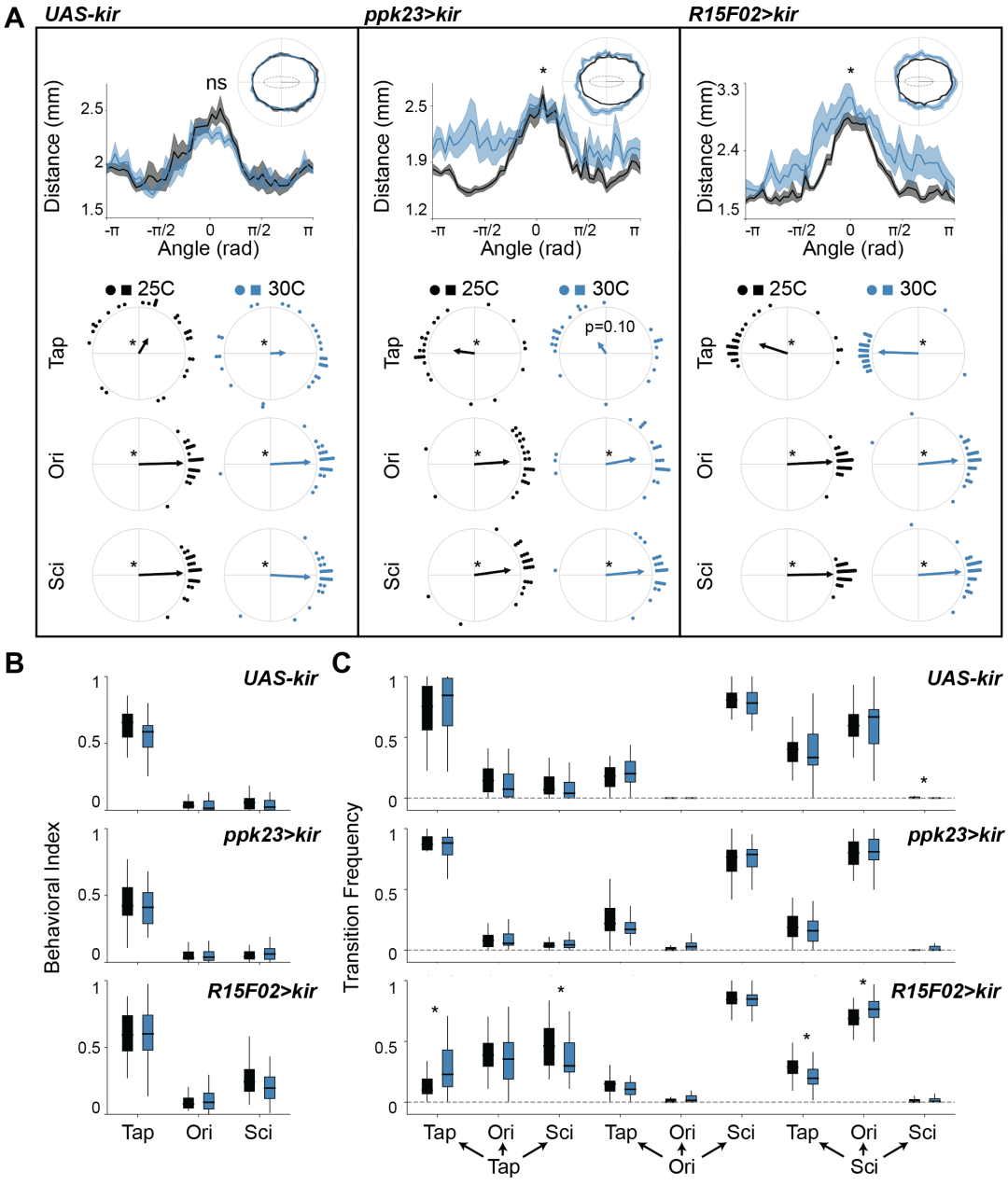

Figure 4.7: **GRN^{fap+} neurons regulate male-female distance, but not other spatiotemporal courtship parameters. (A)** Male-to-female distances during courtship and mean angular locations of males during bouts of tapping (Tap), orienting (Ori), and scissoring (Sci) for *UAS-kir* controls and the GRN^{fap+}, *ppk23*, and *R15F02* lines. Asterisks in distance plots signify that there was a significant difference in the average (across all angles) male-female distance between control (black) and experimental (blue) groups ($p < 0.05$, One-way ANOVA). Asterisks in angular plots signify that behavioral locations were significantly different from uniformity ($p < 0.05$, Rayleigh Test). Caption continued on next page.

Figure 4.7: **(B)** Individual levels of different courtship elements are shown for *UAS-kir*, *ppk23*, and *R15F02* lines. There were no significant differences between any of the experimental and control groups for each genotype. **(C)** Transitions between Tap, Ori, and Sci, are shown for each line. Asterisks signify significant differences between groups ($p < 0.05$, One-way ANOVA).

The subsequent decision to engage in any particular mode of courtship, for instance, one which biases the display of scissoring over tapping, seems to be dependent on other sensory circuits. Since we did not find robust spatial deficits that aligned with those following ablation of female pheromone-producing cells (Figure 4.1), we decided to focus specifically on the role of GRN^{fap+} neurons in the regulation of courtship drive, as described below.

4.3.5 GRN^{fap+} Midline-Crossing Axonal Projections Regulate Courtship Maintenance

We then asked whether the regulation of courtship maintenance by GRN^{fap+} neurons was specifically due to signaling mediated via midline-crossing axonal projections. Previous research has shown that midline-crossing by foreleg axonal projections in the VNC is regulated, in part, by the chemotrophic factor *roundabout-1* (*robo1*) [Mellert et al., 2010, Ito et al., 2016] and that over-expression of *robo1* in *poxn+* neurons prevents axonal midline-crossing [Mellert et al., 2010]. We therefore prevented axonal projections from crossing the midline during development by over-expressing *robo1* in *poxn+* neurons and examined the effects on male courtship behavior (Figure 4.8).

We found that eliminating midline-crossing from GRN^{fap+} neurons led to a significantly decreased courtship index when compared to controls ($p < 0.05$, Kruskal Test; Figure 4.8B), but it did not impact the latency at which males started to court females ($p > 0.05$, Kruskal Test; Figure 4.8C). Further, the decrease in courtship index was a result of an inability of males to maintain long bouts of courtship; whereas control males displayed rela-

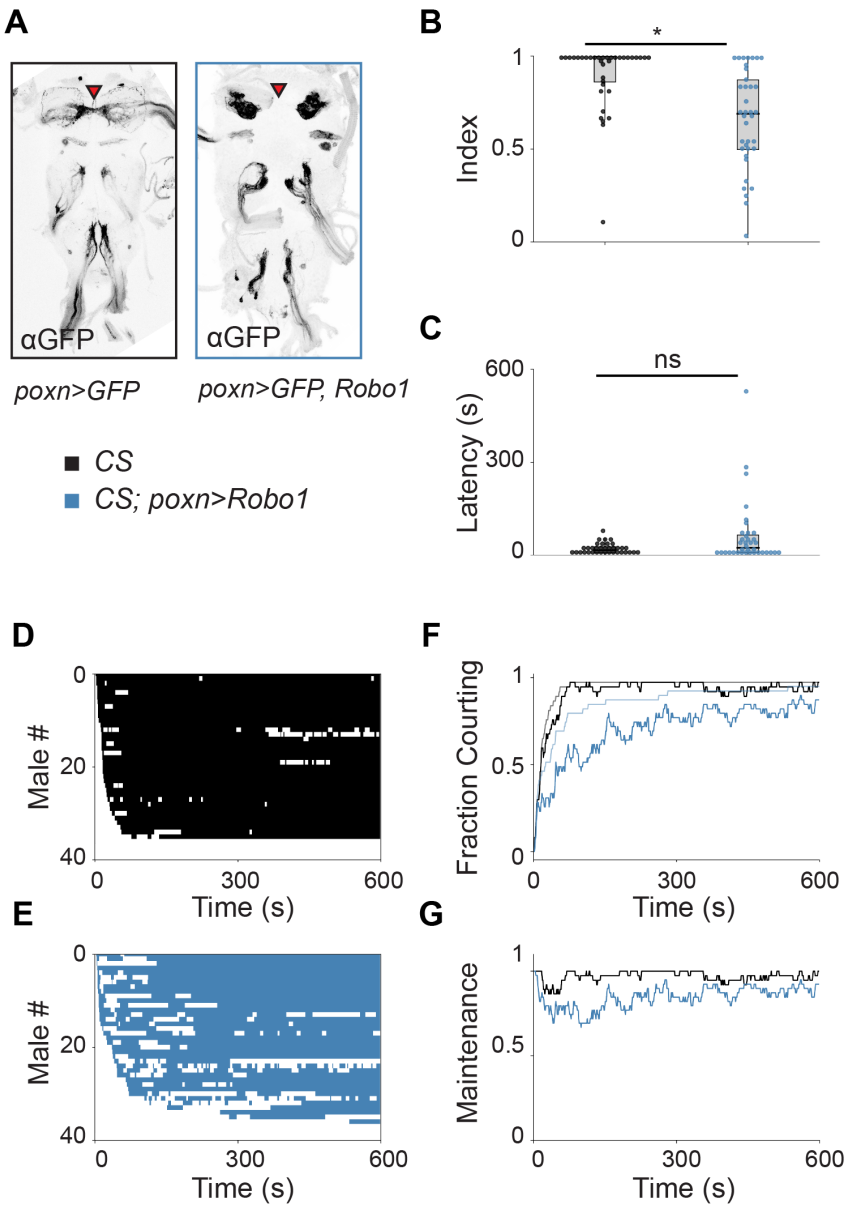

Figure 4.8: **GRN^{fap+} axonal midline crossing is necessary for the maintenance of courtship.** **(A)** Over-expression of Robo1 in *poxn+* neurons prevents axonal midline crossing in GRN^{fap+} neurons. (Left) GFP expression in *poxn+* neurons. (Right) GFP expression in *poxn+* neurons over-expressing Robo1. **(B)** The courtship index is decreased in *CS; poxn>Robo1* males ($p < 0.01$, Kruskal Test), but **(C)** the courtship latency is intact ($p > 0.05$, Kruskal Test). **(D-E)** Ethograms showing bouts of courtship for *CS* and *CS;poxn>Robo1* males. **(F)** Fractions of males engaging in courtship over time (thick lines) shown along with cumulative fractions of males engaging in courtship (thin lines) for each group of flies. **(G)** Courtship maintenance is impaired in *CS;poxn>Robo1* males.

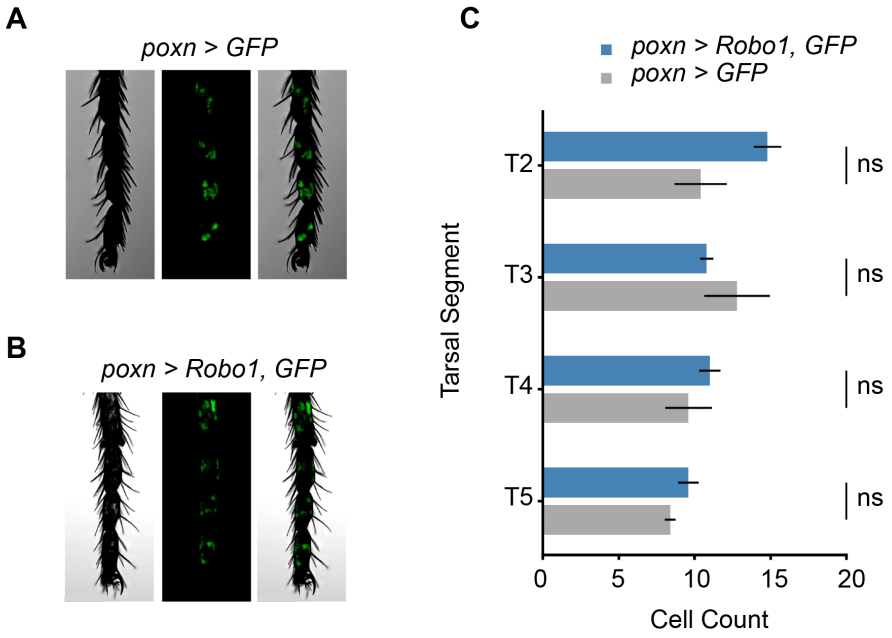

Figure 4.9: **Inhibiting midline crossing in GRN^{fap+} neurons does not lead to cell death. (A-B)** Confocal images (maximal projection, Z-stack) of *poxn+* neurons in control flies (A, *poxn>GFP*) and in flies that overexpress Robo1 in *poxn+* neurons (B, *poxn>GFP, Robo1*). **(C)** Quantification of *poxn+* cells in each tarsal segment in *poxn>GFP* and *poxn>Robo1, GFP* flies.

tively uninterrupted courtship, the bouts of experimental male courtship were fragmented (Figure 4.8D-G). Importantly, while cell death can result as a consequence of improperly formed synapses [Hyman and Yuan, 2012], cell death did not result in GRNs following the over-expression of Robo1 (Figure 4.9). These results suggest that VNC midline-crossing, specifically, from foreleg GRNs is required for males to maintain courtship.

4.4 Discussion

In this chapter, I examined the roles of both female pheromones and foreleg GRNs in directing specific aspects of the male courtship ritual. Using the quantitative methodologies for characterizing spatiotemporal aspects of courtship I developed in Chapters 2–3, I demonstrated a novel role for female pheromones in directing male spatial displays dur-

ing courtship. While previous work has shown that various female pheromones can either increase or decrease levels of male courtship, no work has previously shown that female pheromones can alter the behavioral positioning of males during courtship displays [Ferveur, 2005, Billeter et al., 2009]. Additionally, I highlighted two distinct classes of foreleg GRNs — GRN^{fap+} and GRN^{fap-} — that serve varied roles in mediating mating behaviors in male flies. Along with distinguishing between their roles in driving courtship behaviors in *Drosophila* males, I also identified a unique morphological feature of GRN^{fap+} neurons that functions to sustain levels of courtship: the sexually dimorphic axonal midline crossing of GRNs within the prothoracic neuromere of the VNC. The results presented in this chapter build upon previous research in the field of behavioral neuroethology and add new data and approaches for trying to understand how specific neural circuit architectures can lead animals to make specific behavioral decisions.

The behavioral data presented in this chapter suggest that female oenocyte-generated pheromones play a role in directing the spatial release of specific courtship displays by males; however, we did not investigate the identity of that compound. The pheromonal profile of the female fly is quite complex and consists of many different classes of chemical compounds [Antony and Jallon, 1982, Everaerts et al., 2010, Yew et al., 2008]. Previous research has shown that the most abundant compound present on and specific to the female fly is the hydrocarbon 7,11-heptacosadiene (7,11-HD) and most GRN^{fap+} cells seem to be responsive to this pheromone [Toda et al., 2012, Pikielny, 2012, Kallman et al., 2015, Liu et al., 2018, Kimura et al., 2018]. While 7,11-HD has been shown to act as an excitatory pheromone by functioning to stimulate male courtship [Toda et al., 2012], it's role in coordinating the location of spatial courtship displays in male flies remains unclear. It would be interesting to try and determine the specific identity of the female pheromone(s) responsible for mediating this effect. While studies have examined whether 7,11-HD can function as a chemoattractant, there have been no indications that it plays a role in directing the spatial positioning of males during courtship or other social interactions [Agrawal

et al., 2014]. Identifying those compounds that provide spatial information during complex behaviors could be an exciting area of investigation in future studies.

Our results also suggest that in addition to providing behavioral stimulation to males during courtship, GRN^{fap+} cells require commissural connections for proper courtship maintenance. While 7,11-HD could be a key pheromone providing this excitatory input, the exact circuit-level mechanisms that sustain courtship are not known. We did not test whether contralateral GRN^{fap+} axons make synaptic connections with one another, but if this were the case, axo-axonal excitation may be an important component of this circuit which fuels increased courtship drive. Alternatively, contralateral inputs to any downstream neurons could provide this excitatory input. Either way, upon unilateral pheromonal stimulation, contralateral connections could place the entire nervous system into an excitatory state; without these connections half of the drive needed to maintain courtship might be lost, thus leading to decreased levels of courtship (as seen in Figure 4.8). Though we did not investigate the exact mechanisms by which GRN^{fap+} projections regulate the maintenance of courtship, it will be important for future studies to address this question for understanding both general circuit function and behavioral decision making.

Chapter 5: Conclusions and Future Directions

Mating rituals vary across diverse animal species, yet they retain many common features which make them interesting systems within which to study decision making. Male *Drosophila* are particularly well-suited for determining the sensory and circuit-level mechanisms that direct mating displays. They engage in a stereotyped and complex courtship ritual when exposed to female conspecifics, and the neural circuitry that underlies some of these mating behaviors has started to be worked out. Within this dissertation, I have developed tools to help quantify the courtship ritual more easily and with a higher spatiotemporal resolution than previously and identified and furthered our understanding of the various visual and chemosensory cues and circuits that mediate behavioral choice in male flies. These results should provide insight for subsequent research aimed at determining how animals choose to engage in alternative behaviors when presented with specific environmental scenarios.

Both visual and chemosensory cues are crucial to the mating success of male flies [Greenspan and Ferveur, 2000]. Here, I demonstrated that whereas visual cues seem to mediate both spatial and temporal aspects of male courtship, chemosensory cues — signalled through GRNs with axonal projects that cross the midline of the VNC — seem to be involved in mainly increasing the sexual drive of a male towards a virgin female fly. While I present a simplified model and description of my findings in Figure 5.1, there are many aspects of this work that warrant further research as I discuss below.

Starting with early investigations into the visual acuity of the fly [Hecht and Wald, 1934], researchers have been interested in understanding how visual stimuli are processed to produce behavioral responses. One behavioral response that has been particularly important for our understanding of how the fly visual system works is the optomotor response (OR) [Borst et al., 2010, Haikala et al., 2013]. In the OR, a fly adjusts its heading in re-

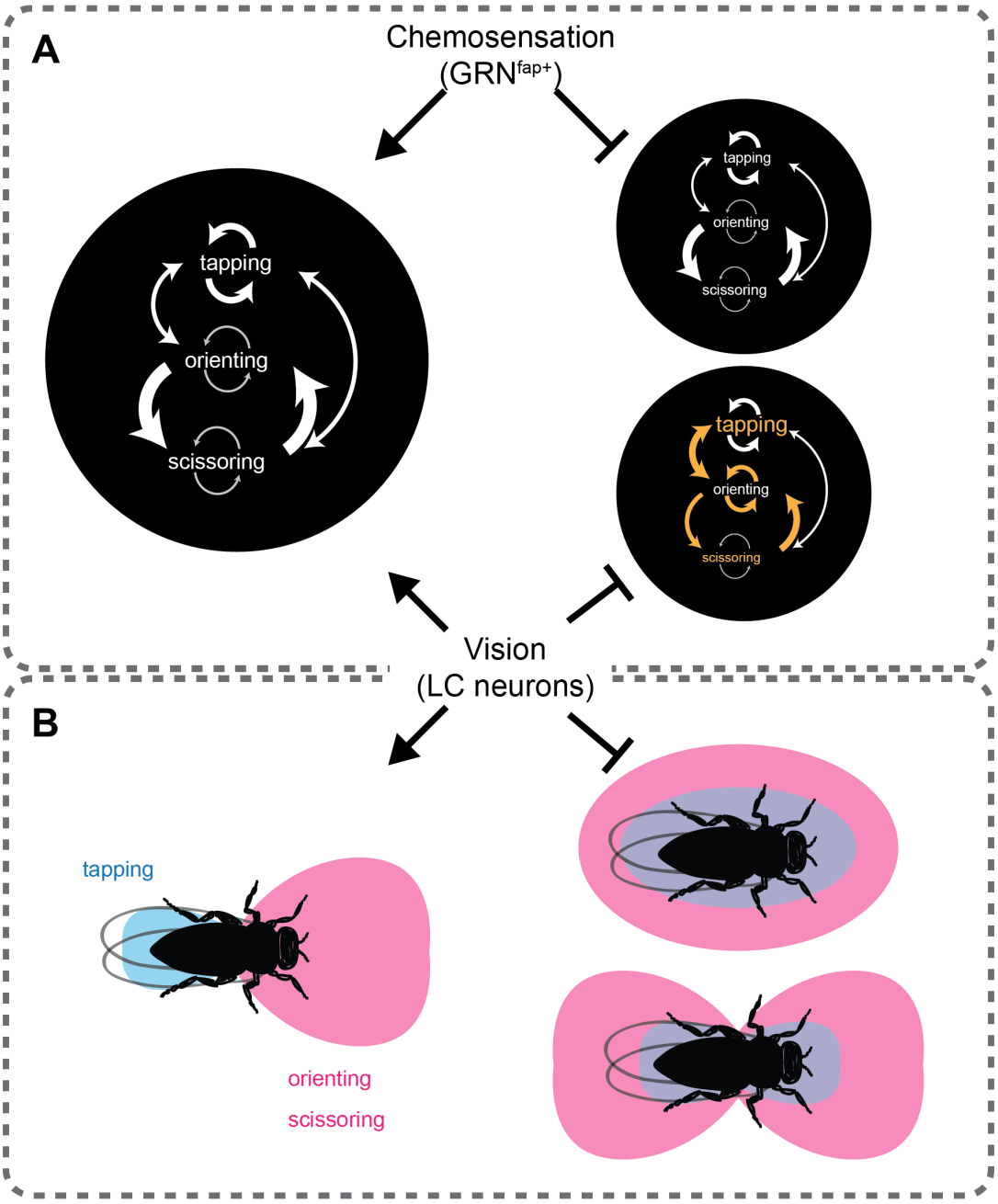

Figure 5.1: **A model of visual and chemosensory inputs related to male courtship.** **(A)** Both vision and chemosensation play roles in mediating the temporal aspects of the male courtship ritual. A schematic of the behavioral components of the courtship ritual are shown by inter-connected arrows within each circle: the size of each circle is proportional to the total amount of time a male spent in courtship; the size and direction of the arrows within each circle are proportional to the fraction of transitions between behavioral elements; and the size of the behavioral label ('tapping', 'orienting', and 'scissoring') is proportional to the amount of time a male spent in each behavioral state during courtship. Caption continued on next page.

Figure 5.1: Colored arrows signify changes in the proportion of transitioning between specific behavioral elements following sensory- or circuit-level manipulations. Whereas suppressing chemosensory signalling through GRN^{fap+} neurons seems to simply decrease the overall amount of courtship, without changing the the amounts of time spent in any particular behavioral state, inhibiting visual signalling both deceases overall courtship and alters the transitional and temporal structure of the courtship ritual. **(B)** Visual signalling, but not chemosensory signalling through GRN^{fap+} neurons, alters the spatial positioning of males during courtship. Blue shaded regions represent location distributions around the female where tapping occurs; pink shaded regions represent location distributions around the female where orienting/scissoring occur. With vision intact, males tap the female on the posterior end and orient/scissor towards the female on the anterior end. Inhibiting visual signalling leads to either complete loss of directionality in orienting/scissoring locations or directs these behaviors to either end of the female's antero-posterior body axis.

sponse to moving bars of alternating light and dark such that the rotation of its body aligns with the direction of the bars' movement. While the ethological purpose of this behavioral response is not entirely clear, it is interesting to consider whether the OR plays a natural role mediating male behavior during the courtship ritual. In particular, the banding pattern on the abdomen of the female closely resembles the contrasting bars of light presented to a fly during the OR. Does the ego-motion of a male around a female during courtship make this banding pattern appear to be moving and thus initiate a rotational response by the male? This would assure that the male's heading remains directed at his courtship target. Further, previous research has shown that ego-motion visual cues, which are sensed as optic flow across the retina, are encoded by visual descending neurons to control flight patterns in the fly [Suver et al., 2016]. Are there similar visual neurons that encode for ego-motion-induced optic flow to generate an OR-like response in males as they engage in courtship? My results presented in Chapter 3 suggest that while the head of the female plays a crucial role in the spatiotemporal dynamics of male courtship, it is not the only visual signal required for appropriate behavioral responses. It would be interesting for future studies to try to determine the identity of these other visual signals and to connect the OR to naturalistic behaviors espoused by males during courtship.

The neuronal architecture that regulates mating decisions in the fly is complex, and in-

cludes many features which likely play distinct roles in mediating different aspects of behavior. While my results overall suggest that GRN^{fap+} neurons are important for increasing courtship drive in males, the precise role(s) of GRN^{fap-} neurons in courtship behavior are largely unknown. For instance, while some GRN^{fap-} have been shown to express *fru* [Kimura et al., 2018], and are thus a component of the male sex circuit, we do not know the behavioral role of these particular cells. It is possible that these neurons actually inhibit courtship behaviors. Indeed, previous work has shown that *fru/ppk23*$^{+}$ neurons are responsive to pheromones that can either increase or decrease levels of male courtship [Thistle et al., 2012, Kallman et al., 2015]. Do *fru/ppk23*$^{+}$ GRNs with different axonal architectures play alternative roles in the detection of pheromones? For instance, do GRN^{fap+} cells detect excitatory pheromones which promote courtship whereas GRN^{fap-} detect inhibitory ones which suppress it? Unfortunately, my work could not determine this due to a ceiling effect in the courtship index, where control flies were almost always courting. Experiments examining male courtship towards mated females could distinguish between these two scenarios, as males tend to court mated females less than virgins; thus, a ceiling effect should be preventable. Future research should provide insights into the specific cell types that detect various pheromones and how these neurons regulate social behaviors.

Recent work has started to examine how signals from disparate sensory circuits interact with one another to produce behavior [Stein et al., 2014]. In particular, the fly has started to be used as a model for this research as the neural circuits that coordinate various behavioral responses have become better characterized [Duistermars and Frye, 2010, LaRue et al., 2015, Hu et al., 2017]. In my work, I demonstrated that both visual and non-GRN chemosensory cues are likely utilized by males for localization of female body axis during courtship. While my experiments were not designed to directly test interactions between visual and chemosensory circuits, we did find that even when visual inputs are intact, loss of female pheromonal cues leads to disrupted male spatial posi-

tioning. These results suggest that concurrent inputs from both sensory modalities are required for appropriate mating decisions. Future experiments could examine how these inputs are integrated in the nervous system to generate specific behavioral responses. In particular, P1 interneurons in the brain have been shown to respond to both visual and chemosensory stimuli [Pan et al., 2012, Kohatsu and Yamamoto, 2015, Clowney et al., 2015] and are known to be important for regulating overall courtship drive; however, the physiology of these neurons in response to both visual and chemosensory inputs has not been examined. As P1 neurons are believed to be the central integration center for commanding male sexual behavior, understanding the circuit-level mechanisms that allow for these neurons to coordinate multiple aspects of courtship will be an important goal for the field in the future.

References

Jan M. Ache, Jason Polsky, Shada Alghailani, Ruchi Parekh, Patrick Breads, Martin Y. Peek, Davi D. Bock, Catherine R. von Reyn, and Gwyneth M. Card. Neural Basis for Looming Size and Velocity Encoding in the Drosophila Giant Fiber Escape Pathway. Current Biology, 0(0), February 2019. ISSN 0960-9822. doi: 10.1016/j.cub.2019.01.079.

S Agrawal, S Safarik, and M Dickinson. The relative roles of vision and chemosensation in mate recognition of Drosophila melanogaster. J Exp Biol, 217(Pt 15):2796–2805, 2014.

Marcus J. Allen, Tanja A. Godenschwege, Mark A. Tanouye, and Pauline Phelan. Making an escape: Development and function of the Drosophila giant fibre system. Seminars in Cell & Developmental Biology, 17(1):31–41, February 2006. ISSN 1084-9521. doi: 10.1016/j.semcdb.2005.11.011.

C Antony, T L Davis, D A Carlson, J M Pechine, and J M Jallon. Compared behavioral responses of maleDrosophila melanogaster (Canton S) to natural and synthetic aphrodisiacs. J Chem Ecol, 11(12):1617–1629, 1985.

Claude Antony and Jean-Marc Jallon. The chemical basis for sex recognition in Drosophila melanogaster. Journal of Insect Physiology, 28(10):873–880, January 1982. ISSN 0022-1910. doi: 10.1016/0022-1910(82)90101-9.

R. A. Baines, J. P. Uhler, A. Thompson, S. T. Sweeney, and M. Bate. Altered electrical properties in Drosophila neurons developing without synaptic transmission. The Journal of Neuroscience: The Official Journal of the Society for Neuroscience, 21(5):1523–1531, March 2001. ISSN 1529-2401.

G J Berman, D M Choi, W Bialek, and J W Shaevitz. Mapping the stereotyped behaviour of freely moving fruit flies. J R Soc Interface, 11(99), 2014.

Shuangyu Bi and Victor Sourjik. Stimulus sensing and signal processing in bacterial chemotaxis. Current Opinion in Microbiology, 45:22–29, October 2018. ISSN 1369-5274. doi: 10.1016/j.mib.2018.02.002.

J C Billeter, J Atallah, J J Krupp, J G Millar, and J D Levine. Specialized cells tag sexual and species identity in Drosophila melanogaster. Nature, 461(7266):987–991, 2009.

N Boeddeker, R Kern, and M Egelhaaf. Chasing a dummy target: Smooth pursuit and velocity control in male blowflies. Proc Biol Sci, 270(1513):393–399, 2003.

W Boll and M Noll. The Drosophila Pox neuro gene: Control of male courtship behavior and fertility as revealed by a complete dissection of all enhancers. Development, 129 (24):5667–5681, 2002.

Alexander Borst and Moritz Helmstaedter. Common circuit design in fly and mammalian motion vision. Nature Neuroscience, 18(8):1067–1076, August 2015. ISSN 1546-1726. doi: 10.1038/nn.4050.

Alexander Borst, Juergen Haag, and Dierk F. Reiff. Fly Motion Vision. Annual Review of Neuroscience, 2010. ISSN 0147-006X. doi: 10.1146/annurev-neuro-060909-153155.

K Branson, A A Robie, J Bender, P Perona, and M H Dickinson. High-throughput ethomics in large groups of Drosophila. Nat Methods, 6(6):451–457, 2009.

Barrie Burnet, Kevin Connolly, and John Beck. Phenogenetic studies on visual acuity in Drosophila melanogaster. Journal of Insect Physiology, 14(6):855–860, June 1968. ISSN 0022-1910. doi: 10.1016/0022-1910(68)90196-0.

F. M. Butterworth. Lipids of Drosophila: A newly detected lipid in the male. Science (New York, N.Y.), 163(3873):1356–1357, March 1969. ISSN 0036-8075.

Gwyneth M. Card. Escape Behaviors in Insects. 2012. ISBN 1873-6882. doi: 10.1016/j.conb.2011.12.009.

C. E. Carr and M. Konishi. Axonal delay lines for time measurement in the owl's brainstem. Proceedings of the National Academy of Sciences of the United States of America, 85 (21):8311–8315, November 1988. ISSN 0027-8424.

Jan Clemens, Philip Coen, Frederic A. Roemschied, Talmo D. Pereira, David Mazumder, Diego E. Aldarondo, Diego A. Pacheco, and Mala Murthy. Discovery of a New Song Mode in Drosophila Reveals Hidden Structure in the Sensory and Neural Drivers of Behavior. Current Biology, 28(15):2400–2412.e6, August 2018. ISSN 0960-9822. doi: 10.1016/j.cub.2018.06.011.

E J Clowney, S Iguchi, J J Bussell, E Scheer, and V Ruta. Multimodal Chemosensory Circuits Controlling Male Courtship in Drosophila. Neuron, 87(5):1036–1049, 2015.

Philip Coen, Jan Clemens, Andrew J. Weinstein, Diego A. Pacheco, Yi Deng, and Mala Murthy. Dynamic sensory cues shape song structure in Drosophila. Nature, 507(7491): 233–237, March 2014. ISSN 1476-4687. doi: 10.1038/nature13131.

Philip Coen, Marjorie Xie, Jan Clemens, and Mala Murthy. Sensorimotor Transformations Underlying Variability in Song Intensity during Drosophila Courtship. Neuron, 89(3): 629–644, February 2016. ISSN 1097-4199. doi: 10.1016/j.neuron.2015.12.035.

Kevin M Collins, Addys Bode, Robert W Fernandez, Jessica E Tanis, Jacob C Brewer, Matthew S Creamer, and Michael R Koelle. Activity of the C. elegans egg-laying behavior circuit is controlled by competing activation and feedback inhibition. eLife, 5:e21126, November 2016. ISSN 2050-084X. doi: 10.7554/eLife.21126.

Kevin Connolly, Barrie Burnet, and David Sewell. Selective mating and eye pigmentation: An analysis of the visual component in he courtship behavior of Drosophila melanogaster. Evolution, 23(4):548–559, 1969. doi: 10.1111/j.1558-5646.1969.tb03540.x.

Robert Cook. The courtship tracking of Drosophila melanogaster. Biological Cybernetics, 34(2):91–106, October 1979. ISSN 1432-0770. doi: 10.1007/BF00365473.

Robert Cook. The extent of visual control in the courtship tracking of D. melanogaster. Biological Cybernetics, 37(1):41–51, May 1980. ISSN 1432-0770. doi: 10.1007/BF00347641.

S. Crossley and E. Zuill. Courtship behaviour of some Drosophila melanogaster mutants. Nature, 225(5237):1064–1065, March 1970. ISSN 0028-0836.

Heiko Dankert, Liming Wang, Eric D. Hoopfer, David J. Anderson, and Pietro Perona. Automated monitoring and analysis of social behavior in Drosophila. Nature Methods, 2009. ISSN 15487091. doi: 10.1038/nmeth.1310.

Anne-Sophie Darmaillacq, Nawel Mezrai, Caitlin E. O'Brien, and Ludovic Dickel. Visual Ecology and the Development of Visually Guided Behavior in the Cuttlefish. Frontiers in Physiology, 8, 2017. ISSN 1664-042X. doi: 10.3389/fphys.2017.00402.

S R Datta, M L Vasconcelos, V Ruta, S Luo, A Wong, E Demir, J Flores, K Balonze, B J Dickson, and R Axel. The Drosophila pheromone cVA activates a sexually dimorphic neural circuit. Nature, 452(7186):473–477, 2008.

E Demir and B J Dickson. Fruitless splicing specifies male courtship behavior in Drosophila. Cell, 121(5):785–794, 2005.

B J Duistermars, D M Chow, and M A Frye. Flies require bilateral sensory input to track odor gradients in flight. Curr Biol, 19(15):1301–1307, 2009.

Brian J Duistermars and Mark A Frye. Multisensory integration for odor tracking by flying Drosophila. Communicative & Integrative Biology, 3(1):60–63, 2010. ISSN 1942-0889.

L. Eastwood and B. Burnet. Courtship latency in male Drosophila melanogaster. Behavior Genetics, 7(5):359–372, September 1977. ISSN 0001-8244.

L. Ehrman. A genetic constitution frustrating the sexual drive in Drosophila paulistorum. Science (New York, N.Y.), 131(3410):1381–1382, May 1960. ISSN 0036-8075.

A Ejima and Griffith. Courtship initiation is stimulated by acoustic signals in Drosophila melanogaster. PLOS ONE, 3(9), 2008. doi: 0.1371/journal.pone.0003246.

Damian O. Elias, Wayne P. Maddison, Christina Peckmezian, Madeline B. Girard, and Andrew C. Mason. Orchestrating the score: Complex multimodal courtship in the Habronattus coecatus group of Habronattus jumping spiders (Araneae: Salticidae). Biological Journal of the Linnean Society, 105(3):522–547, March 2012. ISSN 0024-4066. doi: 10.1111/j.1095-8312.2011.01817.x.

Timothy A. Evans, Celine Santiago, Elise Arbeille, and Greg J. Bashaw. Robo2 acts in trans to inhibit Slit-Robo1 repulsion in pre-crossing commissural axons. eLife, 4: e08407, July 2015. ISSN 2050-084X. doi: 10.7554/eLife.08407.

Claude Everaerts, Jean-Pierre Farine, Matthew Cobb, and Jean-François Ferveur. Drosophila cuticular hydrocarbons revisited: Mating status alters cuticular profiles. PloS One, 5(3):e9607, March 2010. ISSN 1932-6203. doi: 10.1371/journal.pone.0009607.

J F Ferveur. Cuticular hydrocarbons: Their evolution and roles in Drosophila pheromonal communication. Behav Genet, 35(3):279–295, 2005.

J F Ferveur, F Savarit, C J O'Kane, G Sureau, R J Greenspan, and J M Jallon. Genetic feminization of pheromones and its behavioral consequences in Drosophila males. Science, 276(5318):1555–1558, 1997.

K. F. Fischbach and A. P.M. Dittrich. The optic lobe of Drosophila melanogaster. I. A Golgi analysis of wild-type structure. Cell and Tissue Research, 1989. ISSN 0302766X. doi: 10.1007/BF00218858.

Yoav Freund and Robert E. Schapire. A Decision-Theoretic Generalization of On-Line Learning and an Application to Boosting. Journal of Computer and System Sciences, 1997. ISSN 00220000. doi: 10.1006/jcss.1997.1504.

DA Gailey, RC Lacaillade, and JC Hall. Chemosensory elements of courtship in normal and mutant, olfaction-deficient Drosophila melanogaster. Behav Genet, 16(3):375–405, 1986.

Q Gaudry, E J Hong, J Kain, B L de Bivort, and R I Wilson. Asymmetric neurotransmitter release enables rapid odour lateralization in Drosophila. Nature, 493(7432):424–428, 2013.

Joshua I. Gold and Michael N. Shadlen. The Neural Basis of Decision Making. Annual Review of Neuroscience, 30(1):535–574, 2007. doi: 10.1146/annurev.neuro.29.051605.113038.

A Gomez-Marin, J J Paton, A R Kampff, R M Costa, and Z F Mainen. Big behavioral data: Psychology, ethology and the foundations of neuroscience. Nat Neurosci, 17(11): 1455–1462, 2014.

Paloma T. Gonzalez-Bellido, Samuel T. Fabian, and Karin Nordström. Target detection in insects: Optical, neural and behavioral optimizations. Current Opinion in Neurobiology, 41:122–128, December 2016. ISSN 1873-6882. doi: 10.1016/j.conb.2016.09.001.

Ralph J Greenspan and J F Ferveur. Courtship in Drosophila. Annual review of genetics, 2000. ISSN 0066-4197. doi: 10.1146/annurev.genet.34.1.205.

B Grothe, M Pecka, and D McAlpine. Mechanisms of sound localization in mammals. Physiol Rev, 90(3):983–1012, 2010.

Gaëlle Guiraudie-Capraz, Dang Ba Pho, and Jean-Marc Jallon. Role of the ejaculatory bulb in biosynthesis of the male pheromone cis-vaccenyl acetate in Drosophila

melanogaster. Integrative Zoology, 2(2):89–99, June 2007. ISSN 1749-4869. doi: 10.1111/j.1749-4877.2007.00047.x.

J. Haag, A. Vermeulen, and A. Borst. The intrinsic electrophysiological characteristics of fly lobula plate tangential cells: III. Visual response properties. Journal of Computational Neuroscience, 7(3):213–234, 1999. ISSN 0929-5313.

Väinö Haikala, Maximilian Joesch, Alexander Borst, and Alex S. Mauss. Optogenetic control of fly optomotor responses. The Journal of Neuroscience: The Official Journal of the Society for Neuroscience, 33(34):13927–13934, August 2013. ISSN 1529-2401. doi: 10.1523/JNEUROSCI.0340-13.2013.

Selig Hecht and George Wald. The Visual Acuity and Intensity Discrimination of Drosophila. The Journal of General Physiology, 17(4):517–547, March 1934. ISSN 0022-1295, 1540-7748. doi: 10.1085/jgp.17.4.517.

Chun Hu, Meike Petersen, Nina Hoyer, Bettina Spitzweck, Federico Tenedini, Denan Wang, Alisa Gruschka, Lara S. Burchardt, Emanuela Szpotowicz, Michaela Schweizer, Ananya R. Guntur, Chung-Hui Yang, and Peter Soba. Modality-specific sensory integration and neuropeptide-mediated feedback facilitate mechano-nociceptive behavior in Drosophila. Nature neuroscience, 20(8):1085–1095, August 2017. ISSN 1097-6256. doi: 10.1038/nn.4580.

Rafiq Huda, Michael J. Goard, Gerald N. Pho, and Mriganka Sur. Neural mechanisms of sensorimotor transformation and action selection. European Journal of Neuroscience, 0(0), 2018. ISSN 1460-9568. doi: 10.1111/ejn.14069.

Bradley T. Hyman and Junying Yuan. Apoptotic and non-apoptotic roles of caspases in neuronal physiology and pathophysiology. Nature Reviews Neuroscience, 13(6):395–406, June 2012. ISSN 1471-0048. doi: 10.1038/nrn3228.

Martin Irestedt, Knud A. Jønsson, Jon Fjeldså, Les Christidis, and Per G. P. Ericson. An unexpectedly long history of sexual selection in birds-of-paradise. BMC evolutionary biology, 9:235, September 2009. ISSN 1471-2148. doi: 10.1186/1471-2148-9-235.

Hiroki Ito, Kosei Sato, Shu Kondo, Ryu Ueda, and Daisuke Yamamoto. Fruitless Represses robo1 Transcription to Shape Male-Specific Neural Morphology and Behavior in Drosophila. Current biology: CB, 26(12):1532–1542, June 2016. ISSN 1879-0445. doi: 10.1016/j.cub.2016.04.067.

Lloyd A. Jeffress. A place theory of sound localization. Journal of Comparative and Physiological Psychology, 41(1):35–39, 1948. ISSN 0021-9940(Print). doi: 10.1037/h0061495.

Arnim Jenett, Gerald M. Rubin, Teri-T. B. Ngo, David Shepherd, Christine Murphy, Heather Dionne, Barret D. Pfeiffer, Amanda Cavallaro, Donald Hall, Jennifer Jeter, Nirmala Iyer, Dona Fetter, Joanna H. Hausenfluck, Hanchuan Peng, Eric T. Trautman, Robert R. Svirskas, Eugene W. Myers, Zbigniew R. Iwinski, Yoshinori Aso, Gina M. DePasquale, Adrianne Enos, Phuson Hulamm, Shing Chun Benny Lam, Hsing-Hsi Li, Todd R. Laverty, Fuhui Long, Lei Qu, Sean D. Murphy, Konrad Rokicki, Todd Safford, Kshiti Shaw, Julie H. Simpson, Allison Sowell, Susana Tae, Yang Yu, and Christopher T. Zugates. A GAL4-Driver Line Resource for Drosophila Neurobiology. Cell Reports, 2(4):991–1001, October 2012. ISSN 2211-1247. doi: 10.1016/j.celrep.2012.09.011.

Maximilian Joesch, Johannes Plett, Alexander Borst, and Dierk F. Reiff. Response properties of motion-sensitive visual interneurons in the lobula plate of Drosophila melanogaster. Current biology: CB, 18(5):368–374, March 2008. ISSN 0960-9822. doi: 10.1016/j.cub.2008.02.022.

M Kabra, A A Robie, M Rivera-Alba, S Branson, and K Branson. JAABA: Interactive

machine learning for automatic annotation of animal behavior. Nat Methods, 10(1): 64–67, 2013.

J Kain, C Stokes, Q Gaudry, X Song, J Foley, R Wilson, and B de Bivort. Leg-tracking and automated behavioural classification in Drosophila. Nat Commun, 4:1910, 2013.

B R Kallman, H Kim, and K Scott. Excitation and inhibition onto central courtship neurons biases Drosophila mate choice. Elife, 4:e11188, 2015.

Ken Ichi Kimura, Chiaki Sato, Kana Yamamoto, and Daisuke Yamamoto. From the back or front: The courtship position is a matter of smell and sight in Drosophila melanogaster males. Journal of Neurogenetics, 2015. ISSN 15635260. doi: 10.3109/01677063.2014.968278.

Ken-Ichi Kimura, Akira Urushizaki, Chiaki Sato, and Daisuke Yamamoto. A novel sex difference in Drosophila contact chemosensory neurons unveiled using single cell labeling. Journal of Neurogenetics, pages 1–9, November 2018. ISSN 1563-5260. doi: 10.1080/01677063.2018.1531858.

N C Klapoetke, A Nern, M Y Peek, E M Rogers, P Breads, G M Rubin, M B Reiser, and G M Card. Ultra-selective looming detection from radial motion opponency. Nature, 551 (7679):237–241, 2017.

U Klibaite, G J Berman, J Cande, D L Stern, and J W Shaevitz. An unsupervised method for quantifying the behavior of paired animals. Phys Biol, 14(1):15006, 2017.

T W Koh, Z He, S Gorur-Shandilya, K Menuz, N K Larter, S Stewart, and J R Carlson. The Drosophila IR20a clade of ionotropic receptors are candidate taste and pheromone receptors. Neuron, 83(4):850–865, 2014.

S Kohatsu and D Yamamoto. Visually induced initiation of Drosophila innate courtship-like following pursuit is mediated by central excitatory state. Nat Commun, 6:6457, 2015.

S Kohatsu, M Koganezawa, and D Yamamoto. Female contact activates male-specific interneurons that trigger stereotypic courtship behavior in Drosophila. Neuron, 69(3): 498–508, 2011.

John W. Krakauer, Asif A. Ghazanfar, Alex Gomez-Marin, Malcolm A. MacIver, and David Poeppel. Neuroscience Needs Behavior: Correcting a Reductionist Bias. Neuron, 93 (3):480–490, February 2017. ISSN 0896-6273. doi: 10.1016/j.neuron.2016.12.041.

H. G. Krapp and R. Hengstenberg. Estimation of self-motion by optic flow processing in single visual interneurons. Nature, 384(6608):463–466, December 1996. ISSN 0028-0836. doi: 10.1038/384463a0.

H. G. Krapp, B. Hengstenberg, and R. Hengstenberg. Dendritic structure and receptive-field organization of optic flow processing interneurons in the fly. Journal of Neurophysiology, 79(4):1902–1917, April 1998. ISSN 0022-3077. doi: 10.1152/jn.1998.79.4.1902.

D Krstic, W Boll, and M Noll. Sensory integration regulating male courtship behavior in Drosophila. PLoS One, 4(2):e4457, 2009.

Michael Krumin, Julie J Lee, Kenneth D Harris, and Matteo Carandini. Decision and navigation in mouse parietal cortex. eLife, 7:e42583, November 2018. ISSN 2050-084X. doi: 10.7554/eLife.42583.

Joshua J. Krupp, Clement Kent, Jean-Christophe Billeter, Reza Azanchi, Anthony K.-C. So, Julia A. Schonfeld, Benjamin P. Smith, Christophe Lucas, and Joel D. Levine. Social experience modifies pheromone expression and mating behavior in male Drosophila melanogaster. Current biology: CB, 18(18):1373–1383, September 2008. ISSN 0960-9822. doi: 10.1016/j.cub.2008.07.089.

Ron Kupers and Maurice Ptito. Compensatory Plasticity and Cross-Modal Reorganization

Following Early Visual Deprivation. 2014. ISBN 1873-7528. doi: 10.1016/j.neubiorev.2013.08.001.

A Kurtovic, A Widmer, and B J Dickson. A single class of olfactory neurons mediates behavioural responses to a Drosophila sex pheromone. Nature, 446(7135):542–546, 2007.

Lukas Landler, Graeme D. Ruxton, and E. Pascal Malkemper. Circular data in biology: Advice for effectively implementing statistical procedures. Behavioral Ecology and Sociobiology, 72(8), 2018. ISSN 0340-5443. doi: 10.1007/s00265-018-2538-y.

Kelly M LaRue, Jan Clemens, Gordon J Berman, and Mala Murthy. Acoustic duetting in Drosophila virilis relies on the integration of auditory and tactile signals. eLife, 4, 2015. ISSN 2050-084X. doi: 10.7554/eLife.07277.

G. Lee, M. Foss, S. F. Goodwin, T. Carlo, B. J. Taylor, and J. C. Hall. Spatial, temporal, and sexually dimorphic expression patterns of the fruitless gene in the Drosophila central nervous system. Journal of Neurobiology, 43(4):404–426, June 2000. ISSN 0022-3034.

Russell A. Ligon, Christopher D. Diaz, Janelle L. Morano, Jolyon Troscianko, Martin Stevens, Annalyse Moskeland, Timothy G. Laman, and Edwin Scholes Iii. Evolution of correlated complexity in the radically different courtship signals of birds-of-paradise. PLOS Biology, 16(11):e2006962, November 2018. ISSN 1545-7885. doi: 10.1371/journal.pbio.2006962.

Tong Liu, Ying Wang, Yue Tian, Jin Zhang, Jianjian Zhao, and Aike Guo. The receptor channel formed by ppk25, ppk29 and ppk23 can sense the Drosophila female pheromone 7,11-heptacosadiene. Genes, Brain and Behavior, 0(0):e12529, 2018. ISSN 1601-183X. doi: 10.1111/gbb.12529.

M Louis, T Huber, R Benton, T P Sakmar, and L B Vosshall. Bilateral olfactory sensory input enhances chemotaxis behavior. Nat Neurosci, 11(2):187–199, 2008.

B Lu, A LaMora, Y Sun, M J Welsh, and Y Ben-Shahar. Ppk23-Dependent chemosensory functions contribute to courtship behavior in Drosophila melanogaster. PLoS Genet, 8 (3):e1002587, 2012.

B Lu, K M Zelle, R Seltzer, A Hefetz, and Y Ben-Shahar. Feminization of pheromone-sensing neurons affects mating decisions in Drosophila males. Biol Open, 3(2):152–160, 2014.

Devanand S. Manoli, Margit Foss, Adriana Villella, Barbara J. Taylor, Jeffrey C. Hall, and Bruce S. Baker. Male-specific fruitless specifies the neural substrates of Drosophila courtship behaviour. Nature, 436(7049):395–400, July 2005. ISSN 1476-4687. doi: 10.1038/nature03859.

Fabrice Marcillac, François Bousquet, Josiane Alabouvette, Fabrice Savarit, and Jean-François Ferveur. A mutation with major effects on Drosophila melanogaster sex pheromones. Genetics, 171(4):1617–1628, December 2005. ISSN 0016-6731. doi: 10.1534/genetics.104.033159.

T. A. Markow. Behavioral and sensory basis of courtship success in Drosophila melanogaster. Proceedings of the National Academy of Sciences of the United States of America, 84(17):6200–6204, September 1987. ISSN 0027-8424.

Therese A. Markow and Stephen J. Hanson. Multivariate analysis of Drosophila courtship. Proceedings of the National Academy of Sciences of the United States of America, 78 (1):430–434, January 1981. ISSN 0027-8424.

Therese A N N Markow. Effect of light on egg-laying rate and mating speed in phototactic strains of Drosophila. Nature, 258:712, December 1975.

David McAlpine and Benedikt Grothe. Sound localization and delay lines – do mammals fit the model? Trends in Neurosciences, 26(7):347–350, July 2003. ISSN 0166-2236. doi: 10.1016/S0166-2236(03)00140-1.

R M McKinney, C Vernier, and Y Ben-Shahar. The neural basis for insect pheromonal communication. Curr Opin Insect Sci, 12:86–92, 2015.

D J Mellert, J M Knapp, D S Manoli, G W Meissner, and B S Baker. Midline crossing by gustatory receptor neuron axons is regulated by fruitless, doublesex and the Roundabout receptors. Development, 137(2):323–332, 2010.

Richard G. M. Morris. Spatial localization does not require the presence of local cues. Learning and Motivation, 12(2):239–260, May 1981. ISSN 0023-9690. doi: 10.1016/0023-9690(81)90020-5.

M C Neville, T Nojima, E Ashley, D J Parker, J Walker, T Southall, B de Sande, A C Marques, B Fischer, A H Brand, S Russell, M G Ritchie, S Aerts, and S F Goodwin. Male-specific fruitless isoforms target neurodevelopmental genes to specify a sexually dimorphic nervous system. Curr Biol, 24(3):229–241, 2014.

V Orgogozo, F Schweisguth, and Y Bellaiche. Slit-Robo signalling prevents sensory cells from crossing the midline in Drosophila. Mech Dev, 121(5):427–436, 2004.

Hideo Otsuna and Kei Ito. Systematic analysis of the visual projection neurons of Drosophila melanogaster. I. Lobula-specific pathways. Journal of Comparative Neurology, 2006. ISSN 00219967. doi: 10.1002/cne.21015.

Camillo Padoa-Schioppa and John A. Assad. Neurons in the orbitofrontal cortex encode economic value. Nature, 441(7090):223–226, May 2006. ISSN 1476-4687. doi: 10.1038/nature04676.

Yufeng Pan, Geoffrey W. Meissner, and Bruce S. Baker. Joint control of Drosophila male courtship behavior by motion cues and activation of male-specific P1 neurons. Proceedings of the National Academy of Sciences, 109(25):10065–10070, June 2012. ISSN 0027-8424, 1091-6490. doi: 10.1073/pnas.1207107109.

Fabian Pedregosa, Gaël Varoquaux, Alexandre Gramfort, Vincent Michel, Bertrand Thirion, Olivier Grisel, Mathieu Blondel, Peter Prettenhofer, Ron Weiss, Vincent Dubourg, Jake Vanderplas, Alexandre Passos, David Cournapeau, Matthieu Brucher, Matthieu Perrot, and Édouard Duchesnay. Scikit-learn: Machine Learning in Python. Journal of Machine Learning Research, 2012. ISSN 15324435. doi: 10.1007/s13398-014-0173-7.2.

B D Pfeiffer, T T Ngo, K L Hibbard, C Murphy, A Jenett, J W Truman, and G M Rubin. Refinement of tools for targeted gene expression in Drosophila. Genetics, 186(2):735–755, 2010.

Claudio W. Pikielny. Sexy DEG/ENaC channels involved in gustatory detection of fruit fly pheromones. Science Signaling, 5(249):pe48, November 2012. ISSN 1937-9145. doi: 10.1126/scisignal.2003555.

Michael L. Platt and Paul W. Glimcher. Neural correlates of decision variables in parietal cortex. Nature, 400(6741):233–238, July 1999. ISSN 1476-4687. doi: 10.1038/22268.

D R Possidente and R K Murphey. Genetic control of sexually dimorphic axon morphology in Drosophila sensory neurons. Dev Biol, 132(2):448–457, 1989.

Meredith E. Protas and Nipam H. Patel. Evolution of Coloration Patterns. Annual Review of Cell and Developmental Biology, 24(1):425–446, November 2008. ISSN 1081-0706. doi: 10.1146/annurev.cellbio.24.110707.175302.

Inês M.A. Ribeiro, Michael Drews, Armin Bahl, Christian Machacek, Alexander Borst, and Barry J. Dickson. Visual Projection Neurons Mediating Directed Courtship in Drosophila. Cell, 174(3):607–621.e18, July 2018. ISSN 00928674. doi: 10.1016/j.cell.2018.06.020.

Alice A. Robie, Jonathan Hirokawa, Austin W. Edwards, Lowell A. Umayam, Allen Lee, Mary L. Phillips, Gwyneth M. Card, Wyatt Korff, Gerald M. Rubin, Julie H. Simpson,

Michael B. Reiser, and Kristin Branson. Mapping the Neural Substrates of Behavior. Cell, 170(2):393–406.e28, July 2017. ISSN 1097-4172. doi: 10.1016/j.cell.2017.06.032.

V Ruta, S R Datta, M L Vasconcelos, J Freeland, L L Looger, and R Axel. A dimorphic pheromone circuit in Drosophila from sensory input to descending output. Nature, 468 (7324):686–690, 2010.

William F. Schafer. Genetics of egg-laying in worms. Annual Review of Genetics, 40: 487–509, 2006. ISSN 0066-4197. doi: 10.1146/annurev.genet.40.110405.090527.

R Sen, M Wu, K Branson, A Robie, G M Rubin, and B J Dickson. Moonwalker Descending Neurons Mediate Visually Evoked Retreat in Drosophila. Curr Biol, 27(5):766–771, 2017.

R. W. Siegel and J. C. Hall. Conditioned responses in courtship behavior of normal and mutant Drosophila. Proceedings of the National Academy of Sciences, 76(7):3430–3434, July 1979. ISSN 0027-8424, 1091-6490. doi: 10.1073/pnas.76.7.3430.

M B Sokolowski. Drosophila: Genetics meets behaviour. Nat Rev Genet, 2(11):879–890, 2001.

M B Sokolowski. Social interactions in ”simple” model systems. Neuron, 65(6):780–794, 2010.

Herman T. Spieth. Courtship Behavior in Drosophila. Annual Review of Entomology, 19 (1):385–405, 1974. doi: 10.1146/annurev.en.19.010174.002125.

Herman T Spieth and T C Hsu. The influence of light on the mating behavior of seven species of the Drosophila melanogaster species group. Evolution, 4(4):316–325, 1950. doi: 10.1111/j.1558-5646.1950.tb01401.x.

E Starostina, T Liu, V Vijayan, Z Zheng, K K Siwicki, and C W Pikielny. A Drosophila

DEG/ENaC subunit functions specifically in gustatory neurons required for male courtship behavior. J Neurosci, 32(13):4665–4674, 2012.

Barry E. Stein, Terrence R. Stanford, and Benjamin A. Rowland. Development of multisensory integration from the perspective of the individual neuron. Nature reviews. Neuroscience, 15(8):520–535, August 2014. ISSN 1471-003X.

Richard M. Stern, Andrew S. Zeiberg, and Constantine Trahiotis. Lateralization of complex binaural stimuli: A weighted-image model. The Journal of the Acoustical Society of America, 84(1):156–165, July 1988. ISSN 0001-4966. doi: 10.1121/1.396982.

Nicholas J. Strausfeld and Jun Ya Okamura. Visual system of calliphorid flies: Organization of optic glomeruli and their lobula complex efferents. Journal of Comparative Neurology, 2007. ISSN 00219967. doi: 10.1002/cne.21196.

Andrew D. Straw and Michael H. Dickinson. Motmot, an open-source toolkit for realtime video acquisition and analysis. Source Code for Biology and Medicine, 4:5, July 2009. ISSN 1751-0473. doi: 10.1186/1751-0473-4-5.

A. H. Sturtevant. Experiments on sex recognition and the problem of sexual selection in Drosoophilia. Journal of Animal Behavior, 1915. ISSN 00959928. doi: 10.1037/h0074109.

Marie P. Suver, Ainul Huda, Nicole Iwasaki, Steve Safarik, and Michael H. Dickinson. An Array of Descending Visual Interneurons Encoding Self-Motion in Drosophila. Journal of Neuroscience, 36(46):11768–11780, November 2016. ISSN 0270-6474, 1529-2401. doi: 10.1523/JNEUROSCI.2277-16.2016.

Sean T. Sweeney, Kendal Broadie, John Keane, Heiner Niemann, and Cahir J. O'Kane. Targeted expression of tetanus toxin light chain in Drosophila specifically eliminates synaptic transmission and causes behavioral defects. Neuron, 1995. ISSN 08966273. doi: 10.1016/0896-6273(95)90290-2.

N A Swierczek, A C Giles, C H Rankin, and R A Kerr. High-throughput behavioral analysis in C. elegans. Nat Methods, 8(7):592–598, 2011.

E Tauber and DF Eberl. Song production in auditory mutants of Drosophila: The role of sensory feedback. J Comp Physiol A, 187(5):341–8, 2001.

R Thistle, P Cameron, A Ghorayshi, L Dennison, and K Scott. Contact chemoreceptors mediate male-male repulsion and male-female attraction during Drosophila courtship. Cell, 149(5):1140–1151, 2012.

H Toda, X Zhao, and B J Dickson. The Drosophila female aphrodisiac pheromone activates ppk23(+) sensory neurons to elicit male courtship behavior. Cell Rep, 1(6): 599–607, 2012.

W. W. Tso and J. Adler. Negative chemotaxis in Escherichia coli. Journal of Bacteriology, 118(2):560–576, May 1974. ISSN 0021-9193.

Virginie Uhlmann, Pavan Ramdya, Ricard Delgado-Gonzalo, Richard Benton, and Michael Unser. FlyLimbTracker: An active contour based approach for leg segment tracking in unmarked, freely behaving Drosophila. PLOS ONE, 12(4):e0173433, April 2017. ISSN 1932-6203. doi: 10.1371/journal.pone.0173433.

Stéfan van der Walt, Johannes L. Schönberger, Juan Nunez-Iglesias, François Boulogne, Joshua D. Warner, Neil Yager, Emmanuelle Gouillart, and Tony Yu. Scikit-image: Image processing in Python. PeerJ, 2014. ISSN 2167-8359. doi: 10.7717/peerj.453.

C R von Reyn, A Nern, W R Williamson, P Breads, M Wu, S Namiki, and G M Card. Feature Integration Drives Probabilistic Behavior in the Drosophila Escape Response. Neuron, 94(6):1190—-1204.e6, 2017.

Leslie B. Vosshall. Scent of a Fly. Neuron, 59(5):685–689, September 2008. ISSN 0896-6273. doi: 10.1016/j.neuron.2008.08.014.

E Vrontou, S P Nilsen, E Demir, E A Kravitz, and B J Dickson. Fruitless regulates aggression and dominance in Drosophila. Nat Neurosci, 9(12):1469–1471, 2006.

Sijie Jason Wang and Zhao-Wen Wang. Track-A-Worm, An Open-Source System for Quantitative Assessment of C. elegans Locomotory and Bending Behavior. PLOS ONE, 8(7):e69653, July 2013. ISSN 1932-6203. doi: 10.1371/journal.pone.0069653.

Pinsker Wilhelm and Elfriede Doschek. On the role of light in the mating behavior of Drosophila subobscura. Z. Naturforsch, 34(c):1253–1260, 1979.

Patricia J. Wittkopp and Patrícia Beldade. Development and Evolution of Insect Pigmentation: Genetic Mechanisms and the Potential Consequences of Pleiotropy. 2009. ISBN 1084-9521 (Print). doi: 10.1016/j.semcdb.2008.10.002.

Joy S. Wu and Liqun Luo. A protocol for dissecting Drosophila melanogaster brains for live imaging or immunostaining. Nature Protocols, 1(4):2110–2115, November 2006. ISSN 1750-2799. doi: 10.1038/nprot.2006.336.

M Wu, A Nern, W R Williamson, M M Morimoto, M B Reiser, G M Card, and G M Rubin. Visual projection neurons in the Drosophila lobula link feature detection to distinct behavioral programs. Elife, 5, 2016.

Robert J Wyman, David G King, John B Thomas, and Lawrence Salkoff. The Drosophila Giant Fiber System. In Neural Mechanisms of Startle Behavior, pages 133–161. Plenum Press, 1984.

J Y Yew and H Chung. Insect pheromones: An overview of function, form, and discovery. Prog Lipid Res, 59:88–105, 2015.

Joanne Y. Yew, Robert B. Cody, and Edward A. Kravitz. Cuticular hydrocarbon analysis of an awake behaving fly using direct analysis in real-time time-of-flight mass spectrome-

try. Proceedings of the National Academy of Sciences, 105(20):7135–7140, May 2008. ISSN 0027-8424, 1091-6490. doi: 10.1073/pnas.0802692105.

Zhihao Zheng, J. Scott Lauritzen, Eric Perlman, Camenzind G. Robinson, Matthew Nichols, Daniel Milkie, Omar Torrens, John Price, Corey B. Fisher, Nadiya Sharifi, Steven A. Calle-Schuler, Lucia Kmecova, Iqbal J. Ali, Bill Karsh, Eric T. Trautman, John A. Bogovic, Philipp Hanslovsky, Gregory S. X. E. Jefferis, Michael Kazhdan, Khaled Khairy, Stephan Saalfeld, Richard D. Fetter, and Davi D. Bock. A Complete Electron Microscopy Volume of the Brain of Adult Drosophila melanogaster. Cell, 174 (3):730–743.e22, July 2018. ISSN 0092-8674. doi: 10.1016/j.cell.2018.06.019.

Appendix A: Tables Related to Tracking Software

Metadata	Feature	Python Accessibility
Arena	Center Pixel, Column	`summary.arena.center_pixel_cc`
Arena	Center Pixel, Row	`summary.arena.center_pixel_rr`
Arena	Diameter (mm)	`summary.arena.diameter`
Arena	Radius (mm)	`summary.arena.radius`
Arena	Shape	`summary.arena.shape`
Arena	Vertices	`summary.arena.vertices`
Software	Date Tracked	`summary.software.date_tracked`
Software	Loose Threshold	`summary.software.loose_threshold`
Software	Tight Threshold	`summary.software.tight_threshold`
Software	Version	`summary.software.version`
Video	Total Frames	`summary.video.duration_frames`
Video	Total Seconds	`summary.video.duration_seconds`
Video	Start Time	`summary.video.start_time`
Video	Start Time	`summary.video.end_time`
Video	Frames per Second	`summary.video.fps`
Video	Timestamps	`summary.video.timestamps`
Video	Filename	`summary.video.filename`
Video	Pixels per mm	`summary.video.pixels_per_mm`
Experiment	Group	`summary.group`

Table A.1: **Metadata stored in tracking output.** Note that for 'Python Accessibility', this assumes that the user has loaded a .fcts file into the variable `summary`.

Fly Part	Tracked Feature	Python Accessibility
Body	Centroid Pixel Column	summary.male.body.centroid.col
Body	Centroid Pixel Row	summary.male.body.centroid.row
Body	Head Pixel Column	summary.male.body.head.col
Body	Head Pixel Row	summary.male.body.head.row
Body	Ellipse Major Axis Length	summary.male.body.major_axis_length
Body	Ellipse Minor Axis Length	summary.male.body.minor_axis_length
Body	Ellipse Orientation	summary.male.body.orientation
Body	Rear Pixel Column	summary.male.body.rear.col
Body	Rear Pixel Row	summary.male.body.rear.row
Body	Ellipse Rotation Angle	summary.male.body.rotation_angle
Left Wing	Centroid Pixel Column	summary.male.left_wing.centroid.col
Left Wing	Centroid Pixel Row	summary.male.left_wing.centroid.row
Left Wing	Ellipse Major Axis Length	summary.male.left_wing.major_axis_length
Left Wing	Ellipse Minor Axis Length	summary.male.left_wing.minor_axis_length
Left Wing	Ellipse Orientation	summary.male.left_wing.orientation
Right Wing	Centroid Pixel Column	summary.male.right_wing.centroid.col
Right Wing	Centroid Pixel Row	summary.male.right_wing.centroid.row
Right Wing	Ellipse Major Axis Length	summary.male.right_wing.major_axis_length
Right Wing	Ellipse Minor Axis Length	summary.male.right_wing.minor_axis_length
Right Wing	Ellipse Orientation	summary.male.right_wing.orientation
NA	Timestamp of Video Frame	summary.male.timestamps

Table A.2: **Tracking data stored in tracking output.** This data is available for both the male and female fly in each pair, though the Python Accessibility is only shown for the male. Note that for 'Python Accessibility', this assumes that the user has loaded a .fcts file into the variable `summary`.

Feature	Description	units
θ_{wings}	Angle between $C_{LW} > C_{body} > C_{RW}$	rad
θ_{LW}	Angle between $C_{LW} > C_{body} >$ x-axis	rad
θ_{RW}	Angle between $C_{RW} > C_{body} >$ x-axis	rad
A_{LW}	Area of left wing	mm^2
A_{RW}	Area of right wing	mm^2
D_{wing}	Total distance between C_{LW}, C_{body}, C_{RW}	mm
D_{CC}	Male-to-female distance (centroid)	mm
D_{HE}	Male-head to female-ellipse distance	mm
D_{RE}	Male-rear to female-ellipse distance	mm
ΔD	$D_{RE} - D_{HE}$	mm
Θ_{Rel}	Relative heading of male w.r.t female	rad
$\lvert\Theta_{Rel}\rvert$	Absolute value of Θ_{Rel}	rad
v_Θ	Angular velocity of male	rad/sec
$\lvert v_\Theta\rvert$	Absolute value of v_Θ	rad/sec
$\lvert v_C\rvert$	Velocity of male centroid	mm/sec
L_{maj}	Maj. axis length of male ellipse	mm
L_{min}	Min. axis length of male ellipse	mm
A	Area of male ellipse	mm^2
Θ	Angle of male ellipse w.r.t. x-axis	rad
D_{CE}	Male-centroid to arena edge distance	mm

Table A.3: **General features input into behavioral classifiers.** First and second derivatives were calculated for all features. Abbreviations are as follows: C_{LW}, centroid of male fly's left wing; C_{RW}, centroid of male fly's right wing; C_{body}, centroid of male fly's body. Windowed statistics, as shown in Table A.4 were also calculated for all features listed in this table.

Statistic	Window Sizes	DI	Description
Mean	3, 11, 21	NA	Mean value of sliding window
Median	3, 11, 21	NA	Median value of sliding window
Max	3, 11, 21	NA	Maximum value of sliding window
Min	3, 11, 21	NA	Minimum value of sliding window
Median diff	3, 11, 21	0, $i/2$, i	Diff. between window median and value at DI
Max diff	3, 11, 21	0, $i/2$, i	Diff. between window max and value at DI
Min diff	3, 11, 21	0, $i/2$, i	Diff. between window min and value at DI

Table A.4: **General windowed statistics input into behavioral classifiers.** Each tracked feature consisted of an array of N video frames. We applied sliding windows to these arrays to extract informative features which could be used in a boosted decision tree. These windows were of varying sizes (shown above) and were similar to those used in [Branson et al., 2009]. Note that DI stands for "Difference Index", and i in this context refers to the size of the window.